Joint Source Channel Coding in Broadcast and Relay Channels: A Non-Asymptotic End-to-End Distortion Approach

by

James Ho

A thesis
presented to the University of Waterloo
in fulfillment of the
thesis requirement for the degree of
Doctor of Philosophy
in
Electrical and Computer Engineering

Waterloo, Ontario, Canada, 2013

I hereby declare that I am the sole author of this thesis. This is a true copy of the thesis, including any required final revisions, as accepted by my examiners.

I understand that my thesis may be made electronically available to the public.

Abstract

The paradigm of separate source-channel coding is inspired by Shannon's separation result, which implies the asymptotic optimality of designing source and channel coding independently from each other. The result exploits the fact that channel error probabilities can be made arbitrarily small, as long as the block length of the channel code can be made arbitrarily large. However, this is not possible in practice, where the block length is either fixed or restricted to a range of finite values. As a result, the optimality of source and channel coding separation becomes unknown, leading researchers to consider joint source-channel coding (JSCC) to further improve the performance of practical systems that must operate in the finite block length regime. With this motivation, this thesis investigates the application of JSCC principles for multimedia communications over point-to-point, broadcast, and relay channels. All analyses are conducted from the perspective of end-to-end distortion (EED) for results that are applicable to channel codes with finite block lengths in pursuing insights into practical design.

The thesis first revisits the fundamental open problem of the separation of source and channel coding in the finite block length regime. Derived formulations and numerical analyses for a source-channel coding system reveal many scenarios where the EED reduction is positive when pairing the channel-optimized source quantizer (COSQ) with an optimal channel code, hence establishing the invalidity of the separation theorem in the finite block length regime. With this, further improvements to JSCC systems are considered by augmenting error detection codes with the COSQ. Closed-form EED expressions for such system are derived, from which necessary optimality conditions are identified and used in proposed algorithms for system design. Results for both the point-to-point and broadcast channels demonstrate significant reductions to the EED without sacrificing bandwidth when considering a tradeoff between quantization and error detection coding rates. Lastly, the JSCC system is considered under relay channels, for which a computable measure of the EED is derived for any relay channel conditions with nonzero channel error probabilities. To emphasize the importance of analyzing JSCC systems under finite block lengths, the large sub-optimality in performance is demonstrated when solving the power allocation configuration problem according to capacity-based formulations that disregard channel errors, as opposed to those based on the EED.

Although this thesis only considers one JSCC setup of many, it is concluded that consideration of JSCC systems from a non-asymptotic perspective not only is more meaningful, but also reveals more relevant insight into practical system design. This thesis accomplishes such by maintaining the EED as a measure of system performance in each of the considered point-to-point, broadcast, and relay cases.

Acknowledgements

Throughout the Waterloo years, it has always been the people both near and far that have empowered me to persevere through all the expected, inevitable, and unforeseeable obstacles of life. As the years progress, the list of people I am indebted to grows ever longer. This section serves to acknowledge some of the most important people of my journey, without whom this thesis could never be.

My deepest appreciation and gratitude are reserved for my supervisors, Professor Pin-Han Ho and Professor En-Hui Yang. Through them, I became inspired to constantly seek out challenges for self-growth in both academics and character. Only through their influence and guidance could I have gathered the strength necessary to persist through the entirety of this degree.

I am truly grateful of my examining committee members, consisting of Professor Liang-Liang Xie, Professor Sagar Naik, and Professor Fatma Gzara, for their valuable recommendations during my comprehensive examination and their commitment to my thesis defense. Additional thanks to Professor Xie for attending my seminar and providing lots of valuable advice in preparation of my defense. Furthermore, I would like to thank Professor Sorina Dumitrescu from McMaster University for serving as my external examining committee member.

I am also fortunate to have Professor Bill Bishop's guidance since the first year of my undergraduate studies.

I would like to thank previous and current members of the Multimedia Communications Laboratory, many of whom I have forged strong friendships and collaborations with, including Dr. Jin Meng, Dr. Lin Zheng, Dr. Xiang Yu, Dr. Mehdi Torbatian, Chang Sun, Nan Hu, Yueming Gao, Mahshad Eslamifar, Jie Zhang, Krzysztof Hebel, and Krishna Rapaka.

The remainder of the people are those who have kept me sane throughout various stages of my journey. I would like to thank Kevin Keung, Jaimal Soni, Tariq Nanji, Alan Kuurstra, Dan Weisser, Rajiv Tanna, Tracy Kong, Ifan Wang, Dr. Nicholas Allec, Shiva Abbaszadeh, Dr. Ahmad Dhaini, Payam Padidar, and Scott Chen.

Thank you Christie for putting up with any me.

To my beloved parents, who have always shown unwavering love and support.

Table of Contents

List of Tables

List of Figures

Chapter 1

Introduction

The design of effective information exchange over digital communication systems is most generally separated into two stages: source coding and channel coding. At the transmitter, the original source is encoded by a source and channel encoder before transmission over the communication channel, while at the receiver, channel and source decoders process the output of the channel to reconstruct the original source. In general, the purpose of source coding is data compression, accomplished by the removal of redundancies in the original source to represent it using fewer bits. On the other hand, channel coding generally inserts redundancies that assist in maintaining data integrity by effectively minimizing transmission error.

In the first few decades of research into communication systems, the two stages of source and channel coding were mostly designed independent of each other. In this case, the source encoder targets to represent the original source in the most compact bitstream manner regardless of channel statistics. Meanwhile, the channel encoder treats the source encoder output as only bitstreams without consideration of source statistics in minimizing information loss or error. This design paradigm, commonly known as *separate* source-channel coding, was originally inspired by Shannon's separation result, which states that for the point-to-point channel, it is asymptotically optimal to design source and channel coding independently from each other. The result hinges on the fact that the error probability of

the channel can be made arbitrarily small, as long as the block length of the channel code can grow without bound. However, in practice, the block length of the channel cannot be unbounded, and is often restricted to a particular range of finite values to satisfy delay constraints of the application or erratic conditions of the communication channel. Without the assumption of asymptotically large block lengths, channel error probabilities can no longer be made arbitrarily small, resulting in the unknown optimality of source and channel coding separation. Hence, researchers have turned to consider *joint* source-channel coding to further improve the receiver reconstruction quality of the source over communication systems.

1.1 Joint Source Channel Coding Systems

In contrast to the separate design paradigm, systems based on joint source-channel coding (JSCC) allow the source coding and channel coding stages to be jointly designed. While the degree to which they are jointly designed can widely vary from the minor sharing of statistics to treating the two stages as a singularity, any system that does not maintain the strict independence of source and channel coding in its design is considered to employ JSCC principles.

As an example, Fig. 1.1 depicts a general source-channel coding system. At the transmitter, the original scalar or vector source $\boldsymbol{z}$ is processed by the source and channel encoder prior to transmission over the channel. At the receiver, the channel and source decoder eventually outputs $\hat{\boldsymbol{z}}$, a reconstruction of the original source $\boldsymbol{z}$.

For designs based strictly on Shannon's separation result, the source encoder and decoder are designed according to only the statistics of $\boldsymbol{z}$, and the channel encoder and decoder are tailored to only the particular channel of the system. Systems based on JSCC principles allow source coding design based on channel coding information, or *vice versa*, leading to designs such as source-optimized channel coding or channel-optimized source coding. In the former, the channel code is tailored to the source coding of the system while the latter enables source codes that are tailored to the channel coding. JSCC principles

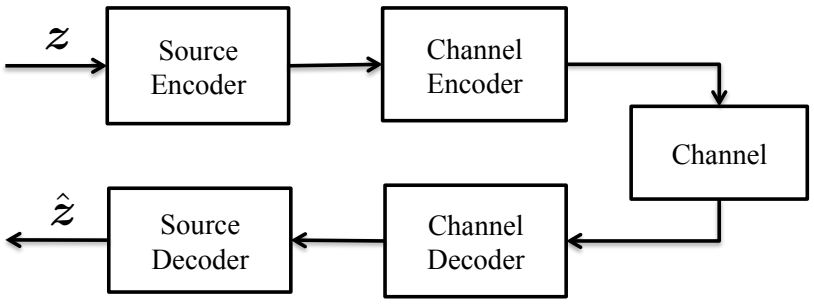

Figure 1.1: General point-to-point source-channel coding system.

can be taken further by considering a combination thereof using iterative methods, further blurring the boundaries between source and channel coding and demonstrating the increased suitability for their treatment as a single source-channel encoder or decoder during design and operation.

For point-to-point channels, such as those depicted in Fig. 1.1, there are indeed indications in some earlier results that suggest joint as opposed to separate source-channel coding yields some notable advantages. For example, numerous investigations into systems employing JSCC have been carried out ([1], [2], [3], [4], [5], [6], [7], and some references therein), all of which exhibit potential advantages over their separate design counterparts in terms of end-to-end distortion (EED), defined as the average per-symbol mean-squared error (MSE) between the original source and its receiver reconstruction to capture the distortion introduced by the source coding, channel coding, as well as the channel itself.

Motivations of employing JSCC principles span beyond the unknown optimality of source and channel coding separation in the finite block length regime for point-to-point channels. For the broadcast channel, JSCC principles have been applied to pair scalable source coding (SSC) with superposition channel coding (SPC) through a natural ordering map of each source code resolution to the corresponding channel code resolution [8][9][10][11]. As such, multiple resolutions of the source information can be decoded from the single channel broadcast, resulting in improved utilization of channel resources under diverse multi-user channel conditions. Moreover, such SSC-SPC pairing enables evaluation of performance in terms of the source end-to-end distortion introduced by the

source-channel coding system, which for practical multimedia communications, may be significantly more meaningful than traditional channel coding metrics such as achievable rate or channel capacity.

As an example, for the transmission of a two-resolution successively refinable source over a degraded broadcast channel with two receivers, it is possible to reconstruct the source at either the lower resolution using only partial information, or the higher resolution using the complete information. By the exact mapping of the lower resolution source symbol to the lower resolution of the SPC codeword that is more tolerant to the channel noise, receivers experiencing poorer channel conditions can better preserve service continuity at the lower resolution instead of service outage. On the other hand, receivers able to decode the full SPC codeword obtain the higher resolution of source reconstruction. As a result of such natural ordering mapping of resolutions between source and channel coding, the awkward situation where correctly-decoded refinement information cannot be used due to loss of corresponding lower resolution information is avoided. The architecture whereby SSC is paired with SPC has also been extended to the transmission of multiresolution sources over wireless relay networks by using a variety of cooperative strategies to exploit the successively refinement nature of the source [12][13][14][15][16].

1.2 End-to-End Distortion

Conducting analysis of separate or joint source-channel coding systems for broadcast or relay channels in a non-asymptotic, practical manner is no easy task. Hence, numerous research efforts have pursued theoretical results in the asymptotic setting by evaluating performance using metrics such as channel capacity or distortion exponent [12][17][18][19][20]. These performance measures are asymptotic in the sense that they are only applicable when the block length of the channel code can grow without bound. As such, they do not include the effects of potentially large error probabilities that applications operating under finite block lengths must tolerate. Hence, while investigations based on these metrics reveal some insights into the design of their considered systems in asymptotic scenarios,

they are less applicable to practical systems operating in the finite block length regime. Furthermore, studies based on channel capacity have unclear associations to the distortions introduced to the source by the entire system in multimedia communication applications, for which evaluations from the perspective of distortion may be more meaningful.

Some research on JSCC systems have employed distortion as a performance metric, but relies on other asymptotic assumptions for its evaluation, such as [13], which computes the expected distortion from outage probabilities based on channel capacity. Efforts in [14] include rigorous theoretical analyses with results based on outage-based end-to-end distortion followed by actual simulations, resulting in unclear implications of their theoretical results on the demonstrated gains in their simulations from the perspective of source distortion. Works in [15][16][21][22] begin with the MSE distortion measure but relies on the assumption of high SNR for analysis and evaluation, again restricting their results' applicability from non-asymptotic practical systems.

While the evaluation of system performance using end-to-end distortion is more natural for multimedia applications, doing so in a non-asymptotic end-to-end manner for systems that include both source and channel coding may often result in rather complex formulations and hence difficulty in conducting analysis. Consider a JSCC system employing channel-optimized source quantizers (COSQ), or noisy channel quantizers. In general, the COSQ is composed of two parts, specifically, a scalar or vector quantizer, and an index assignment mapping, both of which can impact the average EED of the JSCC system. For fixed index assignments, earlier works in [1][2][3][4][5][23] presented effective algorithms for the design of optimal noisy channel quantizers and demonstrated their superiority over traditional quantizers designed based on Lloyd-Max [24][25]. However, they are unable to provide strong analytical results because of using a fixed index assignment in their system setting, resulting in the lack of an analytical closed-form expression for the EED and high complexity in quantizer design. For example, vector quantizers designed in [1] and [5] are based on necessary conditions that depend on all transitional probabilities from channel input symbols to channel output symbols, hence making it difficult to analyze not only the optimal quantizer itself, but also to compute the EED. On the other hand, earlier work by Zeger and Manzella [26] investigated the source quantization problem under random index

assignment (RIA) to transform any discrete memoryless channel (DMC) to a symmetric channel in pursuing analytical results. However, their results are only valid in the high-rate asymptotic case. Meanwhile, efforts by Yu *et al.* and Teng *et al.* in applying RIA led to the derivation of closed-form non-asymptotic EED formulae for both the point-to-point [6] and broadcast [7] channels. With the closed-form EED formula, theoretical analysis of optimal noisy channel quantizers became tractable, and algorithm design required only the average channel error probability, as opposed to the entire matrix of transitional probabilities necessary for the fixed case. Although treatment of the COSQ design problem under the assumption of RIA may initially seem counterintuitive or impractical, RIA has obvious equivalence to scramblers, which are already widely employed in practical communications systems such as LTE systems [27]. Furthermore, it was shown in [6] that quantizers designed based on RIA can partially alleviate the poor performance observed in [1] under channel mismatch.

1.3 Organization and Contributions

This thesis investigates the application of joint source-channel coding principles in broadcast and relay channels. The entirety of the thesis maintains the employment of end-to-end distortion, defined as the exact mean-squared error between the original source and its receiver reconstruction, as the performance metric for system evaluation. Our derivations of closed-form EED expressions for JSCC systems are conducted for systems that link source and channel coding with random index assignment, and holds with full accuracy for any non-asymptotic channel settings. This is in contrast to some prior literatures that rely on asymptotic assumptions to proceed with their analyses. We envision that this style of non-asymptotic analysis allows deeper insight to provide larger implications on practical system and coding design than the studies conducted under asymptotic and unrealistic scenarios. Furthermore, the techniques that enable our non-asymptotic theoretical analysis are not limited to the particular considered setup; they can be similarly applied to any JSCC system, transmission scheme, or relay strategy.

To motivate the consideration of JSCC principles in broadcast or relay scenarios, Chap-

ter 2 first revisits the fundamental problem of the validity of source and channel coding separation in the non-asymptotic finite block length regime. This fundamental problem remains open in general, yet its investigation is necessary to justify the increase in design and operation complexity of joint source-channel coding over separate source-channel coding in practical communication systems, for which operation in the finite block length regime results in channel error probabilities that are strictly greater than zero.

To demonstrate the invalidity of source-channel coding separation, Chapter 2 considers a JSCC system that employs the channel-optimized source quantizer given channel information in the form of transition probabilities between channel input and output symbols, and show its advantages over separate design counterparts. While there are earlier efforts that have considered such a problem, they have assumed system settings with either no channel coding or with a fixed channel code that may be close to or far from optimal, resulting in potentially large overestimations of channel symbol error probabilities and in turn, the reductions to EED as well. Hence, their results do not imply the breakdown of Shannon's separation theorem in the finite block length regime, even though the fact of nonzero channel error probabilities for *any* channel code certainly suggests so. In Chapter 2, our treatment of the problem differs in our employment of optimal channel coding, and as a result, quantifies the lower bound of the achievable reductions to EED when applying JSCC principles to the considered source-channel coding setup through the pairing of the COSQ with an optimal channel code. Our results show that achievable reductions of some magnitude to the EED are possible when considering the joint versus separate design, even under optimal channel coding. Hence, the results of the investigation in Chapter 2 firmly imply that the separation of source and channel coding no longer holds for practical applications that operate in the finite block length regime. Moreover, the yielded reductions to the EED may even be fairly large under certain system settings or channel conditions, hence justifying the employment of joint source-channel coding in practical multimedia communications. This work was published in [28].

With the potential advantages of employing JSCC principles established even under the most idealistic scenario of an optimal channel code, Chapter 3 builds upon prior related work for a particular SSC-SPC pairing, where the noisy multiresolution vector quantizer is

linked to superposition channel codes with random index assignment to enable the closed-form derivation of the EED and its rigorous theoretical analysis. Under this setup, we investigate and analyze further improvements to the performance of such SSC-SPC pairing through the joint design of the multiresolution source quantizer with added error detection codes at the application layer when the channel code and error probability statistics are fixed. The EED for the system with error detection codes are formulated, from which necessary optimality conditions are derived. Iterative algorithms are proposed for multiresolution vector quantization design and analysis, with their performance evaluated for both point-to-point and broadcast channels under the employment of several cyclic redundancy checks of various polynomial lengths as the error detection code.

Our motivation for including error detection into the consideration of source coding design in Chapter 3 stems from earlier work that attributed a large portion of distortion contribution to a structural parameter named the scatter factor of the noisy channel quantizer, and that its contribution to the EED occurs for only undetected symbol errors. Hence, reductions to the scatter factor's contribution to the EED may also significantly reduce the EED itself by transforming any arbitrary discrete memoryless channel to a partial erasure channel, for which the scatter factor's contribution to the EED are reduced to only symbol errors that are undetectable by the error detection code as opposed to all symbol errors. Portions of this work were published in [29] and [30].

Investigations of the SSC-SPC pairing based on JSCC principles are further extended to the three-node relay network in Chapter 4 from the context of end-to-end distortion performance. In contrast to any previously reported research based on asymptotic capacity-based distortion (CBD) measures, the study proceeds with the derivation of the EED for the transmission of a real-valued Gaussian source with error detection codes under random index assignment. Maintaining system formulation and analyses using EED under the non-asymptotic channel coding assumptions serves to achieve better applicability in practice, where channel codes with predetermined finite block lengths subject the multimedia application to large error probabilities. Using the derived EED formulation for the relay network, achievable gains of the SSC-SPC pairing are quantified versus a number of conventional single-resolution or point-to-point transmission schemes. Portions of this

work were published in [31], [32], and [33].

To better motivate the analysis of JSCC systems in a non-asymptotic manner using EED, Chapter 4 further considers the problem of power allocation optimization inherent to the broadcast channel when solved based on the derived EED formulations in comparison to using an asymptotic CBD measure, for which symbol losses caused by channel errors are disregarded. The performance gap between results solved from EED versus CBD are numerically quantified for a variety of relay channel conditions, and demonstrate that the SSC-SPC pairing exhibits potential suboptimal and awkward performance when power allocation configuration is performed based on CBD measures. Portions of this work were published in [31], [34], and [35].

Chapter 5 concludes the thesis and summarizes potential future work, including ongoing research in furthering the development and analysis of joint source-channel coding systems from the non-asymptotic perspective of end-to-end distortion.

Chapter 2

Separation of Source and Channel Coding

Consider the transmission of a real-valued source z over a general point-to-point source-channel coding system. By Shannon's classic separation result, it is asymptotically optimal to design the source and channel coding of z independently from each other, as long as the block length of the channel code is allowed to grow without bound. However, in practice, the block length of the channel code cannot be unbounded, and is often restricted to a particular range of finite values to satisfy delay constraints of the application or erratic conditions of the wireless channel. Without the assumption of asymptotically large block lengths, the question of whether or not the separation theorem holds in the finite block length regime remains a problem yet to be completely analyzed and solved.

In this chapter, we revisit the validity of source and channel coding separation in the finite block length regime. To demonstrate the invalidity of source-channel coding separation for finite block lengths, we employ JSCC principles and consider the usage of channel-optimized source quantizers under optimal channel coding. Our analyses are distinguished from prior work that consider either no channel coding or fixed channel codes that may be close to or far from optimal, and hence do not address the fundamental open problem of whether or not the separation theorem holds for the finite block length regime.

2.1 Background and Related Work

There are indeed indications from earlier results that suggest the separation theorem no longer holds in the finite block length regime; in other words, it is no longer optimal for source and channel coding to be designed independently of each other when the block length of the channel code cannot be made arbitrarily large. For example, numerous investigations into systems employing joint source-channel coding (JSCC) have been carried out, such as source-optimized channel coding, channel-optimized source coding, or a combination thereof (see [1], [6], and references therein), all of which exhibit potentially large advantages over their separate design counterparts in terms of end-to-end distortion (EED). However, much of these prior works consider system settings either without channel coding, or with a particular channel code that may be close to or far from optimal. Without considering the optimal channel code in their system settings, gains yielded from designs based on joint versus separate source-channel coding cannot imply the breakdown of Shannon's separation theorem in the finite block length regime, even though the fact of nonzero channel error probabilities certainly suggests so.

There has been some recent efforts to analytically establish the performance advantage of JSCC designs over separate ones in the finite block length regime. In [36], the problem of lossy compression is considered, where JSCC principles are applied at the decoder side by decoding the source with available channel information. Their analysis is conducted from the perspective of excess-distortion probability (EDP), defined as the probability that the distortion incurred by the source reconstruction exceeds some level d. However, because their code construction varies as a function of d, their results cannot imply an achievability from the perspective of EED, which becomes difficult to evaluate for a fixed coding scheme.

This chapter revisits the validity of source and channel coding separation in the finite block length regime by investigating source quantization when paired with optimal channel coding. Our treatment of this problem is enabled by recent developments in finite block length analysis (see [37], [38], and [39]), which accurately characterizes the tradeoff between coding rate and error probability under optimal channel coding. In contrast to [36], we investigate the problem from the classical perspective of end-to-end distortion, which

can be derived in closed-form when source and channel coding are linked via random index assignment (RIA). Although treatment of the problem under the assumption of RIA may initially seem counterintuitive or impractical, RIA has obvious equivalence to scramblers, which are already widely employed in practical communications systems such as LTE systems [27]. Further, it was shown in [6] that designs of channel-optimized source quantizers (COSQ) based on RIA are more robust against fluctuating channel conditions, which is one of the critical reasons for practical systems to operate under finite block lengths.

Given an arbitrary discrete-input memoryless channel (DIMC) and optimal channel code with a finite block length n to represent k source samples, we seek to disprove the separation theorem by benchmarking a JSCC system employing COSQs, also known as *noisy channel* quantizers, versus one with quantizers following separation principles. Under RIA, both systems employ the optimal tradeoff between the coding rate $\frac{k}{n}$ and channel block error probability ϵ governed by finite block length analysis to minimize EED, while the joint case allows for further channel-optimized source quantizer design based on ϵ for each $\left(\frac{k}{n}, \epsilon\right)$ pair. Note that such comparison considers the best possible design based on separation principles, since completely separate quantizers cannot even exploit the tradeoff between coding rate and channel error probability.

To ensure optimality of the quantizer in the separate design scenario, we consider a scalar quantizer that is applied k times to feed channel coding, as seen in Fig. 2.1. A scalar quantizer is assumed since under separate design, the Lloyd-Max algorithm guarantees optimality and convergence [24][25] for sources with log-concave probability distribution for the squared-error distortion; these characteristics are unclear for an arbitrary k-dimensional vector quantizer and hence would not be suitable to serve as an optimal benchmark.

The rest of the chapter is organized as follows. Section 2.2 details the derivation of EED given the tradeoff between coding rate and block error probability based on finite block length analysis. Section 2.3 details the quantizers employed in both joint and separate design scenarios. To investigate whether or not the separation of source and channel coding still holds in the finite block length regime, Section 2.4 presents numerical comparisons between separate and joint designs under a particular DIMC and the binary symmetric channel (BSC). Closing remarks for the chapter are presented in Section 2.5.

2.2 End-to-End Distortion in the Finite Block Length Regime

Let $z \in \Lambda \subset \mathbb{R}$ be an independent and identically distributed source with zero mean, σ^2 variance, and probability density function $f(z)$. With reference to Fig. 2.1, suppose k samples of z are to be individually quantized and transmitted over a DIMC under optimal channel coding with block length n. Let $(\mathfrak{A}, \mathfrak{Z})$ represent a particular scalar quantizer employed in the system, where $\mathfrak{A} = \{\mathcal{A}_i, 1 \leq i \leq N\}$ is the partitioning of Λ into N disjoint regions $\{\mathcal{A}_1, \cdots, \mathcal{A}_N\}$, which are respectively represented by the codewords, $\{z_1, \cdots, z_N\}$, or simply their indices $\{1, \cdots, N\}$. Let $\pi_t(i^k) = r^k$ be one particular index assignment out of $N^k!$ that links every k quantizer outputs to the optimal channel encoder in a one-to-one mapping manner such that $\{1, \cdots, N^k\} \mapsto \{1, \cdots, N^k\}$.

The DIMC concatenated with optimal channel coding takes $r^k \in \{1, \cdots, N^k\}$ as input and outputs $\hat{r}^k \in \{1, \cdots, N^k\}$ to the source decoder with a block error probability ϵ. We observe here that based on the results of finite block length analysis developed in [37], [38], and [40], ϵ not only depends on the block length n, but also depends on $\log_2(N)$, the rate per source symbol of the scalar quantizer. Let $\epsilon_n(R)$ denote the minimum achievable block error probability at the rate R bits per channel use with block length n. With reference to Fig. 2.1, it is easy to see that $k \log_2(N) = nR$.

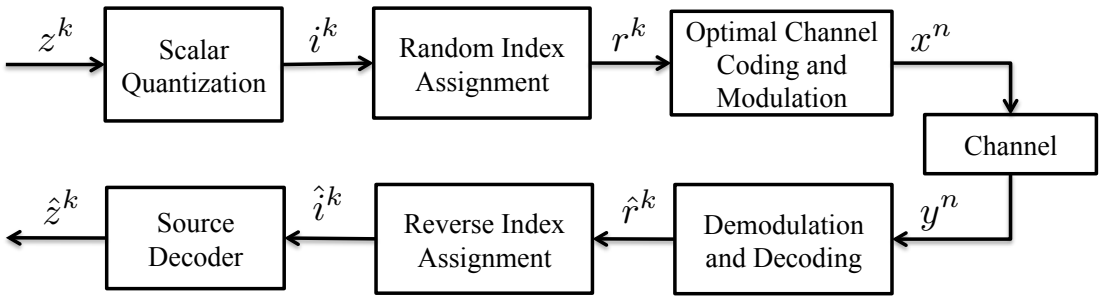

Figure 2.1: A lossy compression joint source-channel coding system with optimal channel coding and random index assignment.

Suppose the DIMC is characterized by the set of transition probability functions $P = \{p(y|x), x \in \mathcal{X}, y \in \mathcal{Y}\}$, where $\mathcal{X}$ and $\mathcal{Y}$ are respectively the channel input and output alphabets. Let $t(x)$ denote the input distribution of P. Given n and R (in nats), the block error probability was shown in [37] and [38] to be well-approximated under optimal channel coding by[1]

$$\epsilon_n(R) \approx \exp\left(\frac{n}{2}\lambda^2\sigma_D^2(\lambda)\right) Q(\sqrt{n}\lambda\sigma_D(\lambda)) \exp\left(-nr_-(\lambda)\right), \tag{2.1}$$

where

$$\begin{aligned}
r_-(\lambda) &= -\lambda R - \sum_{x\in\mathcal{X}} t(x) \ln \int_{\mathcal{Y}} p(y|x) \left[\frac{p(y_x)}{q(y)}\right]^{-\lambda} dy, \\
\sigma_D^2(\lambda) &= \sum_{x\in\mathcal{X}} t(x) \int_{\mathcal{Y}} p(y|x) f_{-\lambda}(y|x) \left[\ln \frac{p(y|x)}{q(y)}\right]^2 dy \\
&\qquad - \sum_{x\in\mathcal{X}} t(x) \left(\int_{\mathcal{Y}} p(y|x) f_{-\lambda}(y|x) \ln \frac{p(y|x)}{q(y)} dy\right)^2, \\
f_{-\lambda}(y|x) &= \frac{\left[\frac{p(y|x)}{q(y)}\right]^{-\lambda}}{\int_{\mathcal{Y}} p(v|x) \left[\frac{p(v|x)}{q(v)}\right]^{-\lambda} dv}, \\
q(y) &= \sum_{x\in\mathcal{X}} t(x) p(y|x), \\
Q(x) &= \int_x^{+\infty} \frac{1}{\sqrt{2\pi}} \exp\left(-\frac{v^2}{2} dv\right),
\end{aligned}$$

such that λ satisfies

$$R = \sum_{x\in\mathcal{X}} \int_{\mathcal{Y}} t(x) p(y|x) f_{-\lambda}(y|x) \ln \frac{p(y|x)}{q(y)} dy.$$

[1]We proceed for a DIMC with continuous output. For discrete output, use summations in place of integrals.

Given any n, k, and any DIMC defined in this section, an N-level scalar quantizer in the system depicted in Fig. 2.1 is associated with a block error probability $\epsilon_n(R)$ expressed by (2.1), where $R = \frac{k}{n}\log_2(N)$.

Suppose the index assignment π_t in Fig. 2.1 is randomly and uniformly selected out of $N^k!$ possible assignments. The EED under RIA for any N-level scalar quantizer associated with a block error probability $\epsilon_n(R)$ is expressed in Theorem 2.1, which is a straightforward extension of the derivations in [6] to the block coding case.

Theorem 2.1. *For any scalar quantizer with N levels paired with optimal channel coding, where the scalar quantizer is applied k times and mapped to a single channel codeword with block length n and block error probability $\epsilon_n(R)$, the end-to-end distortion is expressed as*

$$\bar{D} = \left(1 - \frac{\epsilon_n(R)N^k}{N^k - 1}\right) D_Q + \frac{\epsilon_n(R)N^k}{N^k - 1}(\sigma^2 + S_Q), \tag{2.2}$$

where

$$D_Q = \sum_{i=1}^{N} \int_{z \in \mathcal{A}_i} |z - z_i|^2 f(z) dz, \tag{2.3}$$

$$S_Q = \frac{1}{N} \sum_{i=1}^{N} |z_i|^2. \tag{2.4}$$

Remark 2.1. It was demonstrated in [6] that under the assumption of RIA, an exact closed-form per-symbol EED expression can be derived for a tandem JSCC system. In this paper, Theorem 2.1 is a straightforward extension of the tandem EED expression into the block coding case. As in [6], the EED derived under RIA is dependent on only the average error probability $\Pr\{\hat{r}^k \neq r^k\}$ of the channel, as opposed to the entire set of transitional probability functions $\{p(\hat{r}^k|r^k) : r, \hat{r} \in \{1, \cdots, N^k\}\}$. Observe that due to the employment of RIA, the average error probability defined for the EED formulation in [6] is actually exactly equal to the block error probability governed by finite block length analysis for the optimal channel code with block length n. In other words, we have $\epsilon_n(R) = \Pr\{\hat{r}^k \neq r^k\}$.

Proof of Theorem 2.1. The techniques applied in the proof of Theorem 3.1 for the tandem system with error detection codes can be simplified by removing error detection capability and straightforwardly extended to the block channel case considered here. Hence, the proof is omitted. □

2.3 Quantizers for the Finite Block Lengths Regime

Under the assumption of optimal channel coding, the previous section applied finite block length analysis to approximate an one-to-one association between N and $\epsilon_n(R)$ given block length n. However, the source coding rate becomes discretized due to limitations of the scalar quantizer, and hence, it is more appropriate to minimize the EED over all possible values of N, with corresponding values of $\epsilon_n(R)$, which is approximated by (2.1). We proceed with our analysis by first seeking the optimal tradeoff between N and $\epsilon_n(R)$ for the system employing a separate quantizer.

Let $Q_s^*(N)$ denote the class of optimal separate scalar quantizers designed using the Lloyd-Max algorithm for a source with a log-concave distribution. Formally, given any block length n, number of source symbols k, DIMC with the set of transition probability functions P, and $Q_s^*(N)$, we wish to solve the following optimization problem:

$$\bar{D}_s \triangleq \min_N \left[\left(1 - \frac{\epsilon_n(R) N^k}{N^k - 1} \right) D_Q(Q_s^*(N)) + \frac{\epsilon_n(R) N^k}{N^k - 1} (\sigma^2 + S_Q(Q_s^*(N))) \right], \tag{2.5}$$

where $N \in \{1, 2, \ldots, \lfloor \alpha^{n/k} \rfloor\}$, α denotes the cardinality of the channel input alphabet, and $R = \frac{k}{n} \log_2(N)$. Since $\epsilon_n(R)$ cannot be exactly computed, its approximation as expressed by (2.1) is employed in (2.5). Let N_s^* (or $R_s^* = \frac{k}{n} \log_2(N_s^*)$) denote the solution to (2.5) that achieves the minimum EED, $\bar{D}_s^*(n, k, P)$, which is the optimal performance for the system that pairs the optimal separate quantizer with an optimal channel code through random index assignments.

For the JSCC case, we seek an N-level channel-optimized scalar quantizer that replaces the separate quantizer designed independent of $\epsilon_n(R)$ with one that considers $\epsilon_n(R)$ in

minimizing (2.2). From Theorem 2.1, for any N and its corresponding $\epsilon_n(R)$ governed by finite block length analysis, (2.2) can be further minimized with respect to $(\mathfrak{A}, \mathfrak{Z})$. Hence, given $\epsilon_n(R)$ and N, the joint quantizer should solve

$$\min_{\mathfrak{A},\mathfrak{Z}} \left[\left(1 - \frac{\epsilon_n(R) N^k}{N^k - 1} \right) D_Q \left(\mathfrak{A}, \mathfrak{Z} \right) + \frac{\epsilon_n(R) N^k}{N^k - 1} (\sigma^2 + S_Q \left(\mathfrak{A}, \mathfrak{Z} \right)) \right], \tag{2.6}$$

where the minimization is over all possible pairs of $(\mathfrak{A}, \mathfrak{Z})$.

Given any channel with an optimal channel code with a block error probability $\epsilon_n(R)$, and a desired N-level scalar quantizer, the solution to (2.6) is characterized by two necessary optimality conditions that can be derived from (2.2):

1) Given $\mathfrak{A}$, the optimal code vectors to minimize $\bar{D}$ is computed by[2]

$$z_i = \frac{\int_{z \in \mathcal{A}_i} z f(z) dz}{\frac{\epsilon_n(R)}{(1-\epsilon_n(R))N^k} + \Pr\{z \in \mathcal{A}_i\}}, i = 1, \cdots, N. \tag{2.7}$$

2) Given $\mathfrak{Z}$, the optimal partitioning of Λ follows the nearest neighbour rule. In other words, it satisfies

$$\mathcal{A}_i = \{z : |z - z_i|^2 \leq |z - z_j|^2, j \neq i\}, i = 1, \cdots, N. \tag{2.8}$$

To solve (2.6), the iterative descent algorithm proposed in [6] can be slightly modified with (2.7)-(2.8) to design our noisy joint quantizer without loss of guaranteed convergence. Begin with the initial optimal separate quantizer $Q^0 = Q_s^*(N) = (\mathfrak{A}^0, \mathfrak{Z}^0)$. For each iteration $l > 0$, alternate between computing $\mathfrak{Z}^{l+1}$ according (2.7) given $\mathfrak{A}^l$, followed by $\mathfrak{A}^{l+1}$ according to (2.8) given $\mathfrak{Z}^{l+1}$. Continue for $l = 1, 2, \ldots$ until the decrease in EED between iterations falls below a threshold. Then, output $(\mathfrak{A}^{l+1}, \mathfrak{Z}^{l+1})$ as the desired joint quantizer based on JSCC principles. Note that such quantizer based on (2.7)-(2.8) targets to solve (2.6) for a given N and its corresponding $\epsilon_n(R)$. To further improve the performance of the

[2]Since N^k is large in general, we have assumed $\frac{N^k}{N^k-1} \approx 1$ for clarity.

joint quantizer, the objective should be further optimized over N itself. This is considered in the next section.

2.4 Numerical Analysis

In this section, we investigate the separation of source and optimal channel coding in the finite block length regime by quantifying the achievable gains of employing the joint noisy quantizer versus the separate quantizer based on the Lloyd-Max algorithm. The threshold below which the decrease in EED between iterations is considered small enough to output the final quantizer is set at 10^{-7}. Numerical analyses are conducted for the transmission of a one-dimensional Gaussian source with zero mean and unit variance over both the DIMC and BSC. The separate design case is considered under optimal tradeoffs between N and $\epsilon_n(R)$ as the solution to (2.5). The joint quantizer is designed by solving:

$$\bar{D}_j \triangleq \min_{N,\mathfrak{A},\mathfrak{Z}} \left[\left(1 - \frac{\epsilon_n(R) N^k}{N^k - 1} \right) D_Q\left(\mathfrak{A}, \mathfrak{Z}\right) + \frac{\epsilon_n(R) N^k}{N^k - 1} (\sigma^2 + S_Q\left(\mathfrak{A}, \mathfrak{Z}\right)) \right], \tag{2.9}$$

where the EED is jointly minimized over all possible triples of $(N, \mathfrak{A}, \mathfrak{Z})$. Given a channel with channel input cardinality α, (2.9) can be solved by individually solving (2.6) for every $N \in \{1, 2, \cdots, \lfloor \alpha^{n/k} \rfloor\}$, and then selecting the N and corresponding $(\mathfrak{A}, \mathfrak{Z})$ that minimizes the EED. Denote the final quantizer by $(N_j^*, \mathfrak{A}_j^*, \mathfrak{Z}_j^*)$, and note that N_j^* is unique under our numerical setting such that any $N > N_j^*$ cannot be optimal; this fact allows us to largely reduce the set of possible N when solving (2.9) by enumeration.

2.4.1 Discrete Input Memoryless Channel

We first consider the DIMC depicted in Fig. 2.2 by transmitting using QPSK over an AWGN channel with noise power $\frac{N_0}{2}$. The output of the QPSK modulator serves as input into a DIMC, where the input alphabet $\mathcal{X}$ of the channel is exactly the coordinates of the QPSK signal constellation determined by the channel SNR $\gamma \triangleq \frac{h^2 E}{N_0}$. The output alphabet

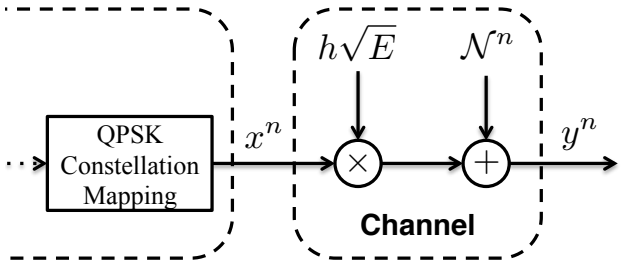

Figure 2.2: The considered DIMC: QPSK modulation over an AWGN channel.

is the complex plane, i.e. $\mathcal{Y} = \mathbb{C}$. Block lengths of $n = 360$ and $n = 720$ are considered, which are on the same order of those in state-of-the-art wireless systems such as LTE [27]. Further note that the achievability and converse bounds from finite block length analysis are rather tight for the considered block lengths to reasonably apply (2.1) in approximating $\epsilon_n(R)$ [37][38].

Table 2.1-2.2 present the respective results for channel SNR $\gamma = -10$ dB and $\gamma = -7$ dB under various bandwidth expansion ratios $\frac{n}{k}$ in terms of PSNR $\triangleq 10\log_{10}(\sigma^2/\bar{D})$. Observe that PSNR gains may be large, but could also be rather small in magnitude, which is due to our consideration of a theoretical setup with optimal channel coding; for practical systems employing actual channel codes that are not optimal, actual block error probabilities would likely be larger and yield larger PSNR gains as well.

The most interesting phenomenon seen from Table 2.1-2.2 is the potential increase in source coding rate when the joint noisy quantizer is employed. As an example, for $n = 360$, $n/k = 72$, and $\gamma = -10$ dB, replacing the separate quantizer with the joint quantizer allows the source rate to be increased from $\log_2 12 = 3.585$ to $\log_2 16 = 4$ bits per symbol while yielding a PSNR gain of 0.247 dB, indicating the potential for improved system end-to-end performance with increased source coding rates and block error probabilities, which the joint quantizer is designed according to. The scenarios exhibiting such behaviour are indicated with bold text. Also, note that the results in Table 2.1-2.2 do not contradict the separation of source and channel coding for asymptotically large block lengths; as suggested by the general decrease in PSNR gains with increasing n and observed in other experiments, further increases to n would eventually reduce both the block error probability and the

Table 2.1: PSNR gains for AWGN with QPSK, $n = 360$, and various n/k.

	$\gamma = -10$ dB			$\gamma = -7$ dB		
n/k	Gains [dB]	N_j^*	N_s^*	Gains [dB]	N_j^*	N_s^*
45	0.177	8	8	0.088	38	38
60	0.092	10	10	0.173	**80**	**71**
72	0.247	**16**	**12**	0.200	**128**	**111**
90	0.187	19	19	0.223	215	215
120	0.331	32	32	0.284	512	406
180	0.544	64	64	0.181	1024‡	1024‡

Table 2.2: PSNR gains for AWGN with QPSK, $n = 720$, and various n/k.

	$\gamma = -10$ dB			$\gamma = -7$ dB		
n/k	Gains [dB]	N_j^*	N_s^*	Gains [dB]	N_j^*	N_s^*
36	0.083	**8**	**7**	0.038	45	45
45	0.058	**11**	**10**	0.059	**90**	**86**
60	0.106	19	19	0.052	228	228
72	0.047	24	24	0.077	**477**	**445**
90	0.124	**45**	**41**	0.032	1024‡	1024‡
120	0.145	**90**	**80**	$\mathcal{O}(10^{-6})$	1024‡	1024‡
180	0.231	**256**	**215**	$\mathcal{O}(10^{-5})$	1024‡	1024‡

gains of using the joint quantizer to zero, hence supporting the optimality of separate source and channel coding design in the asymptotic $n \to \infty$ case.

The observed PSNR gains in this subsection only suggest that the separation of source and channel coding no longer holds in the finite block length regime. This is due to two reasons. First, only an approximation of the block error probability is used to evaluate the EED and hence, we cannot establish that the PSNR gains will *always* be larger than the observed ones. Second, the Lloyd-Max algorithm is only optimal for infinite iterations; as a result, separate quantizers designed in practice are never strictly optimal for the Gaussian source. In the next subsection, we overcome these shortcomings and strengthen our claims to establish the breakdown of Shannon's separation result in the finite block length regime.

‡Our results are restricted to scalar quantizers with rates of no more than 10 bits per source symbol.

2.4.2 Lower Bound of Gains – Binary Symmetric Channel

In this subsection, we quantify the lower bound of the gains achievable from using the joint versus separate quantizer for finite uses of the binary symmetric channel (BSC) with an optimal channel code. This is accomplished by relying on the largest computable lower bound and smallest computable upper bound of the block error probability $\epsilon_n(R)$ for the BSC, as opposed to an approximation of the actual $\epsilon_n(R)$, such as that expressed in (2.1) for the DIMC. We consider the separate quantizer using the lower bound of $\epsilon_n(R)$ and the joint quantizer using the upper bound of $\epsilon_n(R)$, and quantify the performance gap between them. While computation of the performance gap in this manner sharply underestimates it, such analysis allows us to draw a stronger conclusion regarding the separation of source and channel coding in the finite block length regime.

The separate quantizer considered in this subsection solves the following minimization problem:

$$\bar{D}_s^l \triangleq \min_N \left[\left(1 - \frac{\epsilon_n^l(R) N^k}{N^k - 1} \right) D_Q(Q_s^*(N)) + \frac{\epsilon_n^l(R) N^k}{N^k - 1} (\sigma^2 + S_Q(Q_s^*(N))) \right], \tag{2.10}$$

where $N \in \{1, 2, \ldots, \lfloor 2^{n/k} \rfloor\}$ and $\epsilon_n^l(R)$ is the lower bound of $\epsilon_n(R)$. The joint noisy quantizer considered in this subsection solves the following minimization problem:

$$\bar{D}_j^u \triangleq \min_{N, \mathfrak{A}, \mathfrak{Z}} \left[\left(1 - \frac{\epsilon_n^u(R) N^k}{N^k - 1} \right) D_Q(\mathfrak{A}, \mathfrak{Z}) + \frac{\epsilon_n^u(R) N^k}{N^k - 1} (\sigma^2 + S_Q(\mathfrak{A}, \mathfrak{Z})) \right], \tag{2.11}$$

where $N \in \{1, 2, \ldots, \lfloor 2^{n/k} \rfloor\}$ and $\epsilon_n^u(R)$ is the upper bound of $\epsilon_n(R)$.

As of this writing, the tightest known and computable lower and upper bounds that capture the tradeoff between R and $\epsilon_n(R)$ for the BSC are the converse and achievability results derived in [39]. We employ such bounds on the block error probability given n, k, and p and present the gap between $\bar{D}_s^l$ and $\bar{D}_j^u$ in Table 2.3-2.4 for a zero mean unity variance Gaussian source and Table 2.5-2.6 for a zero mean unit variance uniform source distributed over $[-\sqrt{3}, \sqrt{3}]$. For the uniform source, applying the lower and upper bounds in the separate and joint quantizers, respectively, allows us to quantify the *minimum* PSNR

Table 2.3: PSNR gains for Gaussian source over BSC with $n = 200$ and various n/k.

$p = 0.17$				$p = 0.11$			
n/k	Gains [dB]	N_j^u	N_s^l	n/k	Gains [dB]	N_j^u	N_s^l
28.6	0.037	35	35	18.2	0.039	46	46
33.3	0.076	57	57	22.2	0.019	80	80
40.0	0.057	97	84	25.0	0.017	117	117
50.0	0.069	181	181	28.6	0.020	190	190

Table 2.4: PSNR gains for Gaussian source over BSC with $n = 800$ and various n/k.

$p = 0.25$				$p = 0.20$			
n/k	Gains [dB]	N_j^u	N_s^l	n/k	Gains [dB]	N_j^u	N_s^l
40.0	0.022	27	27	26.7	0.027	35	35
50.0	0.022	51	51	33.3	0.013	67	67
57.1	0.024	78	78	36.4	0.019	93	93
66.7	0.032	135	135	40.0	0.011	132	128
72.7	0.033	186	186	44.4	0.021	203	203

gains achievable from using the joint noisy quantizer that solves (2.9) in place of the optimal separate quantizer that solves (2.5) without needing to evaluate the actual $\epsilon_n(R)$.

The results for the uniform source in Table 2.5-2.6 reveal that there are indeed scenarios where $\bar{D}_s^l > \bar{D}_j^u$, as the lower bound of the performance gap can now be quantified by using the uniform quantizer that exactly satisfies the centroid conditions for optimality when designing a quantizer for a uniform source. Whenever $\bar{D}_s^l - \bar{D}_j^u > 0$, we also have $\bar{D}_s - \bar{D}_j \geq \bar{D}_s^l - \bar{D}_j^u > 0$ since $\bar{D}_s \geq \bar{D}_s^l$ and $\bar{D}_j \leq \bar{D}_j^u$. With this, we have argued the strict performance gap between the separate and joint quantizers in terms of EED under certain scenarios in the finite block length regime, hence validating the breakdown of source and channel coding separation for finite usages of the BSC. Note that it is necessary to to establish $\bar{D}_s - \bar{D}_j > 0$ in this manner as there is currently no exact evaluation of the actual block error probability $\epsilon_n(R)$ in the finite block length regime for the BSC.

Table 2.5: PSNR gains for uniform source over BSC with $n = 200$ and various n/k.

$p = 0.17$				$p = 0.11$			
n/k	Gains [dB]	N_j^u	N_s^l	n/k	Gains [dB]	N_j^u	N_s^l
28.6	>0.030	23	23	18.2	>0.003	32	32
33.3	>0.036	32	32	22.2	>0.007	50	50
40.0	>0.028	48	48	25.0	>0.013	69	69
50.0	>0.041	90	90	28.6	>0.022	105	95

Table 2.6: PSNR gains for uniform source over BSC with $n = 800$ and various n/k.

$p = 0.25$				$p = 0.20$			
n/k	Gains [dB]	N_j^u	N_s^l	n/k	Gains [dB]	N_j^u	N_s^l
40.0	>0.018	21	21	26.7	>0.006	27	27
50.0	>0.013	36	36	33.3	>0.008	49	49
57.1	>0.020	52	52	36.4	>0.014	62	62
66.7	>0.027	80	80	40.0	>0.011	84	84

2.5 Summary

This chapter investigates the validity of Shannon's classical result of separate source and channel coding in the finite block length regime. A joint source-channel coding system is considered, where the channel-optimized source quantizer is paired with optimal channel coding to demonstrate achievable reductions to the end-to-end distortion in comparison to separate design. Under the optimal tradeoff between coding rate and block error probability, the joint quantizer is shown to outperform the optimal separate quantizer designed via Lloyd-Max for many scenarios. Although the magnitude of the gains can vary, we are still able to argue that from the perspective of end-to-end distortion, the separation of source and channel coding fails to hold in the finite block length regime. The lower bound of the possible reductions to the end-to-end distortion is also evaluated, and indicates the potential for performance advantages favouring joint source-channel coding for practical applications that must always operate in the finite block length regime.

Chapter 3

Noisy Quantization with Error Detection for Broadcast Channels

With the potential advantages of joint source-channel coding established in the previous chapter, this chapter considers the inclusion of error detection codes at the application layer in the transmission of real-valued sources over the wireless point-to-point or broadcast channel. Employment of error detection serves to further improve system performance for applications that must tolerate potentially large channel error probabilities caused by operation in the finite block length regime. As before, we proceed with a non-asymptotic end-to-end distortion approach to characterize the JSCC system, followed by further design and analysis in the joint design of noisy quantization with error detection codes for both point-to-point and broadcast channels.

3.1 Background and Related Work

Consider applying JSCC principles in the design of quantizers that sample a real-valued source for transmission over a discrete memoryless channel (DMC). In the literature, this problem has been well-formulated as a concatenation of quantization with block channel coding, with such quantizers referred to as channel-optimized source quantizers (COSQ),

or noisy channel quantizers. In general, the COSQ is composed of two parts, specifically, a scalar or vector quantizer, and an index assignment mapping, both of which can impact the average end-to-end distortion (EED) of the JSCC system.

It is no easy task to accomplish both the design *and* analysis of the optimal quantizer and index assignment to minimize EED. Hence, the majority of the literature have mainly studied their joint design from the index assignment point of view, i.e., COSQ design to minimize EED given a fixed index assignment. For example, early works such as [2] and [3] proposed algorithms to design optimal noisy channel scalar quantizers for a fixed index assignment. Subsequent work included extension to the vector case by Farvardin and Vaishampayan [4] and Kumazawa *et al.* [5], where optimality conditions under noisy channels were identified and experimentally demonstrated to outperform their counterparts designed via the Lloyd-Max algorithm [24][25]. Relatively more recent work by Goldsmith and Effros [1] considered the joint design of channel-optimized vector quantizers with source-optimized rate-compatible punctured convolutional channel codes. For the broadcast channel, [23] paired multiresolution source quantization with hierarchical channel coding [41] to investigate the joint design of both to minimize EED under a fixed transmitter energy constraint. Other more recent advancements on multiresolution quantizer design for the scalar ([42], [43]) or vector [44] case target minimizing the quantization distortion weighted by the probability of operation at each refinement resolution.

While all of the aforementioned work present effective algorithms for the design of optimal noisy or noiseless channel quantizers, they are unable to provide strong analytical results because of using a fixed index assignment in their system setting. For example, vector quantizers designed in [1] and [5] are based on necessary conditions that depend on all transitional probabilities from channel input symbols to channel output symbols, hence making it difficult to analyze not only the optimal quantizer itself, but also the system performance. Furthermore, an observation was made in [1] that quantizers designed in this manner may often perform poorly under channel mismatch or variations.

In pursuit of analytical results, earlier work by Zeger and Manzella [26] investigated the source quantization problem under random index assignment (RIA). However, their analytical results are for vector quantizers that are designed independent of channel statis-

tics in the high-rate asymptotic case. On the other hand, efforts by Yu *et al.* and Teng *et al.* in applying RIA led to the derivation of closed-form non-asymptotic EED formulae for both the point-to-point [6] and broadcast [7] channels. With the closed-form EED formula, theoretical analysis of optimal noisy channel quantizers became tractable, and algorithm design required only the average channel error probability, as opposed to the entire matrix of transitional probabilities necessary for the fixed case. As mentioned before, although use of RIA may seem counterintuitive or impractical, it has obvious equivalence to scramblers that are already widely used in practical communications systems such as LTE systems [27]. Furthermore, it was shown in [6] that quantizers designed based on RIA can partially alleviate the poor performance observed in [1] under channel mismatch.

From the literature, it is well-known that both quantization distortion and channel errors contribute to the EED. Under RIA, formulations in [6] and [7] further attributed a large portion of the distortion contribution from channel errors to a structural parameter named the *scatter factor* of the noisy channel quantizer. It was demonstrated in [6] and [7] that given average channel statistics, this scatter factor is different from and additional to quantization distortion, and hence it is suboptimal to minimize only the quantization distortion when designing the quantizer in a source-channel coding system. They also demonstrated that under RIA, the design of the optimal noisy channel quantizer became a tradeoff between balancing distortion contributions from the scatter factor and the quantization itself. The result of considering such a tradeoff led to significantly reduced EED in comparison to a system employing quantizers designed via Lloyd-Max. Although an optimal noisy channel quantizer partially mitigates distortion contribution from the scatter factor at the expense of larger quantization distortion, it cannot entirely eliminate the effect of the scatter factor on the EED. An interesting question then naturally arises: when the error statistics of the channel are fixed, is there any other way to largely reduce or even eliminate the effect of the scatter factor to further reduce EED?

With this motivation, we observe that in the closed-form EED expression derived in [6], the scatter factor's contribution to EED appears in addition to source variance whenever a source symbol is mapped to some other incorrect symbol during decoder reconstruction. Meanwhile, the scatter factor is exactly equal to the average distance between each

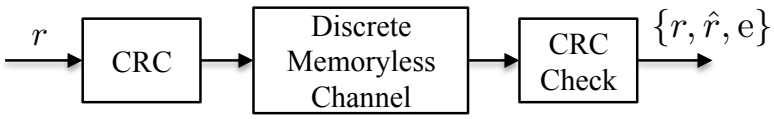

Figure 3.1: Partial erasure channel composed of general DMC augmented with CRC.

codeword vector and the source mean vector. Hence, if the decoder had available side information on the correctness state of a particular symbol, EED performance can be improved by using the source mean vector for the reconstruction of incorrect symbols. Decoding in this manner limits distortion contribution from incorrect symbols to a maximum valued at the source variance and entirely eliminates the scatter factor's contribution to EED.

One particular channel that exposes symbol correctness information to the decoder is the erasure channel. Derivations in [6] can be simplified for this channel and it is indeed the case that the scatter factor drops from the EED expression since the decoder never maps to the wrong codeword; it either outputs the correct codeword or declares an erasure state for each symbol. However, for any general DMC, the erasure state of each symbol is not readily available at the decoder and must be obtained from other means. Such an observation leads us to consider augmenting the DMC with cyclic redundancy checks (CRC) as in Fig. 3.1 to transform the channel into a partial erasure channel.

Inclusion of CRC for error detection impacts the system in two ways. First, we must reallocate certain bits originally used for source quantization for CRC check bits, resulting in increased quantization distortion. Second, inclusion of CRC only partially transforms the DMC channel into an erasure channel; even with the reduction of undetected symbol errors by proportions dependent on the selected CRC, false negative incorrect symbols still occur and contribute to the EED. Hence, we observe yet another interesting tradeoff between quantization design and CRC polynomial selection to further reduce the EED of the JSCC system. From a high level, such tradeoff can be interpreted as a tradeoff between source coding (quantization) and channel coding (CRC), which is a problem well-studied in works such as [1] and [45]. However, it is important to note that the tradeoff considered by these works varies the channel coding rate to adjust the channel error probability, while the above motivation of introducing CRC to eliminate scatter factor effects applies for *any*

fixed channel error probability given by any channel code.

In this chapter, we focus on the design and analysis of optimal multiresolution vector quantizers (MRVQ) in tandem with broadcast channels augmented with CRC similar to that in Fig. 3.1. Like [6] and [7], RIA is adopted to link MRVQ at the source with superposition coding (SPC) at the CRC-coded broadcast channel. The contributions in this chapter are summarized as follows. First, a closed-form expression is derived for the weighted end-to-end distortion of a tandem system of MRVQ, RIA, CRC, and SPC. Second, two necessary conditions to minimize the weighted EED are presented and used to design a controlled iterative algorithm for the scalar case. The proposed algorithm is used for quantization design in both point-to-point and broadcast channels. Numerical results demonstrate that dramatic reductions to EED are possible, even though a portion of the bits available for source quantization is replaced with redundancy bits to enable CRC.

The remainder of this chapter is organized as follows. Section 3.2 provides a comprehensive derivation of the weighted EED. Given channel and error detection statistics, Section 3.3 derives two necessary conditions for minimizing the weighted EED and proposes a controlled iterative algorithm for multiresolution quantization design. Section 3.4 is an analysis of optimal quantization design with error detection codes through experiments based on the point-to-point additive white Gaussian noise (AWGN) channel and the Gaussian broadcast channel. Closing remarks for the chapter are presented in Section 3.5.

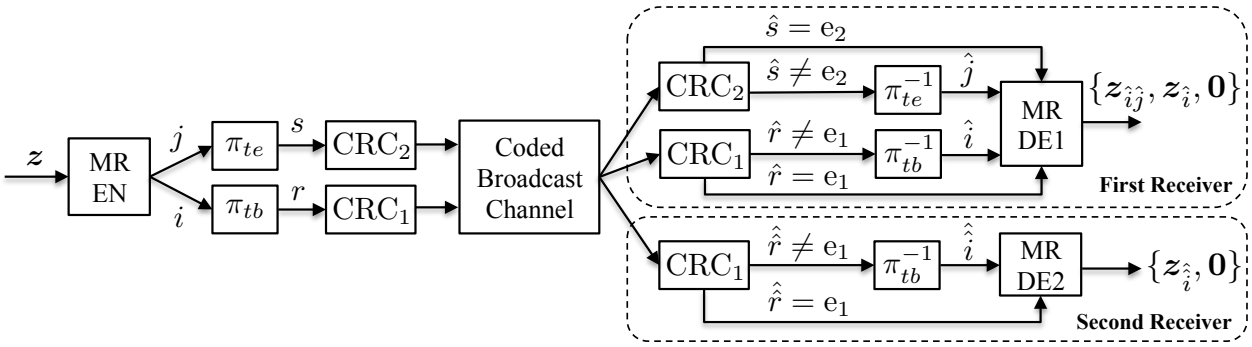

Figure 3.2: The considered source-channel CRC-coded broadcast system.

3.2 End-To-End Distortion

3.2.1 System and Notation

Let $\boldsymbol{z}$ be a k-dimensional real-valued vector source over the Euclidean space Λ with a probability density function $f(\boldsymbol{z})$, $\mathbf{0}$ mean, and variance per dimension $\sigma^2 = \frac{1}{k}\int_\Lambda \|\boldsymbol{z}\|^2 f(\boldsymbol{z})d\boldsymbol{z}$. Suppose $\boldsymbol{z}$ is to be transmitted as a scalably encoded two-resolution source over the tandem source-channel coding broadcast system depicted in Fig. 3.2. For the lower resolution, the quantizer partitions Λ into N_1 disjoint regions denoted by $\{\mathcal{A}_1, \cdots, \mathcal{A}_{N_1}\}$, and represents them with respective codeword vectors $\{\boldsymbol{z}_1, \cdots, \boldsymbol{z}_{N_1}\}$. For the higher resolution, the quantizer further partitions each of the N_1 regions into N_2 subregions denoted by $\{\mathcal{A}_{i1}, \cdots, \mathcal{A}_{iN_2}\}$, and represents them with respective codeword vectors $\{\boldsymbol{z}_{i1}, \cdots, \boldsymbol{z}_{iN_2}\}$. Let $i = 1, \cdots, N_1$ and $j = 1, \cdots, N_2$ index the lower and higher resolution codeword vectors, respectively. The transmitted scalably coded source $\boldsymbol{z}$ is then represented by the index pair (i, j), where the first receiver attempts to reconstruct $\boldsymbol{z}$ at a higher resolution using both i and j while the second receiver only desires a lower resolution reconstruction using i.

Let $\pi_t(i, j) = (\pi_{tb}(i), \pi_{te}(j|i)) = (r, s)$ be a particular index assignment linking the multiresolution source encoder output (i, j) with the CRC-coded broadcast channel[1] input (r, s) in a one-to-one mapping manner such that $i \in \{1, \cdots, N_1\} = m_{\mathrm{b}}$ and $j \in \{1, \cdots, N_2\} = m_2$ are mapped to $r \in m_{\mathrm{b}}$ and $s \in m_2$, respectively. Further let $\hat{m}_{\mathrm{b}} = m_{\mathrm{b}} \cup \mathrm{e}_1$, and $\hat{m}_2 = m_2 \cup \mathrm{e}_2$, where e_1 and e_2 denote the erasure states for r and s.

The CRC-coded broadcast channel takes $(r, s) \in m_{\mathrm{b}} \times m_2 = m_{\mathrm{e}}$ as input and outputs $\hat{m}_e = (\hat{r}, \hat{s}) \in \hat{m}_{\mathrm{b}} \times \hat{m}_2$ to the first receiver and $\hat{m}_b = \hat{\hat{r}} \in \hat{m}_{\mathrm{b}}$ to the second receiver. The entire CRC-coded broadcast channel is hence fully characterized by a matrix of transition probabilities

$$\{p(\hat{m}_e,\hat{m}_b|(r, s)) : (r, s) \in m_{\mathrm{e}}, \hat{m}_b \in \hat{m}_{\mathrm{b}}, \hat{m}_e \in \hat{m}_{\mathrm{b}} \times \hat{m}_2\},$$

[1]Note that since the coded broadcast channel is fixed, CRC is considered here to be at the application layer.

where $p(\hat{m}_e, \hat{m}_b|(r,s))$ is the conditional probability that the CRC-coded broadcast channel outputs $\hat{m}_e$ and $\hat{m}_b$ given the input (r,s). From this matrix, the following transition probability matrices can be further derived to describe the channel for each of the two receivers:

$$\{p_e(\hat{m}_e|(r,s)) : (r,s) \in m_{\rm e}, \hat{m}_e \in \hat{m}_{\rm b} \times \hat{m}_2\}; \tag{3.1}$$

$$\{p_b(\hat{m}_b|(r,s)) : (r,s) \in m_{\rm e}, \hat{m}_b \in \hat{m}_{\rm b}\}. \tag{3.2}$$

In presence of CRC, with reference to Fig. 3.2, let $p_{bd} = \Pr\{\hat{\hat{r}} = {\rm e}_1\}$ and $p_{bu} = \Pr\{\hat{\hat{r}} \neq r, \hat{\hat{r}} \neq {\rm e}_1\}$ be the respective detected and undetected error probabilities of the second receiver. The first receiver is associated with five error probabilities based on the error detection states of r and s: (i) $p_{d_1} = \Pr\{\hat{r} = {\rm e}_1\}$; (ii) $p_{d_2} = \Pr\{\hat{r} = r, \hat{s} = {\rm e}_2\}$; (iii) $p_{ud} = \Pr\{\hat{r} \neq r, \hat{r} \neq {\rm e}_1, \hat{s} = {\rm e}_2\}$; (iv) $p_{u_1} = \Pr\{\hat{r} \neq r, \hat{r} \neq {\rm e}_1, \hat{s} \neq {\rm e}_2\}$; and (v) $p_{u_2} = \Pr\{\hat{r} = r, \hat{s} \neq s, \hat{s} \neq {\rm e}_2\}$. All seven error probabilities are computable from (3.1)-(3.2) under the assumption that (r,s) is uniformly distributed over $m_{\rm e}$, where $|m_{\rm e}| = N_1 N_2$. For the first receiver, we have

$$p_{d1} = \frac{1}{N_1 N_2} \sum_{r=1}^{N_1} \sum_{s=1}^{N_2} p_e \left\{\hat{r} = {\rm e}_1 | r, s\right\},$$

$$p_{d_2} = \frac{1}{N_1 N_2} \sum_{r=1}^{N_1} \sum_{s=1}^{N_2} p_e \left\{r, \hat{s} = e_2 | r, s\right\},$$

$$p_{ud} = \frac{1}{N_1 N_2} \sum_{r=1}^{N_1} \sum_{\substack{\hat{r}=1, \\ \hat{r} \neq r, {\rm e}_1}}^{N_1} \sum_{s=1}^{N_2} p_e \left\{\hat{r}, \hat{s} = e_2 | r, s\right\},$$

$$p_{u_1} = \frac{1}{N_1} \frac{1}{N_2} \sum_{r=1}^{N_1} \sum_{s=1}^{N_2} \sum_{\substack{\hat{r}=1 \\ \hat{r} \neq r, {\rm e}_1}}^{N_1} \sum_{\substack{\hat{s}=1 \\ \hat{s} \neq {\rm e}_2}}^{N_2} p_e \left\{\hat{r}, \hat{s} | r, s\right\},$$

$$p_{u_2} = \frac{1}{N_1 N_2} \sum_{r=1}^{N_1} \sum_{s=1}^{N_2} \sum_{\substack{\hat{s}=1 \\ \hat{s} \neq s, {\rm e}_2}}^{N_2} p_e \left\{r, \hat{s} | r, s\right\}.$$

while for the second receiver,

$$p_{bd} = \frac{1}{N_1}\frac{1}{N_2}\sum_{r=1}^{N_1}\sum_{s=1}^{N_2} p_b\left\{\hat{\hat{r}} = \mathrm{e}_1 | r, s\right\},$$
$$p_{bu} = \frac{1}{N_1}\frac{1}{N_2}\sum_{r=1}^{N_1}\sum_{s=1}^{N_2}\sum_{\hat{r}=1, \hat{\hat{r}}\neq r, \mathrm{e}_1}^{N_1} p_b\left\{\hat{\hat{r}} | r, s\right\}.$$

With reference to Fig. 3.2, CRC introduces per-symbol erasure states for r and s at the decoder input of both receivers. Upon receiving $(\hat{r}, \hat{s})$, the first receiver has three possible outputs: $\boldsymbol{z}_{\hat{i}\hat{j}}$ if $\hat{r} \neq \mathrm{e}_1$, $\hat{s} \neq \mathrm{e}_2$; $\boldsymbol{z}_{\hat{i}}$ if $\hat{r} \neq \mathrm{e}_1$, $\hat{s} = \mathrm{e}_2$; and $\mathbf{0}$ if $\hat{r} = \mathrm{e}_1$. Given π_t, the crossover error probabilities from codeword vector $\boldsymbol{z}_{ij}$ to each of the three outputs are related to the channel transition error probabilities as follows:

$$p_e^{\pi_t}(\boldsymbol{z}_{\hat{i}\hat{j}} | \boldsymbol{z}_{ij}) = p_e\{\hat{r}, \hat{s} | r, s\}, \hat{r} \neq \mathrm{e}_1, \hat{s} \neq \mathrm{e}_2;$$
$$p_e^{\pi_t}(\boldsymbol{z}_{\hat{i}} | \boldsymbol{z}_{ij}) = p_e\{\hat{r}, \hat{s} = \mathrm{e}_2 | r, s\}, \hat{r} \neq \mathrm{e}_1;$$
$$p_e^{\pi_t}(\mathbf{0} | \boldsymbol{z}_{ij}) = p_e\{\hat{r} = \mathrm{e}_1 | r, s\}.$$

The EED is defined as the mean squared error distortion between the quantizer input and the decoder output. Hence, with the codeword crossover probabilities defined above for some given index assignment π_t, the EED for each of the three possible outputs is expressed as follows:

$$D_{e_1}^{\pi_t} \triangleq \frac{1}{k}\sum_{i,j}\int_{z\in\mathcal{A}_{ij}}\sum_{\hat{i},\hat{j}}\|\boldsymbol{z} - \boldsymbol{z}_{\hat{i}\hat{j}}\|^2 p_e^{\pi_t}(\boldsymbol{z}_{\hat{i}\hat{j}} | \boldsymbol{z}_{ij}) f(\boldsymbol{z}) d\boldsymbol{z}; \tag{3.3}$$

$$D_{e_2}^{\pi_t} \triangleq \frac{1}{k}\sum_{i,j}\int_{z\in\mathcal{A}_{ij}}\sum_{\hat{i}}\|\boldsymbol{z} - \boldsymbol{z}_{\hat{i}}\|^2 p_e^{\pi_t}(\boldsymbol{z}_{\hat{i}} | \boldsymbol{z}_{ij}) f(\boldsymbol{z}) d\boldsymbol{z}; \tag{3.4}$$

$$D_{e_3}^{\pi_t} \triangleq \frac{1}{k}\sum_{i,j}\int_{z\in\mathcal{A}_{ij}}\|\boldsymbol{z}\|^2 p_e^{\pi_t}(\mathbf{0} | \boldsymbol{z}_{ij}) f(\boldsymbol{z}) d\boldsymbol{z}. \tag{3.5}$$

The total EED for the first receiver is the sum of (3.3)-(3.5), expressed as

$$D_e^{\pi_t} \triangleq D_{e_1}^{\pi_t} + D_{e_2}^{\pi_t} + D_{e_3}^{\pi_t}. \tag{3.6}$$

Similarly, upon receiving $\hat{\hat{r}}$, the second receiver outputs $\boldsymbol{z}_{\hat{\hat{i}}}$ if $\hat{\hat{r}} \neq \mathrm{e}_1$ and $\mathbf{0}$ if $\hat{\hat{r}} = \mathrm{e}_1$. Given index assignment π_t, the crossover error probabilities from codeword vector $\boldsymbol{z}_{ij}$ to the two possible outputs are related to the channel transition error probabilities as follows:

$$\begin{aligned} p_b^{\pi_t}(\boldsymbol{z}_{\hat{\hat{i}}}|\boldsymbol{z}_{ij}) &= p_b\{\hat{\hat{r}}|r,s\}, \hat{\hat{r}} \neq \mathrm{e}_1; \\ p_b^{\pi_t}(\mathbf{0}|\boldsymbol{z}_{ij}) &= p_b\{\hat{\hat{r}} = \mathrm{e}_1|r,s\}. \end{aligned}$$

Again for the second receiver, the EED for each of the two above decoder outputs given π_t is expressed as

$$D_{b_1}^{\pi_t} \triangleq \frac{1}{k}\sum_{i,j}\int_{z\in\mathcal{A}_{ij}}\sum_{\hat{\hat{i}}}\|\boldsymbol{z}-\boldsymbol{z}_{\hat{\hat{i}}}\|^2 p_b^{\pi_t}(\boldsymbol{z}_{\hat{\hat{i}}}|\boldsymbol{z}_{ij})f(\boldsymbol{z})d\boldsymbol{z}, \tag{3.7}$$

$$D_{b_2}^{\pi_t} \triangleq \frac{1}{k}\sum_{i,j}\int_{z\in\mathcal{A}_{ij}}\|\boldsymbol{z}\|^2 p_b^{\pi_t}(\mathbf{0}|\boldsymbol{z}_{ij})f(\boldsymbol{z})d\boldsymbol{z}, \tag{3.8}$$

such that the total EED for the second receiver is expressed as $D_b^{\pi_t} \triangleq D_{b_1}^{\pi_t} + D_{b_2}^{\pi_t}$.

EED expressions derived in this subsection are visibly dependent on the choice of index assignment mappings. In this paper, we are tasked to study the achievable gains of employing error detecting codes as opposed to optimizing index assignment. Hence, we simply assume a purely random index assignment[2] to obtain the *average* EED. The argument in favor of using random index assignments instead of fixed assignments was made in Section 3.1. By the random coding argument, the EED based on RIA can also serve as an upper bound to the EED performance of an optimal index assignment.

[2]It is worthwhile to point out that scramblers used in practical communication systems such as LTE systems are actually equivalent to RIA.

3.2.2 EED for CRC-Coded Broadcast Channels

Consider a random selection of the index assignment mapping π_t. Let $D_e^{\Pi} = E_{\pi_t} D_e^{\pi_t}$ and $D_b^{\Pi} = E_{\pi_t} D_b^{\pi_t}$ respectively denote the EED for the first and second receiver averaged over all possible $(N_1!)(N_2!)^{N_1}$ assignment mappings.

Theorem 3.1. *For any k-dimensional multiresolution quantizer in tandem with a CRC-coded broadcast channel as in Fig. 3.2,*

$$\begin{aligned} D_b^{\Pi} &= \left(1 - p_{bd} - \frac{N_1 p_{bu}}{N_1 - 1}\right) D_{Q_b} \\ &\quad + \left(\frac{N_1 p_{bu}}{N_1 - 1}\right) \left(\sigma^2 + S_{Q_b}\right) + p_{bd}\sigma^2 \qquad (3.9) \\ D_e^{\Pi} &= \left(1 - p_{d_1} - p_{d_2} - p_{ud} - p_{u_1} - \frac{N_2 p_{u_2}}{N_2 - 1}\right) D_{Q_e} \\ &\quad + \left(p_{d_2} - \frac{p_{ud}}{N_1 - 1}\right) D_{Q_b} + \frac{N_1 p_{u_1}}{N_1 - 1} \left(\sigma^2 + S_{Q_e}\right) \\ &\quad + \left(\frac{N_2 p_{u_2}}{N_2 - 1} - \frac{p_{u_1}}{N_1 - 1}\right) \left(\bar{\sigma}_{Q_e}^2 + \bar{S}_{Q_e}\right) \\ &\quad + \frac{N_1 p_{ud}}{N_1 - 1}(\sigma^2 + S_{Q_b}) + p_{d_1}\sigma^2, \qquad (3.10) \end{aligned}$$

where

$$\begin{aligned} D_{Q_e} &\triangleq \frac{1}{k} \sum_{i=1}^{N_1} \sum_{j=1}^{N_2} \int_{\boldsymbol{z} \in \mathcal{A}_{ij}} \|\boldsymbol{z} - \boldsymbol{z}_{ij}\|^2 f(\boldsymbol{z}) d\boldsymbol{z}, \\ D_{Q_b} &\triangleq \frac{1}{k} \sum_{i=1}^{N_1} \int_{\boldsymbol{z} \in \mathcal{A}_i} \|\boldsymbol{z} - \boldsymbol{z}_i\|^2 f(\boldsymbol{z}) d\boldsymbol{z}, \\ S_{Q_e} &\triangleq \frac{1}{k N_1 N_2} \sum_{i=1}^{N_1} \sum_{j=1}^{N_2} \|\boldsymbol{z}_{ij}\|^2, \\ \bar{S}_{Q_e} &\triangleq \sum_{i=1}^{N_1} \Pr\{\boldsymbol{z} \in \mathcal{A}_i\} \left(\frac{1}{k N_2} \sum_{\hat{j}=1}^{N_2} \|\boldsymbol{z}_{i\hat{j}} - \boldsymbol{y}_i\|^2\right), \end{aligned}$$

$$
\begin{aligned}
S_{Q_b} &\triangleq \frac{1}{kN_1}\sum_{i=1}^{N_1}\|\boldsymbol{z}_i\|^2,\\
\bar{\sigma}^2_{Q_e} &\triangleq \sum_{i=1}^{N_1}\Pr\{\boldsymbol{z}\in\mathcal{A}_i\}\sigma_i^2,\\
\boldsymbol{y}_i &= \frac{1}{\Pr\{\boldsymbol{z}\in\mathcal{A}_i\}}\int_{\boldsymbol{z}\in\mathcal{A}_i}\boldsymbol{z}f(\boldsymbol{z})d\boldsymbol{z},\\
\sigma_i^2 &= \frac{1}{k\Pr\{\boldsymbol{z}\in\mathcal{A}_i\}}\int_{\boldsymbol{z}\in\mathcal{A}_i}\|\boldsymbol{z}-\boldsymbol{y}_i\|^2 f(\boldsymbol{z})d\boldsymbol{z},
\end{aligned}
$$

such that $\boldsymbol{y}_i$ is the conditional mean of $\boldsymbol{z}$ given $\mathcal{A}_i$, and σ_i^2 is the conditional variance per dimension of $\boldsymbol{z}$ given $\mathcal{A}_i$.

Remark 3.1. Observe that D_{Q_b} and D_{Q_e} are the conventional quantization distortions for reconstruction at the lower and higher resolution, respectively. The scatter factors of the lower and higher resolution are respectively denoted by S_{Q_b} and S_{Q_e}, quantifying the average distance of the codeword vectors from the source mean vector $\mathbf{0}$. $\bar{S}_{Q_e}$ denotes the conditional scatter factor of the refinement coding given the set of lower resolution partitions $\{\mathcal{A}_i\}$.

Remark 3.2. (3.9) and (3.10) serve as a generalization of the scenario without error detection considered in [7]. The substitution of $p_{bd} = p_{d_1} = p_{d_2} = p_{ud} = 0$ indeed simplifies (3.9) and (3.10) to the form in [7] without presence of error detection to imply that all errors are undetectable. On its own, (3.9) is the EED for the point-to-point transmission of a single-resolution source with error detection, and is the generalization of [6].

Remark 3.3. It is instructive to compare (3.9) to the scenario without error detection. Suppose high coding rates such that $\frac{N_1}{N_1-1} \approx 1$. (3.9) can then be interpreted on a per-symbol basis where the per-symbol distortion is weighted by the decoded status of each symbol. Under this interpretation, detectable symbol errors contribute only σ^2 to the EED as opposed to $(\sigma^2 + S_{Q_b})$ for undetectable symbol errors, thus eliminating effects of the scatter factor for detectable errors. Naturally, there is a tradeoff between this reduction of the EED with increased D_{Q_b}, since N_1 is halved for each additional bit assigned for error detection redundancy.

Remark 3.4. The comparison of (3.10) with no error detection is even more interesting. Interpreting (3.10) in the same manner as Remark 3.3 indicates that the portion of p_{d_2} symbols with a correct lower resolution index, but an erasure declared for the higher resolution observe a distortion equal to the quantization distortion of the second receiver, D_{Q_b}. Hence, error detection further exploits the advantages of the coded broadcast channel by introducing an incremental lower resolution quality for the first receiver. From an EED perspective, these symbols have their distortion dramatically reduced from $\left(\bar{\sigma}^2_{Q_e} + \bar{S}_{Q_e}\right)$ to D_{Q_b}. For the portion of p_{d_1} symbols with error detected in the lower resolution index, they contribute σ^2 to the distortion instead of $(\sigma^2 + S_{Q_e})$, again partially eliminating scatter factor contribution to EED. Lastly for p_{ud}, these symbols have their contribution reduced from $(\sigma^2 + S_{Q_e})$ to $(\sigma^2 + S_{Q_b})$, since $S_{Q_e} > S_{Q_b}$ in general.

Proof of Theorem 3.1. We first prove the EED for the first receiver given by (3.10). For presentation clarity, the EED for each of the three possible decoder outputs are considered separately. Given a specific index assignment π_t, consider the portions of the EED from (3.3)-(3.5) as follows:

$$\begin{aligned}
D_{e_1}^{\pi_t} &= \frac{1}{k}\sum_{i,j}\int_{z\in\mathcal{A}_{ij}}\sum_{\hat{i},\hat{j}}\|\boldsymbol{z}-\boldsymbol{z}_{\hat{i}\hat{j}}\|^2 p_e^{\pi_t}(\boldsymbol{z}_{\hat{i}\hat{j}}|\boldsymbol{z}_{ij})f(\boldsymbol{z})d\boldsymbol{z} \\
&= \frac{1}{k}\sum_{i,j}\int_{z\in\mathcal{A}_{ij}}\sum_{\hat{i},\hat{j}}\left[\|\boldsymbol{z}-\boldsymbol{z}_{ij}\|^2+2(\boldsymbol{z}-\boldsymbol{z}_{ij})(\boldsymbol{z}_{ij}-\boldsymbol{z}_{\hat{i}\hat{j}})' + \|\boldsymbol{z}_{ij}-\boldsymbol{z}_{\hat{i}\hat{j}}\|^2\right] p_e^{\pi_t}(\boldsymbol{z}_{\hat{i}\hat{j}}|\boldsymbol{z}_{ij})f(\boldsymbol{z})d\boldsymbol{z} \\
&= \frac{1}{k}\sum_{i,j}\int_{z\in\mathcal{A}_{ij}}\|\boldsymbol{z}-\boldsymbol{z}_{ij}\|^2 f(\boldsymbol{z})d\boldsymbol{z}\sum_{\hat{i},\hat{j}}p_e^{\pi_t}(\boldsymbol{z}_{\hat{i}\hat{j}}|\boldsymbol{z}_{ij}) \\
&\quad + \frac{1}{k}\sum_{i,j}\int_{z\in\mathcal{A}_{ij}}\sum_{\hat{j}\neq j}\left[2(\boldsymbol{z}-\boldsymbol{z}_{ij})(\boldsymbol{z}_{ij}-\boldsymbol{z}_{i\hat{j}})' + \|\boldsymbol{z}_{ij}-\boldsymbol{z}_{i\hat{j}}\|^2\right] p_e^{\pi_t}(\boldsymbol{z}_{i\hat{j}}|\boldsymbol{z}_{ij})f(\boldsymbol{z})d\boldsymbol{z} \\
&\quad + \frac{1}{k}\sum_{i,j}\int_{z\in\mathcal{A}_{ij}}\sum_{\hat{i}\neq i,\hat{j}}\left[2(\boldsymbol{z}-\boldsymbol{z}_{ij})(\boldsymbol{z}_{ij}-\boldsymbol{z}_{\hat{i}\hat{j}})' + \|\boldsymbol{z}_{ij}-\boldsymbol{z}_{\hat{i}\hat{j}}\|^2\right] p_e^{\pi_t}(\boldsymbol{z}_{\hat{i}\hat{j}}|\boldsymbol{z}_{ij})f(\boldsymbol{z})d\boldsymbol{z};
\end{aligned} \tag{3.11}$$

$$D_{e_2}^{\pi_t} = \frac{1}{k}\sum_{i,j}\int_{z\in\mathcal{A}_{ij}}\sum_{\hat{i}}\|\boldsymbol{z}-\boldsymbol{z}_{\hat{i}}\|^2 p_e^{\pi_t}(\boldsymbol{z}_{\hat{i}}|\boldsymbol{z}_{ij})f(\boldsymbol{z})d\boldsymbol{z}$$

$$= \frac{1}{k}\sum_{i,j}\int_{z\in\mathcal{A}_{ij}}\sum_{\hat{i}}\left[\|\boldsymbol{z}-\boldsymbol{z}_i\|^2+2(\boldsymbol{z}-\boldsymbol{z}_i)(\boldsymbol{z}_i-\boldsymbol{z}_{\hat{i}})'+\|\boldsymbol{z}_i-\boldsymbol{z}_{\hat{i}}\|^2\right]p_e^{\pi_t}(\boldsymbol{z}_{\hat{i}}|\boldsymbol{z}_{ij})f(\boldsymbol{z})d\boldsymbol{z}$$

$$= \frac{1}{k}\sum_{i,j}\int_{z\in\mathcal{A}_{ij}}\|\boldsymbol{z}-\boldsymbol{z}_i\|^2 f(\boldsymbol{z})d\boldsymbol{z}\sum_{\hat{i}}p_e^{\pi_t}(\boldsymbol{z}_{\hat{i}}|\boldsymbol{z}_{ij})$$

$$+\frac{1}{k}\sum_{i,j}\int_{z\in\mathcal{A}_{ij}}\sum_{\hat{i}\neq i}\left[2(\boldsymbol{z}-\boldsymbol{z}_i)(\boldsymbol{z}_i-\boldsymbol{z}_{\hat{i}})'+\|\boldsymbol{z}_i-\boldsymbol{z}_{\hat{i}}\|^2\right]p_e^{\pi_t}(\boldsymbol{z}_{\hat{i}}|\boldsymbol{z}_{ij})f(\boldsymbol{z})d\boldsymbol{z}; \tag{3.12}$$

$$D_{e_3}^{\pi_t} = \frac{1}{k}\sum_{i,j}\int_{z\in\mathcal{A}_{ij}}\|\boldsymbol{z}\|^2 p_e^{\pi_t}(\mathbf{0}|\boldsymbol{z}_{ij})f(\boldsymbol{z})d\boldsymbol{z}. \tag{3.13}$$

In the above expressions, all vectors are row vectors and the prime symbol indicates matrix transposition. The average EED under random index assignment is thus computed as follows by taking expectation of $D_e^{\pi_t}$ with respect to π_t:

$$D_e^{\Pi} = E_{\pi_t}(D_e^{\pi_t}). \tag{3.14}$$

Expectation taken over π_t for each of the codeword crossover error probabilities are summarized as follows for substitution into (3.14). For a correct low resolution index and undetected high resolution index error such that $\hat{i}=i$ and $(\hat{j}\neq j, \hat{s}\neq \mathrm{e}_2)$, respectively,

$$E_{\pi_t}p_e^{\pi_t}(\boldsymbol{z}_{i\hat{j}}|\boldsymbol{z}_{ij}) = \frac{1}{(N_1!)(N_2!)^{N_1}}\sum_{t=1}^{(N_1!)(N_2!)^{N_1}}p_e^{\pi_t}(\boldsymbol{z}_{i\hat{j}}|\boldsymbol{z}_{ij})$$

$$= \frac{1}{(N_1!)(N_2!)^{N_1}}\sum_{r=1}^{N_1}\sum_{s=1}^{N_2}\sum_{\substack{\hat{s}=1\\ \hat{s}\neq s,\mathrm{e}_2}}^{N_2}\sum_{\substack{t:\pi_{tb}(i)=r\\ \pi_{te}(j|i)=s\\ \pi_{te}(\hat{j}|i)=\hat{s}}}p_e^{\pi_t}(\boldsymbol{z}_{i\hat{j}}|\boldsymbol{z}_{ij})$$

$$= \frac{(N_1-1)!(N_2-2)!(N_2!)^{N_1-1}}{(N_1!)(N_2!)^{N_1}}\sum_{r=1}^{N_1}\sum_{s=1}^{N_2}\sum_{\substack{\hat{s}=1\\ \hat{s}\neq s,\mathrm{e}_2}}^{N_2}p_e\left\{r,\hat{s}|r,s\right\}$$

$$= \frac{1}{N_2-1}\left[\frac{1}{N_1N_2}\sum_{r=1}^{N_1}\sum_{s=1}^{N_2}\sum_{\substack{\hat{s}=1\\ \hat{s}\neq s,\mathrm{e}_2}}^{N_2}p_e\left\{r,\hat{s}|r,s\right\}\right] = \frac{p_{u2}}{N_2-1}. \tag{3.15}$$

For an undetected low resolution index error such that $\hat{i} \neq i$ and $\hat{r} \neq \mathrm{e}_1$,

$$\begin{aligned} E_{\pi_t} p_e^{\pi_t}(\boldsymbol{z}_{\hat{i}\hat{j}}|\boldsymbol{z}_{ij}) &= \frac{(N_1-2)![(N_2-1)!]^2(N_2!)^{N_1-2}}{(N_1!)(N_2!)^{N_1}} \sum_{r=1}^{N_1} \sum_{\substack{\hat{r}=1 \\ \hat{r}\neq r,\mathrm{e}_1}}^{N_1} \sum_{s=1}^{N_2}\sum_{\hat{s}=1}^{N_2} p_e\left\{\hat{r},\hat{s}|r,s\right\} \\ &= \frac{1}{N_2\left(N_1-1\right)} \left[\frac{1}{N_1}\frac{1}{N_2} \sum_{r=1}^{N_1} \sum_{\substack{\hat{r}=1 \\ \hat{r}\neq r,\mathrm{e}_1}}^{N_1} \sum_{s=1}^{N_2}\sum_{\hat{s}=1}^{N_2} p_e\left\{\hat{r},\hat{s}|r,s\right\}\right] \\ &= \frac{p_{u_1}}{N_2\left(N_1-1\right)}. \end{aligned} \tag{3.16}$$

When the lower resolution index is correct and erasure is declared for the higher resolution index such that $\hat{i} = i$ and $\hat{s} = \mathrm{e}_2$, respectively,

$$\begin{aligned} E_{\pi_t} p_e^{\pi_t}(\boldsymbol{z}_{i}|\boldsymbol{z}_{ij}) &= \frac{(N_1-1)!(N_2-1)!(N_2!)^{N_1-1}}{(N_1!)(N_2!)^{N_1}} \sum_{r=1}^{N_1} \sum_{s=1}^{N_2} p_e\left\{r,\hat{s}=\mathrm{e}_2|r,s\right\} \\ &= \frac{1}{N_1N_2} \sum_{r=1}^{N_1} \sum_{s=1}^{N_2} p_e\left\{r,\hat{s}=e_2|r,s\right\} \\ &= p_{d_2}. \end{aligned} \tag{3.17}$$

When the lower resolution index is incorrect and undetected such that $\hat{i} \neq i$ and $\hat{r} \neq \mathrm{e}_1$ while an erasure is declared for the higher resolution index such that $\hat{s} = \mathrm{e}_2$,

$$\begin{aligned} E_{\pi_t} p_e^{\pi_t}(\boldsymbol{z}_{\hat{i}}|\boldsymbol{z}_{ij}) &= \frac{(N_1-2)!(N_2-1)!(N_2!)^{N_1-1}}{(N_1!)(N_2!)^{N_1}} \sum_{r=1}^{N_1} \sum_{\substack{\hat{r}=1, \\ \hat{r}\neq r}}^{N_1} \sum_{s=1}^{N_2} p_e\left\{\hat{r},\hat{s}=\mathrm{e}_2|r,s\right\} \\ &= \frac{1}{N_1-1} \left[\frac{1}{N_1N_2} \sum_{r=1}^{N_1} \sum_{\substack{\hat{r}=1, \\ \hat{r}\neq r}}^{N_1} \sum_{s=1}^{N_2} p_e\left\{\hat{r},\hat{s}=e_2|r,s\right\}\right] \\ &= \frac{p_{ud}}{N_1-1}. \end{aligned} \tag{3.18}$$

When erasure is declared for the lower resolution index,

$$\begin{aligned} E_{\pi_t} p_e^{\pi_t}(\mathbf{0}|\boldsymbol{z}_{ij}) &= \frac{(N_1-1)!(N_2-1)!(N_2!)^{N_1-1}}{(N_1!)(N_2!)^{N_1}} \sum_{r=1}^{N_1}\sum_{s=1}^{N_2} p_e\left\{\hat{r}=\mathrm{e}_1|r,s\right\} \\ &= \frac{1}{N_1N_2}\sum_{r=1}^{N_1}\sum_{s=1}^{N_2} p_e\left\{\hat{r}=\mathrm{e}_1|r,s\right\} \\ &= p_{d1}. \end{aligned} \tag{3.19}$$

Finally, for erasure to not be declared for both lower and higher resolution indices,

$$\begin{aligned} E_{\pi_t}\left[\sum_{\hat{i}=1}^{N_1}\sum_{\hat{j}=1}^{N_2} p_e^{\pi_t}(\boldsymbol{z}_{\hat{i}\hat{j}}|\boldsymbol{z}_{ij})\right] &= 1 - E_{\pi_t} p_e^{\pi_t}(\mathbf{0}|\boldsymbol{z}_{ij}) - E_{\pi_t}\sum_{\hat{i}=1}^{N_1} p_e^{\pi_t}(\boldsymbol{z}_{\hat{i}}|\boldsymbol{z}_{ij}) \\ &= 1 - p_{d_1} - p_{d_2} - p_{ud}. \end{aligned} \tag{3.20}$$

Substitution of (3.15)-(3.20) into (3.14) yields

$$\begin{aligned} D_{e_1}^{\Pi} &= \left(1 - p_{d_1} - p_{d_2} - p_{ud}\right) D_{Q_e} \\ &\quad + \frac{p_{u_2}}{k(N_2-1)} \\ &\qquad \times \sum_{i,j}\int_{z\in\mathcal{A}_{ij}} \sum_{\hat{j}\neq j}\left[2(\boldsymbol{z}-\boldsymbol{z}_{ij})(\boldsymbol{z}_{ij}-\boldsymbol{z}_{i\hat{j}})' + \|\boldsymbol{z}_{ij}-\boldsymbol{z}_{i\hat{j}}\|^2\right] f(\boldsymbol{z})d\boldsymbol{z} \\ &\quad + \frac{p_{u_1}}{kN_2\left(N_1-1\right)} \\ &\qquad \times \sum_{i,j}\int_{z\in\mathcal{A}_{ij}} \sum_{\hat{i}\neq i,\hat{j}}\left[2(\boldsymbol{z}-\boldsymbol{z}_{ij})(\boldsymbol{z}_{ij}-\boldsymbol{z}_{\hat{i}\hat{j}})' + \|\boldsymbol{z}_{ij}-\boldsymbol{z}_{\hat{i}\hat{j}}\|^2\right] f(\boldsymbol{z})d\boldsymbol{z}, \end{aligned} \tag{3.21}$$

$$\begin{aligned} D_{e_2}^{\Pi} &= \left(p_{d_2} + p_{ud}\right)\frac{1}{k}\sum_{i,j}\int_{z\in\mathcal{A}_{ij}} \|\boldsymbol{z}-\boldsymbol{z}_i\|^2 f(\boldsymbol{z})d\boldsymbol{z} \\ &\quad + \frac{p_{ud}}{k(N_1-1)}\sum_{i,j}\int_{z\in\mathcal{A}_{ij}}\sum_{\hat{i}\neq i}\left[2(\boldsymbol{z}-\boldsymbol{z}_i)(\boldsymbol{z}_i-\boldsymbol{z}_{\hat{i}})' + \|\boldsymbol{z}_i-\boldsymbol{z}_{\hat{i}}\|^2\right] f(\boldsymbol{z})d\boldsymbol{z}, \end{aligned} \tag{3.22}$$

$$D_{e_3}^{\Pi} = p_{d_1}\sigma^2. \tag{3.23}$$

First consider simplifying (3.21):

$$
\begin{aligned}
D_{e_1}^{\Pi} &= (1-p_{d_1}-p_{d_2}-p_{ud})\, D_{Q_e} \\
&\quad + \frac{p_{u_2}}{k(N_2-1)} \sum_{i,j} \int_{z\in\mathcal{A}_{ij}} \sum_{\hat{j}\neq j} \left[2(\boldsymbol{z}-\boldsymbol{z}_{ij})(\boldsymbol{z}_{ij}-\boldsymbol{z}_{i\hat{j}})' + \|\boldsymbol{z}_{ij}-\boldsymbol{z}_{i\hat{j}}\|^2\right] f(\boldsymbol{z})d\boldsymbol{z} \\
&\quad + \frac{p_{u_1}}{kN_2\,(N_1-1)} \sum_{i,j} \int_{z\in\mathcal{A}_{ij}} \sum_{\hat{i}\neq i,\hat{j}} \left[2(\boldsymbol{z}-\boldsymbol{z}_{ij})(\boldsymbol{z}_{ij}-\boldsymbol{z}_{\hat{i}\hat{j}})' + \|\boldsymbol{z}_{ij}-\boldsymbol{z}_{\hat{i}\hat{j}}\|^2\right] f(\boldsymbol{z})d\boldsymbol{z} \\
&= (1-p_{d_1}-p_{d_2}-p_{ud})\, D_{Q_e} \\
&\quad + \frac{p_{u_1}}{kN_2\,(N_1-1)} \sum_{i,j} \int_{z\in\mathcal{A}_{ij}} \sum_{\hat{i},\hat{j}} \left[\|\boldsymbol{z}-\boldsymbol{z}_{\hat{i}\hat{j}}\|^2 - \|\boldsymbol{z}-\boldsymbol{z}_{ij}\|^2\right] f(\boldsymbol{z})d\boldsymbol{z} \\
&\quad + \left[\frac{p_{u_2}}{k(N_2-1)} - \frac{p_{u_1}}{kN_2\,(N_1-1)}\right] \sum_{i,j} \int_{z\in\mathcal{A}_{ij}} \sum_{\hat{j}} \left[\|\boldsymbol{z}-\boldsymbol{z}_{i\hat{j}}\|^2 - \|\boldsymbol{z}-\boldsymbol{z}_{ij}\|^2\right] f(\boldsymbol{z})d\boldsymbol{z} \\
&= \left(1-p_{d_1}-p_{d_2}-p_{ud}-p_{u_1}-\frac{N_2p_{u_2}}{N_2-1}\right) D_{Q_e} \\
&\quad + \frac{p_{u_1}}{kN_2\,(N_1-1)} \int_{\Lambda} \sum_{\hat{i},\hat{j}} \|\boldsymbol{z}-\boldsymbol{z}_{\hat{i}\hat{j}}\|^2 f(\boldsymbol{z})d\boldsymbol{z} \\
&\quad + \left[\frac{p_{u_2}}{k(N_2-1)} - \frac{p_{u_1}}{kN_2\,(N_1-1)}\right] \sum_{i} \int_{z\in\mathcal{A}_{i}} \sum_{\hat{j}} \|\boldsymbol{z}-\boldsymbol{y}_i+\boldsymbol{y}_i-\boldsymbol{z}_{i\hat{j}}\|^2 f(\boldsymbol{z})d\boldsymbol{z} \\
&\overset{1}{=} \left(1-p_{d_1}-p_{d_2}-p_{ud}-p_{u_1}-\frac{N_2p_{u_2}}{N_2-1}\right) D_{Q_e} \\
&\quad + \frac{p_{u_1}}{kN_2\,(N_1-1)} \int_{\Lambda} \sum_{\hat{i},\hat{j}} \left[\|\boldsymbol{z}\|^2 + \|\boldsymbol{z}_{\hat{i}\hat{j}}\|^2\right] f(\boldsymbol{z})d\boldsymbol{z} \\
&\quad + \left[\frac{p_{u_2}}{k(N_2-1)} - \frac{p_{u_1}}{kN_2\,(N_1-1)}\right] \sum_{i} \int_{z\in\mathcal{A}_{i}} \sum_{\hat{j}} \left[\|\boldsymbol{z}-\boldsymbol{y}_i\|^2 + \|\boldsymbol{z}_{i\hat{j}}-\boldsymbol{y}_i\|^2\right] f(\boldsymbol{z})d\boldsymbol{z} \\
&= \left(1-p_{d_1}-p_{d_2}-p_{ud}-p_{u_1}-\frac{N_2p_{u_2}}{N_2-1}\right) D_{Q_e} \\
&\quad + \frac{N_1p_{u_1}}{N_1-1}\left(\sigma^2+S_{Q_e}\right) + \left(\frac{N_2p_{u_2}}{N_2-1} - \frac{p_{u_1}}{N_1-1}\right)\left(\bar{\sigma}_{Q_e}^2+\bar{S}_{Q_e}\right), \qquad (3.24)
\end{aligned}
$$

where $\overset{1}{=}$ is by $E(\boldsymbol{z})=\boldsymbol{0}$ and by definition of $\boldsymbol{y}_i$.

Next, we consider simplifying (3.22) and (3.23) together:

$$
\begin{aligned}
D_{e_2}^{\Pi} + D_{e_3}^{\Pi} &= (p_{d_2} + p_{ud}) \frac{1}{k} \sum_{i,j} \int_{z \in \mathcal{A}_{ij}} \|\boldsymbol{z} - \boldsymbol{z}_i\|^2 f(\boldsymbol{z}) d\boldsymbol{z} + p_{d_1} \sigma^2 \\
&\quad + \frac{p_{ud}}{k(N_1 - 1)} \sum_{i,j} \int_{z \in \mathcal{A}_{ij}} \sum_{\hat{i} \neq i} \left[2(\boldsymbol{z} - \boldsymbol{z}_i)(\boldsymbol{z}_i - \boldsymbol{z}_{\hat{i}})' + \|\boldsymbol{z}_i - \boldsymbol{z}_{\hat{i}}\|^2 \right] f(\boldsymbol{z}) d\boldsymbol{z} \\
&= (p_{d_2} + p_{ud}) D_{Q_b} + p_{d_1} \sigma^2 \\
&\quad + \frac{p_{ud}}{k(N_1 - 1)} \sum_{i,\hat{i}} \int_{z \in \mathcal{A}_i} \left[\|\boldsymbol{z} - \boldsymbol{z}_{\hat{i}}\|^2 - \|\boldsymbol{z} - \boldsymbol{z}_i\|^2 \right] f(\boldsymbol{z}) d\boldsymbol{z} \\
&= \left(p_{d_2} + p_{ud} - \frac{N_1 p_{ud}}{N_1 - 1} \right) D_{Q_b} + p_{d_1} \sigma^2 \\
&\quad + \frac{p_{ud}}{k(N_1 - 1)} \int_{\Lambda} \sum_{\hat{i}} \|\boldsymbol{z} - \boldsymbol{z}_{\hat{i}}\|^2 f(\boldsymbol{z}) d\boldsymbol{z} \\
&\overset{2}{=} \left(p_{d_2} - \frac{p_{ud}}{N_1 - 1} \right) D_{Q_b} + p_{d_1} \sigma^2 \\
&\quad + \frac{p_{ud}}{k(N_1 - 1)} \int_{\Lambda} \sum_{\hat{i}} \left[\|\boldsymbol{z}\|^2 + \|\boldsymbol{z}_{\hat{i}}\|^2 \right] f(\boldsymbol{z}) d\boldsymbol{z} \\
&= \left(p_{d_2} - \frac{p_{ud}}{N_1 - 1} \right) D_{Q_b} + p_{d_1} \sigma^2 + \frac{N_1 p_{ud}}{N_1 - 1} \left(\sigma^2 + S_{Q_b} \right), \qquad (3.25)
\end{aligned}
$$

where $\overset{2}{=}$ is again due to $E(\boldsymbol{z}) = \mathbf{0}$. Combining (3.24) and (3.25) yields (3.10). The proof of (3.9) follows the same techniques as the above for (3.10), and is hence omitted. □

3.3 Multiresolution Quantization Design

This section considers MRVQ design and analysis given CRC-coded channel statistics. We begin with the problem definition and derive its necessary optimality conditions, followed by the design of a controlled iterative algorithm to yield tree-structured multiresolution quantizers such as in [42]-[44]. The objective value of the iterative algorithm is shown to be always convergent, and is hence implementable for use in numerical experiments.

Theorem 3.1 provides explicit expressions for D_b^{Π} and D_e^{Π}, the EED for each of the two receivers in the broadcast channel. Since minimizing D_b^{Π} does not necessarily minimize D_e^{Π}, and *vice versa*, we assign certain weights to the two receivers and look to minimize a weighted EED defined as

$$\bar{D} \triangleq pD_e^{\Pi} + (1-p)D_b^{\Pi}, \tag{3.26}$$

where $0 < p < 1$ is the weight assigned to the first receiver to represent the percentage of receivers who are eligible for the higher resolution source reconstruction.

3.3.1 Optimality Conditions for Optimal MRVQ

Let $(\mathfrak{A}, \mathfrak{Z}_1, \mathfrak{Z}_2)$ be a triple representing a two-resolution vector quantizer employed in the system depicted in Fig. 3.2, where $\mathfrak{A} = \{\mathcal{A}_{ij}, 1 \le i \le N_1, 1 \le j \le N_2\}$ is the partitioning of Λ into the higher resolution regions in a way such that $\{\mathcal{A}_i = \cup_j \mathcal{A}_{ij}\}_{i=1}^{N_1}$ is the set of lower resolution regions, $\mathfrak{Z}_1 = \{\boldsymbol{z}_i, i = 1, \cdot, N_1\}$ is the set of codeword vectors respectively representing all source vectors in $\mathcal{A}_i$, and $\mathfrak{Z}_2 = \{\boldsymbol{z}_{ij}, i = 1, \cdot, N_1, j = 1, \cdots, N_2\}$ for all source vectors in $\mathcal{A}_{ij}$. The design of the optimal quantizer thus has an objective function expressed as

$$\min_{\mathfrak{Z}_1, \mathfrak{Z}_2} \min_{\mathfrak{A}} \quad pD_e^{\Pi} + (1-p)D_b^{\Pi}, \tag{3.27}$$

where the minimization is over all possible triples of $(\mathfrak{A}, \mathfrak{Z}_1, \mathfrak{Z}_2)$. The optimal solution to (3.27) is characterized by two necessary conditions derived from Theorem 3.1.

Theorem 3.2. *Given an error detecting coded broadcast channel with p_{bd}, p_{bu}, p_{d_1}, p_{d_2}, p_{ud}, p_{u_1}, and p_{u_2}, the optimal multiresolution vector quantizer to (3.27) satisfies the following two conditions:*

1) Given $\mathfrak{A}$, the optimal code vectors to minimize $\bar{D}$ for the lower and higher resolution are respectively computed by

$$\boldsymbol{z}_i = \frac{\int_{\boldsymbol{z}\in\mathcal{A}_i} \boldsymbol{z} f(\boldsymbol{z}) d\boldsymbol{z}}{\frac{(1-p)p_{bu}+pp_{ud}}{(N_1-1)[(1-p)k_3+pk_4]} + \Pr\{\boldsymbol{z}\in\mathcal{A}_i\}} \tag{3.28}$$

$$\boldsymbol{z}_{ij} = \frac{k_1 \int_{\boldsymbol{z}\in\mathcal{A}_{ij}} \boldsymbol{z} f(\boldsymbol{z}) d\boldsymbol{z} + k_2 \int_{\boldsymbol{z}\in\mathcal{A}_i} \boldsymbol{z} f(\boldsymbol{z}) d\boldsymbol{z}}{\frac{p_{u_1}}{N_2(N_1-1)} + k_1 \Pr\{\boldsymbol{z}\in\mathcal{A}_{ij}\} + k_2 \Pr\{\boldsymbol{z}\in\mathcal{A}_i\}} \tag{3.29}$$

for $i = 1, \cdots, N_1, j = 1, \cdots, N_2$.

2) Given $\mathfrak{Z}_1$ and $\mathfrak{Z}_2$, the optimal higher resolution partitioning of Λ is defined as

$$\mathcal{A}_{ij} = \{\boldsymbol{z} : 2\boldsymbol{\alpha}_{ij}\boldsymbol{z}' - \boldsymbol{\beta}_{ij} \geq 2\boldsymbol{\alpha}_{i'j'}\boldsymbol{z}' - \boldsymbol{\beta}_{i'j'} \; \forall \, (i', j') \neq (i, j)\} \tag{3.30}$$

for $i = 1, \cdots, N_1, j = 1, \cdots, N_2$, where

$$\begin{aligned}
k_1 &\triangleq 1 - p_{u_1} - \frac{N_2 p_{u_2}}{N_2 - 1} - p_{d_1} - p_{d_2} - p_{ud}, \\
k_2 &\triangleq \frac{p_{u_2}}{N_2 - 1} - \frac{p_{u_1}}{N_2(N_1 - 1)}, \\
k_3 &\triangleq 1 - \frac{N_1 p_{bu}}{N_1 - 1} - p_{bd}, \\
k_4 &\triangleq p_{d_2} - \frac{p_{ud}}{N_1 - 1}, \\
\boldsymbol{\alpha}_{ij} &\triangleq pk_1 \boldsymbol{z}_{ij} + pk_2 \sum_{\hat{j}=1}^{N_2} \boldsymbol{z}_{i\hat{j}} + [(1-p)k_3 + pk_4]\boldsymbol{z}_i, \\
\boldsymbol{\beta}_{ij} &\triangleq pk_1 \|\boldsymbol{z}_{ij}\|^2 + pk_2 \sum_{\hat{j}=1}^{N_2} \|\boldsymbol{z}_{i\hat{j}}\|^2 + [(1-p)k_3 + pk_4]\|\boldsymbol{z}_i\|^2.
\end{aligned}$$

Remark 3.5. It is expected and indeed the case that both 1) and 2) appear similar to the case for the coded broadcast channel without error detection in [7]. Given a CRC-coded broadcast channel, the substitution of $p_{bd} = p_{d_1} = p_{d_2} = p_{ud} = 0$ reduces (3.28)-(3.30) into the forms derived in [7].

Remark 3.6. For the single-resolution case without error detection, it was found in [6] that earlier optimality conditions based on a fixed index assignment in [5] could be reduced to those based on a RIA by applying the conditions in [5] to an average symmetric channel. This, however, does not apply in the case with error detection, as the CRC-coded channel is no longer a symmetric channel. Furthermore, extension of the optimality conditions from [5] for a fixed index assignment to the multiresolution case for pairing with a broadcast channel is not a straightforward problem, even for the case without error detection.

Proof of Theorem 3.2. Proof of (3.28)-(3.29) involves the standard technique of taking the derivative of (3.26) with respect to and solving for $\boldsymbol{z}_i$ and $\boldsymbol{z}_{ij}$. We begin with

$$\frac{\partial \bar{D}}{\partial \boldsymbol{z}_i} = \left[(1-p)k_3 + pk_4\right] \frac{\partial D_{Q_b}}{\partial \boldsymbol{z}_i} + \left[(1-p)p_{bu} + pp_{ud}\right] \left(\frac{N_1}{N_1 - 1}\right) \frac{\partial S_{Q_b}}{\partial \boldsymbol{z}_i},$$

from which $\frac{\partial \bar{D}}{\partial \boldsymbol{z}_i} = 0$ could be solved for $\boldsymbol{z}_i$ to yield (3.28). Similarly with respect to $\boldsymbol{z}_{ij}$, we have

$$\frac{\partial \bar{D}}{\partial \boldsymbol{z}_{ij}} = p \left[k_1 \frac{\partial D_{Q_e}}{\partial \boldsymbol{z}_{ij}} + \left(\frac{N_1 p_{u_1}}{N_1 - 1}\right) \frac{\partial S_{Q_e}}{\partial \boldsymbol{z}_{ij}} + k_2 N_2 \frac{\partial \bar{S}_{Q_e}}{\partial \boldsymbol{z}_{ij}} \right],$$

yielding (3.29) when solving for $\boldsymbol{z}_{ij}$ in $\frac{\partial \bar{D}}{\partial \boldsymbol{z}_{ij}} = 0$.

For (3.30), observe that given $\mathfrak{Z}_1$ and $\mathfrak{Z}_2$, (3.26) can be rewritten in integral form as

$$\bar{D} = \int_{\Lambda} G(\boldsymbol{z}) f(\boldsymbol{z}) d\boldsymbol{z} + const, \tag{3.31}$$

where

$$G(\boldsymbol{z}) = F(\boldsymbol{z}, \boldsymbol{z}_i, \boldsymbol{z}_{ij}) \text{ if } \boldsymbol{z} \in \mathcal{A}_{ij}$$

and

$$F(\boldsymbol{z}, \boldsymbol{z}_i, \boldsymbol{z}_{ij}) \triangleq \frac{p}{k}\left(k_1\|\boldsymbol{z}-\boldsymbol{z}_{ij}\|^2 + k_2\sum_{\hat{j}=1}^{N_2}\|\boldsymbol{z}-\boldsymbol{z}_{i\hat{j}}\|^2\right) + \left[\frac{(1-p)k_3+pk_4}{k}\right]\|\boldsymbol{z}-\boldsymbol{z}_i\|^2.$$

For a particular $\boldsymbol{z}$, $G(\boldsymbol{z})$ can only take on one value corresponding to the index pair (i,j) to which $\boldsymbol{z}$ is mapped. Hence, to minimize (3.31), it is sufficient to map that particular $\boldsymbol{z}$ to the index pair (i,j) for which $G(\boldsymbol{z})$ is minimized. Precisely stated, we require

$$\mathcal{A}_{ij} = \left\{\boldsymbol{z} : F(\boldsymbol{z}, \boldsymbol{z}_i, \boldsymbol{z}_{ij}) \leq F(\boldsymbol{z}, \boldsymbol{z}_{i'}, \boldsymbol{z}_{i'j'})\ \forall\ (i',j') \neq (i,j)\right\},$$

which can be simplified and shown to be equivalent to (3.30). □

3.3.2 Quantization Algorithm Design

The two conditions stated by Theorem 3.2 for the vector case suggest an iterative descent algorithm to design the optimal multiresolution vector quantizer. With reference to Theorem 3.2, we propose two algorithms to minimize the EED: a baseline iterative algorithm based strictly on Theorem 3.2 that may produce non-convex quantization partitions, and a controlled version that converges faster, is easier to implement, and like [42] and [43], maintains the convexity of quantization partitions at all resolutions.

The baseline algorithm is stated as follows. Fix all error probabilities p_{bd}, p_{bu}, p_{d_1}, p_{d_2}, p_{ud}, p_{u_1}, p_{u_2}, and the weight p. First select any initial multiresolution quantizer $Q^{(0)} = (\mathfrak{A}^{(0)}, \mathfrak{Z}_1^{(0)}, \mathfrak{Z}_2^{(0)})$ with an objective value $\bar{D}^{(0)}$. Then, for each iteration $n = 1, 2, \ldots$, alternate between computing $\mathfrak{Z}_1^{(n+1)}$ and $\mathfrak{Z}_2^{(n+1)}$ respectively according to (3.28) and (3.29) given $\mathfrak{A}^{(n)}$, followed by computing $\mathfrak{A}^{(n+1)}$ according to (3.30) given $\mathfrak{Z}_1^{(n+1)}$ and $\mathfrak{Z}_2^{(n+1)}$. At the end of each iteration, also compute $\bar{D}^{(n+1)}$. Output $Q^{(n+1)} = (\mathfrak{A}^{(n+1)}, \mathfrak{Z}_1^{(n+1)}, \mathfrak{Z}_2^{(n+1)})$ as the final quantizer once $\bar{D}^{(n)} - \bar{D}^{(n+1)} < \epsilon$ is satisfied for some constant ϵ. Note that at each iteration, the local minimum is found and as a result, $\bar{D}^{(n)}$ is always non-increasing. This along with its lower boundedness imply convergence of the sequence $\{\bar{D}^{(n)}\}$ as $n \to \infty$.

The above baseline algorithm is visibly inspired by the Lloyd-Max algorithm for designing the optimal noiseless vector quantizer. However, in contrast with the traditional centroid rule, we see from (3.28)-(3.29) that the set of $\boldsymbol{z}_i$ are forced to move towards the origin, and the set of $\boldsymbol{z}_{ij}$ are forced towards the weighted centroid of the corresponding $\mathcal{A}_i$. Furthermore, the optimal partition boundaries in (3.30) no longer follow the nearest neighbour rule (as we shall see later, this is actually only true for the lower resolution partitions). To see how convexity is violated, consider the scalar case, where the optimal partition boundaries are no longer the midpoints of the nearest codewords. Based on the updating rules for each iteration defined in (3.28)-(3.30), the updated $\boldsymbol{z}_i$ and $\boldsymbol{z}_{ij}$ may not fall inside $\mathcal{A}_i$ and $\mathcal{A}_{ij}$, respectively, while certain partitions may cease to exist at all. If this was allowed to occur, then $\{\boldsymbol{z}_1, \ldots, \boldsymbol{z}_{N_1}\}$, $\{\boldsymbol{z}_{11}, \ldots, \boldsymbol{z}_{N_1 N_2}\}$, $\{\mathcal{A}_1, \ldots, \mathcal{A}_{N_1}\}$, or $\{\mathcal{A}_{11}, \ldots, \mathcal{A}_{N_1 N_2}\}$ could become arbitrarily ordered at certain iterations. Since we must have $\mathcal{A}_i = \cup_j \mathcal{A}_{ij}$ by definition, then $\mathcal{A}_i$ may no longer be convex. Violating convexity implies the multiresolution quantizer cannot be modeled by a tree structure.

Now consider the scalar case, i.e., $k = 1$. Suppose the source $z \in \mathbb{R}$ is finitely supported in $[T_l, T_u]$. Let Q be any two-resolution scalar quantizer represented by three vectors defined as

$$\begin{aligned}
\boldsymbol{b} &= (b_{1,1}, b_{1,2}, \ldots b_{1,N_2}, b_{2,1}, \ldots, b_{N_1,N_2-1}), \\
\boldsymbol{g} &= (g_{1,1}, g_{1,2}, \ldots g_{1,N_2}, g_{2,1}, \ldots, g_{N_1,N_2}), \\
\boldsymbol{h} &= (h_1, \ldots, h_{N_1}),
\end{aligned}$$

satisfying $T_l = b_{0,N_2} < b_{i,j} < b_{i',j'} < b_{N_1,N_2} = T_u$, $h_i < h_{i'}$, and $g_{i,j} < g_{i',j'}$ for any (i,j) and (i',j') with either $i' > i$ or $i = i'$, $j' > j$. Higher resolution quantization of z proceeds as follows: $Q(z) = g_{1,1}$ for any $z \in L_{1,1} \triangleq [T_l, b_{1,1}]$; $Q(z) = g_{i,j}$ for any $z \in L_{i,j} \triangleq (b_{i,j-1}, b_{i,j}]$, $1 \leq i \leq N_1$, $1 < j \leq N_2$; and $Q(z) = g_{i,1}$ for any $z \in L_{i,1} \triangleq (b_{i-1,N_2}, b_{i,1}]$, $1 < i \leq N_1$. Lower resolution quantization of z occurs such that $Q(z) = h_1$ for any $z \in L_1 \triangleq [T_l, b_{1,N_2}]$ and $Q(z) = h_i$ for any $z \in L_i \triangleq (b_{i-1,N_2}, b_{i,N_2}]$, $1 < i \leq N_1$. Note that by our lengthy definitions here, the scalar quantizer is restricted to having only convex quantization partitions at both lower and higher resolutions.

While (3.28)-(3.30) are necessary optimality conditions of the solution to the general problem defined in (3.27), we restrict our controlled iterative algorithm to the case of convex partitions and solve the following optimization problem:

$$\begin{aligned} \min_{\boldsymbol{g},\boldsymbol{h},\boldsymbol{b}} \quad & \bar{D} = pD_e^{\Pi} + (1-p)D_b^{\Pi} \\ \text{subject to} \quad & h_i < h_{i'}, g_{i,j} < g_{i',j'}, \\ & T_l < b_{i,j} < b_{i',j'} < T_u, \\ & \text{whenever } i' > i \text{ or } i' = i \text{ and } j' > j. \end{aligned} \tag{3.32}$$

The controlled iterative algorithm to solve (3.32) is summarized as follows.

1) Initialization: Set $n = 0$ and pick any quantizer $Q^{(0)}$ with valid $\boldsymbol{b}^{(0)}$, $\boldsymbol{h}^{(0)}$, and $\boldsymbol{g}^{(0)}$ satisfying the constraints of (3.32). Compute $\bar{D}^{(n)}$.

2) Given $\boldsymbol{b}^{(n)}$, compute $\boldsymbol{h}^{(n+1)}$ by $h_i^{(n+1)} = \mu_i^{(n+1)}$, where

$$\mu_i^{(n+1)} = \max\left\{\min\left(\xi_i^{(n+1)}, \sup L_i^{(n)}\right), \inf L_i^{(n)}\right\}, i = 1, \ldots, N_1 \tag{3.33}$$

and

$$\xi_i^{(n+1)} = \frac{\int_{L_i^{(n)}} zf(z)dz}{\frac{(1-p)p_{bu}+pp_{ud}}{(N_1-1)[(1-p)k_3+pk_4]} + \int_{L_i^{(n)}} f(z)dz},$$

and for any set L, $\sup L = \sup_{z\in L} z$ and $\inf L = \inf_{z\in L} z$. Further compute $\boldsymbol{g}^{(n+1)}$ by $g_{i,j}^{(n+1)} = \lambda_{i,j}^{(n+1)}$, where

$$\lambda_{i,j}^{(n+1)} = \max\left\{\min\left(\psi_{i,j}^{(n+1)}, \sup L_{i,j}^{(n)}\right), \inf L_{i,j}^{(n)}\right\}, i = 1, \ldots, N_1, j = 1, \ldots, N_2 \tag{3.34}$$

and

$$\psi_{i,j}^{(n+1)} = \frac{k_1 \int_{L_{i,j}^{(n)}} zf(z)dz + k_2 \int_{L_i^{(n)}} zf(z)dz}{\frac{p_{u_1}}{N_2(N_1-1)} + k_1 \int_{L_{i,j}^{(n)}} f(z)dz + k_2 \int_{L_i^{(n)}} f(z)dz}.$$

3) Given $\boldsymbol{h}^{(n+1)}$ and $\boldsymbol{g}^{(n+1)}$, update $\boldsymbol{b}^{(n+1)}$ by $b_{i,j}^{(n+1)} = \nu_{i,j}^{(n+1)}$, where

$$\nu_{i,j}^{(n+1)} = \begin{cases} \frac{1}{2}\left(g_{i,j}^{(n+1)} + g_{i,j+1}^{(n+1)}\right) \\ \qquad\qquad \text{if } i = 1,\ldots,N_1, j = 1,\ldots,N_2-1, \\ \max\left\{\min\left(\zeta_{i,N_2}^{(n+1)}, g_{i+1,1}^{(n+1)}, h_{i+1}^{(n+1)}\right),\ g_{i,N_2}^{(n+1)}, h_i^{(n+1)}\right\} \\ \qquad\qquad \text{if } i = 1,\ldots,N_1-1, j = N_2, \end{cases} \tag{3.35}$$

and

$$\zeta_{i,N_2}^{(n+1)} = \frac{\beta_{i+1,1}^{(n+1)} - \beta_{i,N_2}^{(n+1)}}{2\left(\alpha_{i+1,1}^{(n+1)} - \alpha_{i,N_2}^{(n+1)}\right)},$$

$$\alpha_{i,j}^{(n+1)} = pk_1 g_{i,j}^{(n+1)} + pk_2 \sum_{\hat{j}=1}^{N_2} g_{i,\hat{j}}^{(n+1)} + [(1-p)k_3 + pk_4] h_i^{(n+1)},$$

$$\beta_{i,j}^{(n+1)} = pk_1 \left[g_{i,j}^{(n+1)}\right]^2 + pk_2 \sum_{\hat{j}=1}^{N_2} \left[g_{i,\hat{j}}^{(n+1)}\right]^2 + [(1-p)k_3 + pk_4] \left[h_i^{(n+1)}\right]^2.$$

4) Compute $\bar{D}^{(n+1)}$. Repeat Steps 2 and 3 for $n = 1, 2, \ldots$ until $\bar{D}^{(n)} - \bar{D}^{(n+1)} < \epsilon$ for some predefined $\epsilon > 0$, then output $\boldsymbol{b}^{(n+1)}$, $\boldsymbol{h}^{(n+1)}$, and $\boldsymbol{g}^{(n+1)}$ as our desired two-resolution scalar quantizer.

Remark 3.7. The reduction of (3.28)-(3.30) to (3.33)-(3.35) for the one-dimensional case merits some discussion. As pointed out in [7], two-resolution quantization design observes impact of channel error probabilities on the quantization partition in contrast to the single-resolution case, where the nearest neighbour decision rule applies independent of the channel. However, inspection of (3.35) reveals that while the nearest neighbour rule does not apply in general, it still applies for only the higher resolution quantization partitions, but not for the lower resolution partitions. Note that there is actually not a non-uniformity in the computation of each partition from (3.35) for $j = N_2$ versus $j \neq N_2$; the equation used to compute $b_{i,j}^{(n+1)}$ for $j = N_2$ actually reduces to the nearest neighbour rule for $j \neq N_2$.

Remark 3.8. Both the baseline and controlled iterative algorithms proposed in this subsection are visibly inspired by the Lloyd-Max algorithm and its generalizations to channel-optimized source quantization studied in [4], [5], and [23]. However, these previous works propose algorithms that require complete knowledge of the channel transitional probabilities, in contrast to ours, which require only the average channel information quantified by the error probabilities p_{bd}, p_{bu}, p_{d_1}, p_{d_2}, p_{ud}, p_{u_1}, and p_{u_2}. In practical systems, we postulate that such average channel statistics are much more readily available than the complete channel transition matrix. Our algorithms are also significantly less computationally intensive than prior proposed algorithms for fixed index assignments; due to RIA, the error probability of the channel is decoupled from the integral in computing the updated codewords. Thus, in contrast to [1], [5], and [23], training sequences are no longer required for quantization design and the source distribution $f(\boldsymbol{z})$ can be directly used at every iteration. Lastly, algorithms designed based on only average channel statistics was shown for the single-resolution case in [6] to be more robust against channel fluctuations, an advantage we expect to be carried over to the multiresolution case with error detection.

Remark 3.9. Due to convexity of the quantization partitions at both lower and higher resolutions, the controlled iterative algorithm is arguably more applicable for practical implementation than the baseline algorithm based strictly on the necessary optimality conditions. Maintaining convexity of the quantization partitions at all resolutions enables efficient encoding and decoding by modeling the quantizer in a tree structure such as in [43] and [44]. As an example, for the noiseless case, efficient computation of the encoder partition step in the iterative algorithm proposed by Dumitrescu in [42] also relies on the convexity of quantization partitions.

Theorem 3.3 (Convergence)**.** *Given $k_i \geq 0$ for $i = 1, 2, 3, 4$, the controlled iterative algorithm is guaranteed to locally converge in the sense that the sequence of objective values $\bar{D}^{(n)}$ converges as $n \to \infty$.*

Proof. We first prove that the objective function in (3.32) is non-increasing after every iteration. To do so, $\bar{D}$ is must be shown to be non-increasing in both Steps 2 and 3 for any arbitrary iteration. In Step 3, consider the computation of a particular $b_{i,j}$ given $\boldsymbol{h}$ and $\boldsymbol{g}$.

As a function of $b_{i,j}$, observe that the objective function can be written as

$$\bar{D} = \int_{T_l}^{T_u} G(z) f(z) dz + const, \tag{3.36}$$

where $G(z) = F(z, h_i, g_{i,j})$ if $z \in L_{i,j}$ and

$$\begin{aligned} F(z, h_i, g_{i,j}) &= pk_1(z - g_{i,j})^2 + pk_2 \sum_{\hat{j}=1}^{N_2} (z - g_{i,\hat{j}})^2 + \left[(1-p)k_3 + pk_4\right](z - h_i)^2 \\ &= \beta_{i,j} - 2z\alpha_{i,j} + z^2 \left[p(k_1 + k_2 N_2 + k_4) + (1-p)k_3\right]. \end{aligned}$$

Hence we have

$$\frac{\partial \bar{D}}{\partial b_{i,j}} = \begin{cases} \left[2b_{i,j}(\alpha_{i,j+1} - \alpha_{i,j}) - (\beta_{i,j+1} - \beta_{i,j})\right] f(b_{i,j}), \\ \qquad\qquad \text{if } i = 1, \ldots, N_1, j = 1, \ldots, N_2 - 1, \\ \left[2b_{i,N_2}(\alpha_{i+1,1} - \alpha_{i,N_2}) - (\beta_{i+1,1} - \beta_{i,N_2})\right] f(b_{i,N_2}), \\ \qquad\qquad \text{if } i = 1, \ldots, N_1 - 1, j = N_2. \end{cases}$$

Since $f(\cdot) > 0$, $(\alpha_{i,j+1} - \alpha_{i,j}) > 0$, and $(\alpha_{i+1,1} - \alpha_{i,N_2}) > 0$, there exists a unique minimizer where $\frac{\partial \bar{D}}{\partial b_{i,j}} = 0$. Computed $\{b_{i,j}\}$ satisfying $\frac{\partial \bar{D}}{\partial b_{i,j}} = 0$ is the unique minimizer and hence cannot increase the objective function. However, careful inspection of (3.35) reveals that a subset of $\{b_{i,N_2} : i = 1, \ldots, N_1 - 1\}$ may not satisfy $\frac{\partial \bar{D}}{\partial b_{i,N_2}} = 0$ but can still be shown to not increase $\bar{D}$. With reference to (3.35), suppose $\zeta_{i,N_2} \leq g_{i,N_2}$. Then $\bar{D}$ is non-increasing if $b_{i,N_2} = g_{i,N_2}$ since $\frac{\partial \bar{D}}{\partial b_{i,N_2}} > 0$ for all $b_{i,N_2} \in (g_{i,N_2}, g_{i+1,1}]$. Similarly for $\zeta_{i,N_2} > g_{i+1,1}$, $\bar{D}$ is non-increasing if $b_{i,N_2} = g_{i+1,1}$ since $\frac{\partial \bar{D}}{\partial b_{i,N_2}} < 0$ for all $b_{i,N_2} \in (g_{i,N_2}, g_{i+1,1}]$.

For Step 2, we need to demonstrate that $\bar{D}$ is non-increasing when computing $\boldsymbol{h}$ and $\boldsymbol{g}$ given $\boldsymbol{b}$. Consider only the i and (i,j) for which $\frac{\partial \bar{D}}{\partial h_i} = 0$ and $\frac{\partial \bar{D}}{\partial g_{i,j}} = 0$ are not respectively satisfied; otherwise, the non-increase is guaranteed. With reference to (3.33), suppose $\xi_i \leq b_{i-1,N_2}$. Then $\bar{D}$ is non-increasing if $h_i = b_{i-1,N_2}$, since it can be shown that $\frac{\partial \bar{D}}{\partial h_i} > 0$ for all $h_i \in (b_{i-1,N_2}, b_{i,N_2}]$. Similarly, suppose $\xi_i > b_{i,N_2}$. Then $\bar{D}$ is non-increasing if $h_i = b_{i,N_2}$ since $\frac{\partial \bar{D}}{\partial h_i} < 0$ for all $h_i \in (b_{i-1,N_2}, b_{i,N_2}]$. The same argument applies for $\boldsymbol{g}$.

With the non-increasing property of the objective function established, the lower boundedness of $\bar{D}$ allows us to conclude that the sequence $\{\bar{D}^{(n)}\}$ is convergent as $n \to \infty$. $\square$

3.4 Numerical Experiments

In this section, experiments are conducted to study the tradeoff between source quantization and error detection performance. We first consider the transmission of a one-dimensional Gaussian source with zero mean and unit variance over the CRC-coded point-to-point channel with additive white Gaussian noise (AWGN); the point-to-point case provides effective means to study the performance gains attributed to trading off source quantization with CRC error detection. Next, we consider the transmission of the same source over a coded broadcast channel using superposition coding (SPC), which can be implemented using layered modulation, a technique well-studied in the literature [41][46][47] and defined in a number of standards such as DVB-T [48] and UMB [49].

For the point-to-point AWGN channel, the continuous source is processed by a single-resolution scalar quantizer and transmitted over two blocks of 16-QAM modulation for a block size of $b_1 = 8$ bits. Let n_1 and l_1 respectively denote the number of data and CRC bits for the quantization index, where $n_1 + l_1 = b_1$. Hence, given a selected CRC polynomial for error detection purposes, we have a $N_1 = 2^{n_1}$-level quantizer, while l_1 is selected from Table 3.1, the list of best-performing polynomials for each CRC size based on [50].

Table 3.1: Considered CRC generator polynomial lengths for source error detection.

l_1 or l_2	Nickname	Polynomial
0	-	`0x00` $= 1$
1	CRC-1/parity	`0x01` $= (x+1)$
3	-	`0x05` $= (x^3+x+1)$
4	CCITT-4	`0x09` $= (x^4+x+1)$
5	CRC-5/USB	`0x12` $= (x^5+x^2+1)$
6	CRC-6/DARC	`0x2c` $= (x+1)(x^5+x^4+x^2+x+1)$

For the broadcast channel, suppose each multiresolution source symbol is transmitted over two uses of a standard 16/64-QAM hierarchical modulation as defined in [41] for a block size of 12 bits, where $b_1 = 8$ and $b_2 = 4$ bits are respectively available for the lower and higher resolution indices. In this case, the CRC code is individually applied to both indices for a pair of CRC polynomials. Let n_1 and l_1 respectively denote the same but for the lower resolution index, where $n_1 + l_1 = b_1$. Similarly, let n_2 and l_2 denote the same for the higher resolution index with $n_2 + l_2 = b_2$. For a particular pair of CRC polynomials, we then have a multiresolution quantizer with $N_1 = 2^{n_1}$ and $N_2 = 2^{n_2}$ levels for the lower and higher resolution, respectively, while l_1 and l_2 are again selected from Table 3.1.

Suppose the Karnaugh map style Gray mapping [41] is employed to map each channel symbol to a bit stream such that adjacent points in the QAM signal constellation differ by one bit. The matrices of transitional probabilities $p(\hat{m}_b|r)$ and $p(\hat{m}_e, \hat{m}_b|(r,s))$ for the CRC-coded point-to-point and broadcast channels, respectively, are then given. For each particular or pair of CRC(s) in Table 3.1, the two matrices allow the exact evaluation of p_{bd} and p_{bu} for the point-to-point channel and p_{bd}, p_{bu}, p_{d_1}, p_{d_2}, p_{ud}, p_{u_1}, and p_{u_2} for the broadcast channel. With these seven error probabilities that govern the entire CRC-coded broadcast channel as well as N_1 and N_2, we apply the controlled iterative algorithm from Section 3.3 to design the two-resolution scalar quantizer. The single-resolution quantizer for the point-to-point case is designed by taking $N_2 = 1$ in computing p_{bd} and p_{bu}, and selectively applying only lower resolution quantization portions of the controlled iterative algorithm with $p = 0$ in (3.32).

Although the controlled algorithm is less general than the baseline version, we have found that even though they converge to drastically different final quantizers, both yield nearly identical objectives at convergence. Specifically, the baseline algorithm is seen to outperform the controlled one by no more than 0.001 dB in terms of PSNR $\triangleq 10\log_{10}(\sigma^2/\bar{D})$. The controlled algorithm also converges faster since the sequence of quantizers can be modeled with a tree structure by convexity of the higher and lower resolution partitions. On the other hand, for every iteration, the baseline algorithm demands a careful record of each codeword-to-partition mapping, as well as higher-to-lower resolution partition mapping.

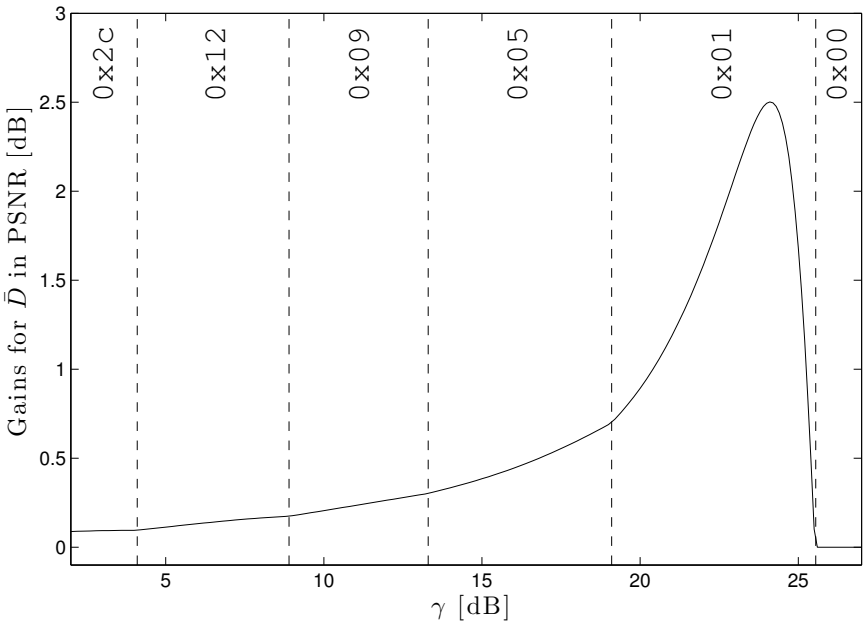

Figure 3.3: PSNR gains yielded from encoder design with versus without error detection under optimal CRCs (labeled) for various AWGN channel γ.

3.4.1 Gains from Error Detection

We first study the performance gains from employing CRC error detection versus without. The gains under the point-to-point channel are presented in terms of PSNR gains to quantify the increase in PSNR when a tradeoff is considered between data and CRC bits instead of the allocation of all bits for data in the case of no error detection. For the point-to-point channel employing a single-resolution scalar quantizer, a range of SNRs γ are considered for the receiver experiencing AWGN power $\frac{N_0}{2}$. Fig. 3.3 plots the quantity of the gain up to approximately 2.5 dB, along with corresponding regions marked with the CRC that achieves the largest PSNR gain.

The overall trend of the PSNR gains in Fig. 3.3 may actually be somewhat surprising at first glance; as the channel condition improves, one would expect the gains yielded from CRC to decrease. This is in contrast to the actuality, where gains from employing CRC initially *increases* as the channel condition improves. We explain the phenomenon

observed in Fig. 3.3 by considering the gains in PSNR within three regions of γ employing the CRCs, `0x2c`, `0x01`, and `0x00`.

In the lowest SNR region employing the CRC polynomial `0x2c`, CRC capability dramatically reduces the contribution of the $(\sigma^2 + S_{Q_b})$ term to the EED. However, this reduction is mostly offset by a large increase in quantization distortion, since the region's high error probabilities require many bits for CRC, leaving little remaining for source quantization. As the channel improves and error probabilities decrease, the system gradually requires a decreasing number of CRC bits to reduce S_{Q_b} effects. This reduces the increase in quantization distortion sacrificed to implement CRC, allowing the CRC-coded system to yield much more pronounced gains peaking in the region employing CRC `0x01`. The third region is characterized by a sharp reduction of the PSNR gain to zero when CRC no longer improves performance; this occurs once the error probabilities are so small that there is little contribution of S_{Q_b} to the EED, and thus, it is no longer worthwhile to sacrifice any quantization bits for error detection capability.

For the broadcast channel, a number of channel SNR combinations (γ_1, γ_2) are considered for the first and second receivers experiencing AWGN power $\frac{N_0}{2}$, where γ_1 and γ_2 respectively denote the SNRs of the first and second receiver. For each (γ_1, γ_2), we consider all combinations of CRC_1 and CRC_2, which denote the CRC polynomials selected from Table 3.1 for the lower and higher resolution indices, respectively. The combination of CRC_1 and CRC_2 that achieves the largest PSNR gain is employed to evaluate performance gains in the broadcast scenario.

Fig. 3.4 depicts the impact of employing CRC on the first receiver's EED in terms of PSNR gains with optimally configured CRC_1 and CRC_2 for $p = 0.5$. The same phenomenon from the point-to-point case is expected and observed for increasing PSNR gains under improved γ_2. This is because in the broadcast scenario, the second receiver behaves like the point-to-point case with interest in source reconstruction using only the lower resolution index. Hence, as before, improving γ_2 requires less CRC_1 check bits to reduce scatter factor effects, and as a result, reduces the increase in quantization distortion sacrificed for error detection of the lower resolution index. Since the lower resolution index is common information, an increase in PSNR gains is observed at both receivers.

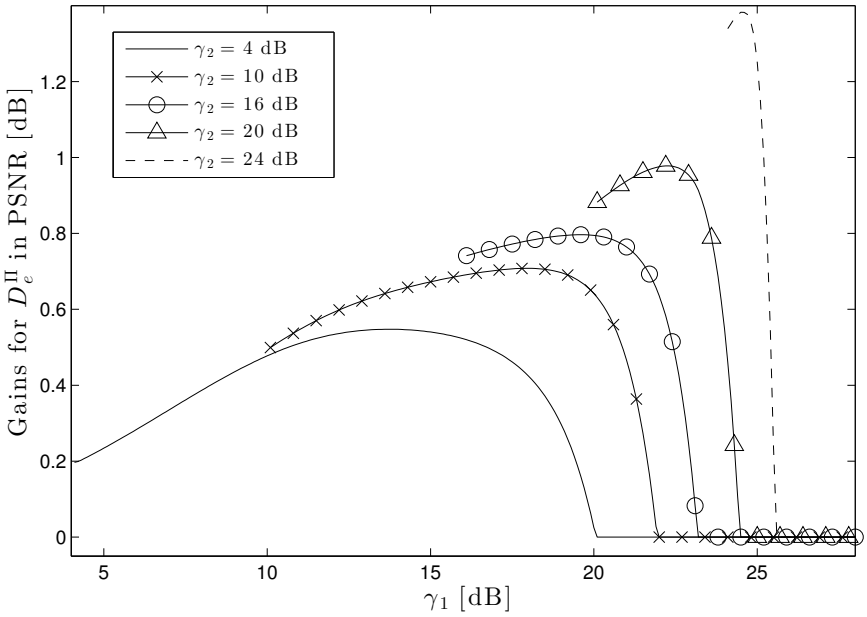

Figure 3.4: PSNR gains yielded for first receiver from encoder design with versus without error detection under optimal CRCs for broadcast channels with varying γ_1, γ_2, and $p = 0.5$.

The increase in PSNR gains with improving γ_1 for a particular fixed γ_2 is, however, due to another phenomenon. Under poorer channel conditions at the first receiver, the lower resolution index has higher likelihood of being incorrect. Hence, its PSNR gains are mainly resulted from employing only CRC_1, since the higher resolution index is discarded along with CRC_2 when an erasure is declared for the lower resolution index. As γ_1 improves, the decoder has an increasingly higher chance to exploit both CRC_1 and CRC_2 to yield larger gains. As in the point-to-point case, PSNR gains drops to zero under sufficiently good channel conditions.

3.4.2 Gains from Noisy Quantizer Design

In this subsection, we contrast the performance of the noisy and noiseless quantizers under various bit allocation levels between quantization and CRC error detection. In Fig. 3.5-3.6, PSNR gains are depicted under several CRC(s) for various channel conditions in the

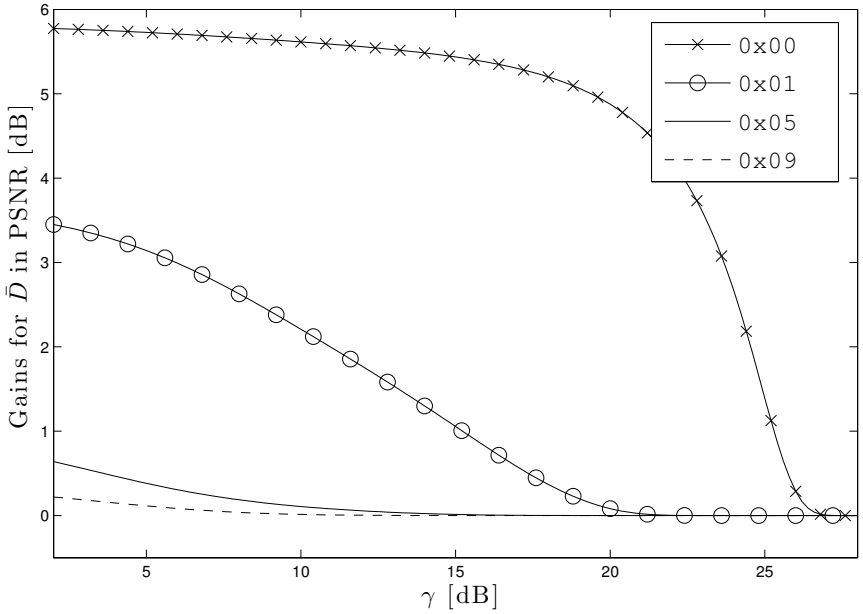

Figure 3.5: PSNR gains yielded from joint versus separate quantizer design under fixed CRCs for various AWGN channel γ.

point-to-point and broadcast channels, respectively. In general, the noisy quantizer always outperforms the noiseless quantizer for any bit allocation level. This is because CRC cannot detect all errors and thus cannot entirely eliminate the scatter factor's contribution to EED. The magnitude of the gain, however, depends on the particular CRC configuration and channel condition.

For the point-to-point case, observe in Fig. 3.5 that gains are largest when no error detection is applied. This is because without error detection, scatter factor contributions to the EED are at its peak and results in the largest sub-optimality if neglected as in the noiseless quantizer. On the other hand, allocating the maximum number of bits for CRC produces the least gains, as the scatter factor's contribution to EED is reduced by the most. In this case, quantization distortion dominates the EED, and the structure of the noisy quantizer would most closely resemble that of the noiseless quantizer. Since the optimal bit allocation level to minimize EED is mostly in between these two extreme scenarios, gains from the noisy channel quantizer may be large or small depending on the

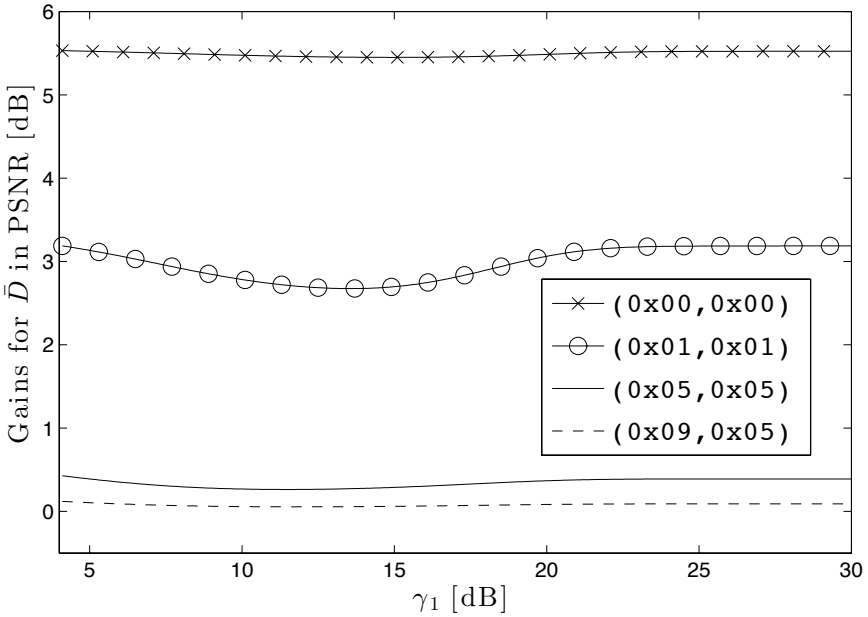

Figure 3.6: PSNR gains yielded from joint versus separate quantizer design under fixed (CRC_1, CRC_2) for broadcast channels with varying γ_1, $\gamma_2 = 4$ dB, and $p = 0.5$.

channel statistics. For each particular CRC, gains are also reduced with improving channel conditions, as the overall error probability is reduced.

For the broadcast channel, Fig. 3.6 shows the same trend, i.e., gains are decreased when more bits are allocated for (CRC_1, CRC_2). Note that for $p = 0.5$, D_b^{Π} contributes largely to $\bar{D}$. Hence, we see from Fig. 3.6 that with respect to a fixed γ_2, the gain with increasing γ_1 remains relatively steady, as there is no impact on the error probability experienced by the second receiver. The large contribution of D_b^{Π} relative to D_e^{Π} in $\bar{D}$ for $p = 0.5$ would also result in decreased PSNR gains for $\bar{D}$ as in the point-to-point case when γ_2 is increased.

3.5 Summary

This chapter investigates the design of channel-optimized multiresolution quantizers over CRC-coded channels, for which a closed-form end-to-end distortion formula is derived. The EED formulation allows for further derivation of necessary optimality conditions, based upon which an iterative algorithm is proposed and employed in numerical experiments. Results for both the point-to-point and broadcast channels demonstrate significant reductions to the EED without sacrificing bandwidth when considering a tradeoff between data and CRC bits in the application layer.

Counterintuitively, gains yielded from employing the optimal CRC increases at first with improving channel conditions still exhibiting moderate to large symbol crossover probabilities. Although gains with CRC vanish as the crossover probability asymptotically approaches zero, inclusion of error detection with quantization design is still concluded to be highly advantageous for applications that operate in the finite block length regime and hence, are constantly subject to non-zero error probabilities. Moreover, for the case of error detection, gains exhibited by the joint versus separate quantizer are observed to still hold with varying degrees depending on the system configuration and channel statistics.

Chapter 4

Transmission of Multiresolution Sources over Relay Channels

For applications that operate in the finite block length regime, it is demonstrated in Chapter 2 that under certain channel scenarios or system settings, reductions to the end-to-end distortion of the system can be achieved using joint source-channel coding as opposed to separate source-channel coding. This result implies that source-channel coding separation is no longer valid and their separate design is actually suboptimal for channel codes with finite block lengths.

While the above fact both motivates and justifies the consideration of JSCC for practical wireless applications, there are other ways for JSCC principles to be exploited for multimedia communication applications. For example, in Chapter 3, JSCC allows the pairing of scalable source coding with superposition channel coding for the broadcast channel. Specifically, the scalably encoded two-resolution quantizer is paired with layered modulation at the channel through a natural ordering map of each quantizer resolution to the corresponding channel modulation resolution. As such, two resolutions of the source information can be decoded from the source broadcast and results in improved utilization of channel resources for the two receivers experiencing different channel conditions. The SSC-SPC pairing also enables the notion of end-to-end distortion to be employed as an

end-to-end performance metric that captures the effects of both source quantization and channel crossover statistics, and as a result, is a more meaningful evaluation of quality for the transmission of real-valued sources, such as those in multimedia applications.

In this chapter, we extend the consideration of the SSC-SPC pairing to a decode-and-forward three-node relay network. In contrast to any previously reported research using asymptotic capacity-based distortion (CBD) measures, we derive the EED of such JSCC system based on a real-valued Gaussian source, aiming to achieve better precision and practicality for applications that are subject to large error probabilities caused by operation in the finite block length regime. The EED evaluation is formulated and applied to demonstrate achievable gains of the SSC-SPC architecture versus a number of conventional approaches. Power allocation optimization is performed based on the developed non-asymptotic EED model and compared to that by using an asymptotic CBD measure, for which symbol losses caused by channel error cannot be considered. We demonstrate the performance gaps between results solved from the EED versus CBD in our numerical example, and conclude that optimization based on the CBD behaves awkwardly in computing proper power allocation configurations in the considered SSC-SPC architecture.

4.1 Background and Related Work

JSCC has also been proven to be a promising approach for multimedia applications where service continuity is favoured over maximum quality delivery. In literature such as [8]-[11], the pairing of scalable source coding with superposition channel coding (SPC) enable multiple resolutions of receptions to effectively mitigate the vicious impact of multi-user channel diversity in the broadcast scenario. For the two-resolution scenario, the successive refinable source allows reconstruction of the original source at either the lower resolution using the partial information, or the higher resolution using the complete information. Hence, through the exact mapping of the lower resolution source symbol to the lower order of the SPC signal constellation that is more tolerant to the channel noise, receivers experiencing poorer channel conditions can better preserve service continuity at the lower

resolution instead of channel outage. Furthermore, receivers able to decode the full SPC signal obtain the higher resolution of source reconstruction.

Although numerous research efforts have been addressed on SPC for multi-layer source transmissions over wireless networks, most of them have employed formulations based on abstract asymptotic performance measures such as channel capacity and distortion exponent. In prior related work such as [17][18][19][20], multi-layer source broadcasting is considered under the three-node relay network with a number of relaying strategies, with extension to the multiple relay case in [12]. While they are all solid contributions, their analyses are based on the information theoretical perspective of channel capacity, thus causing difficulty in evaluating the end-receiver quality under large error probabilities. Some research consider a variety of distortion measures but maintains basis on the asymptotic case, such as [13], which computes the expected distortions from outage probabilities based on channel capacity, and [14], which provides rigorous theoretical analyses with results based on outage-based end-to-end distortion followed by actual simulations. Thus, there are still unclear implications of their theoretical formulation on the mean-squared error (MSE) used to demonstrate gains in their simulations. Other works in [15][16][21][22] begin with the MSE distortion measure but relies on the assumption of high SNR for analysis and evaluation.

Some literatures further perform power allocation optimization under the asymptotic case. In [18], improper power allocation is identified to cause severe detriments to the achievable channel capacity. In [51], the authors consider the joint optimization of power and rate allocation for layered transmission to minimize the expected distortion, which is still derived from an outage-style perspective based on channel SNR thresholds. [15] explores power and rate allocation in a more generalized multiple relay scenario exploiting spatial diversity based on the distortion exponent.

We emphasize that while the use of asymptotic or capacity-based metrics may be suitable for performance evaluation under some circumstances, they are less appropriate for applications that are constantly subject to or must tolerate large symbol error probabilities. Thus, studies focused on practical coding systems have long utilized the notion of end-to-end MSE distortion (EED), henceforth simply referred to as EED, or its PSNR

equivalent, to evaluate performance [52]-[54]. The fundamental difference between the notion of EED and asymptotic or capacity-based metrics lies in the fact that EED includes distortion caused by both source quantization and channel errors, since it precisely captures the average MSE distortion per symbol between the original continuous source and its reconstruction at the end-receiver. Evaluation of the EED from a non-asymptotic, theoretical perspective for a JSCC system, however, would cause highly complex formulations and intractability in theoretical analysis, and hence has remained an open problem without in-depth research thus far.

In this chapter, we consider the transmission of real-valued and continuous Gaussian sources over the fundamental three-node relay network under JSCC with possibly large channel error probabilities. We explore the performance modeling and power allocation optimization under the pairing of scalable source coding and SPC, or referred to as the SSC-SPC pairing architecture, where the source is encoded into two resolutions with successive refinement so as to match two-layer SPC in the physical layer. We take EED as the performance metric, enabled through the technique of random index assignment (RIA) that has also been applied in previous chapters to maintain exact MSE characterization and applicability to any non-asymptotic or asymptotic channel conditions with arbitrarily large error probabilities. To the best of our survey, this is the first study employing EED as the target metric for theoretical analysis of the SSC-SPC pairing for relay channels in a non-asymptotic and practical manner. Through power allocation optimization, we demonstrate that a significant EED reduction is achievable using the proposed model in comparison to the aforementioned conventional asymptotic schemes, which are suboptimal due to the lack of considering potentially large channel error probabilities.

The contributions of this chapter include: 1) a general framework for the transmission of scalable encoded information sources using SPC in a relay network; 2) a detailed system model formulation for the proposed framework over the fading relay channel; 3) generalization of the EED models for all service levels, including service outage at the lower resolution in evaluating the EED reduction capability of the proposed relay framework; and 4) justification of the generalized EED model over formulations based on channel capacity by considering the power allocation optimization at the transmitter and the relay.

The rest of the chapter is organized as follows. Section 4.2 provides a comprehensive overview of the system model upon which the proposed framework is developed. Section 4.3 derives necessary EED formulations used for the results of numerical experiments presented in Section 4.4. Closing remarks for the chapter are presented in Section 4.5.

4.2 System Model

With reference to Fig. 4.1, consider the SSC-SPC architecture over a fundamental three-node relay network, where the s-d, s-r, and r-d channels respectively denote the wireless channel between the source and destination, source and relay, and relay and destination nodes. Suppose a real-valued, continuous, Gaussian source is to be scalably encoded and transmitted to the destination via both the source (s-d) and relay (s-r, r-d) channels. At the source node, the Gaussian source is scalably encoded into two layers with successive refinement to enable two reconstruction resolutions at the destination node. Let the base and enhancement layers refer to specific portions of the source such that the base layer provides a lower resolution reconstruction, while both the base and enhancement layers are required to reconstruct the source at the higher resolution. Bitstreams for the base and enhancement layers are then respectively modulated into layer 1 and layer 2 of the SPC modulation, and superimposed to yield SPC symbols, each with total power E and allocation parameter β_1 such that $\beta_1 E$ and $(1-\beta_1)E$ are the respective powers for layer 1 and layer 2 of the SPC constellation. Note that although we consider only two layers in this work, the proposed model can be extended to a system with any number of layers at the expense of exponentially increased complexity.

Suppose the relay network operates under the most general transmission strategy, in which SPC broadcast occurs at the source node to both relay and destination nodes in the first transmission period, and the source keeps silent in the second transmission period while the relay launches the received data via SPC broadcast to the destination in a decode-and-forward manner to allow a possibly different power allocation. At the end of the first transmission period, the relay and destination nodes employ successive interference cancellation (SIC) to demodulate both layers.

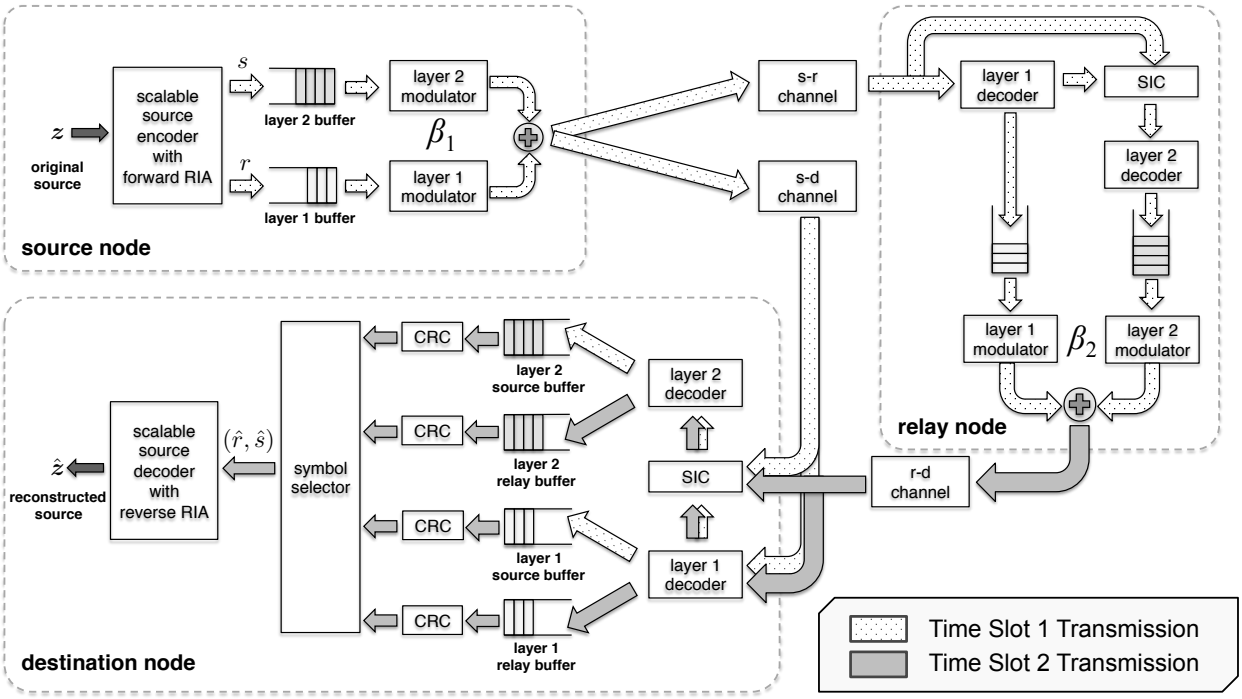

Figure 4.1: General coding structure of scalably encoded sources with successive refinement in overall framework for two layers.

An example of SIC decoding for the SCC-SPC pairing is given as follows. Let BPSK and QPSK be the respective modulation schemes for layer 1 and layer 2 of the SPC signal to illustrate the three stages of SPC decoding, whose constellation diagram is shown in Fig. 4.2 along with corresponding symbol-to-bit mapping. On the receiver side, the decoding of the received SPC signal first applies the BPSK demodulation by identifying whether the abscissa dimension is left or right of the origin. If layer 1 is correctly decoded as identified by error detection mechanisms, it is subtracted from the original received SPC signal, and then demodulated using the QPSK demodulator to obtain layer 2.

Once both layers are decoded, further processing occurs at both relay and destination nodes, as shown in Fig. 4.1. At the destination, bitstreams for the two layers are respectively stored in the layer 1 and layer 2 source buffers while at the relay, the buffered two layers are again modulated into SPC symbols at a power allocation parameter β_2 for

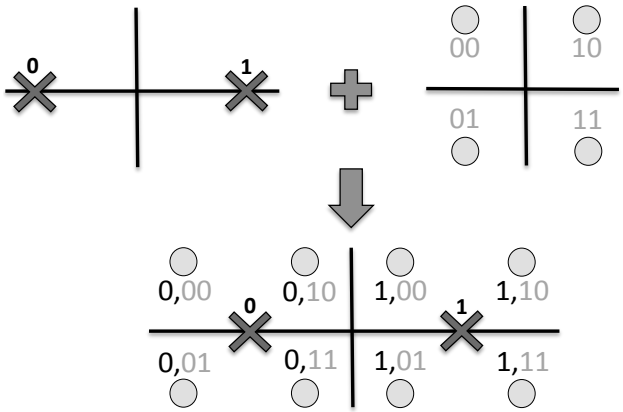

Figure 4.2: SPC encoding of BPSK and QPSK signals with corresponding symbol-to-bit mapping.

broadcast at the beginning of the second transmission period. The outputs from layer 1 and layer 2 decoders during the first and second transmission period are stored in corresponding buffers at the destination node. At the end of the second transmission period, bitstreams in the four buffers are further fed into individual CRC modules for error detection and then processed in the symbol selector. Based on the correctness of the layer 1 and layer 2 bitstreams obtained from the two transmission periods, there can be three possible outcomes: (i) error for both layers; (ii) error for layer 2 but a valid layer 1 bitstream; (iii) valid bitstreams for both layers. The source decoder then reconstructs the original source based on the outcome and valid bitstreams received from the symbol selector output.

By superimposing base layer and corresponding enhancement data in a single SPC broadcast, a notable advantage is that the enhancement layer data can be decoded only if the corresponding base layer is obtained, which effectively avoids the awkward situation where correctly-decoded enhancement layer bits cannot be used due to the loss of corresponding base layer data. This is thanks to the intrinsic nature of SIC-based SPC decoding, where layer 1 data must be correctly decoded before layer 2 data can be obtained. It has been well reported in [8] and [10] that such layered SSC-SPC structure yields merits in overcoming multi-user channel diversity in the scenario of large-scale multicast in which the transmitter cannot adapt its transmission rate with every receiver.

In addition to the additional hardware circuitry required for the implementation of SPC, the operation of the system in Fig. 4.1 is subject to some extra coordination and synchronization requirements among the three nodes. A real system would require minor time durations allocated for control signaling, which are necessary for the exchange of channel state information for each of the three channels in the network. Furthermore, the source node must also inform the relay on how to optimally configure its power allocation parameter. Lastly, since perfect time slot synchronization is difficult to achieve, each source symbol must be either indexed or labeled with added overhead to allow the symbol selector at the destination to wait for all four buffers to be populated with information corresponding to the same original source symbol before attempting reconstruction.

4.3 EED Model for Power Allocation

This section derives the EED model for the two-layer SSC-SPC architecture in the three-node network scenario. Forthcoming formulations are based upon the assumption of random index assignment similar to [6], and is positioned as the first analytical model for EED that exploits the logical mapping between the source and channel coding structures in relay networks under the SSC-SPC architecture.

4.3.1 Background of EED Derivation

Fading and path loss are the two major elements governing symbol error over wireless channels. This subsection serves as a background to further EED derivation by first formulating symbol error expressions for SIC-based SPC demodulation in presence of noisy wireless channels.

Suppose the Nakagami m-distribution [55] is used to model fading in a particular wireless channel with an average SNR $\overline{\gamma}$. Note that the m parameter varies the fading rapidity of the channel, and reduces the m-distribution to the Rayleigh slow fading channel when $m = 1$. The *pdf* and *cdf* of the Nakagami m-distributed instantaneous channel SNR

denoted by γ are given by:

$$f_\Gamma(\gamma) = \left(\frac{m}{\overline{\gamma}}\right)^m \frac{\gamma^{m-1}}{\Gamma(m)} \exp\left(-\frac{m}{\overline{\gamma}}\gamma\right); \tag{4.1}$$

$$F_\Gamma(\gamma) = \frac{\gamma(m, \frac{m}{\overline{\gamma}}\gamma)}{\Gamma(m)} = \frac{1 - \Gamma(m, \frac{m}{\overline{\gamma}}\gamma)}{\Gamma(m)}, \tag{4.2}$$

where $\gamma(\cdot,\cdot)$, and $\Gamma(\cdot,\cdot)$ are respectively the incomplete lower and upper gamma functions, and $\overline{\gamma}$ is the average *attenuated* receiver SNR (i.e. average SNR) such that $\overline{\gamma} = \frac{E}{N_0 d^\alpha} = \frac{E'}{N_0}$ once the total power of the SPC broadcast E is subject to AWGN power $\frac{N_0}{2}$ and path loss constant α at a distance d.

In general, the *pdf* in (4.1) can be divided into L fading categories indexed by l such that the receiver decodes up to layer l of the SPC broadcast whenever its channel SNR belongs to category l. Hence, category l encompasses the realized SNR range $[\gamma_{th,l}, \gamma_{th,l+1})$ for $0 \leq l \leq L-1$ and $[\gamma_{th,L}, \infty)$ for $l = L$. Each category corresponds to a realization probability p_l at an average categorial SNR $\overline{\gamma}_l$. Thus, the average channel SNR must satisfy

$$\overline{\gamma} = \sum_{l=0}^{L} p_l \overline{\gamma}_l. \tag{4.3}$$

For each category, the realization probability p_l and average SNR $\overline{\gamma}_l$ can also be derived using (4.2). Results of the derivations are presented as follows, where $\alpha_{th,l} = \frac{m}{\overline{\gamma}}\gamma_{th,l}$ is substituted for clarity:

$$p_l = \begin{cases} \frac{\gamma(m,\alpha_{th,l+1}) - \gamma(m,\alpha_{th,l})}{\Gamma(m)} & \text{if } 0 \leq l < L \\ \frac{\Gamma(m,\alpha_{th,l})}{\Gamma(m)} & \text{if } l = L \end{cases} \tag{4.4}$$

The corresponding average SNR for each category are expressed as follows:

$$\overline{\gamma}_l = \begin{cases} \overline{\gamma}\left[1 - \frac{1}{m}\frac{e^{-\alpha_{th,l+1}}\alpha_{th,l+1}^m - e^{-\alpha_{th,l}}\alpha_{th,l}^m}{\gamma(m,\alpha_{th,l+1}) - \gamma(m,\alpha_{th,l})}\right] & \text{if } 0 \leq l < L; \\ \overline{\gamma}\left[1 + \frac{1}{m}\frac{e^{-\alpha_{th,L}}\alpha_{th,L}^m}{\Gamma(m,\alpha_{th,L})}\right] & \text{if } l = L. \end{cases} \tag{4.5}$$

The SNR boundary $\gamma_{th,l}$ that defines the layer l channel category is set to the minimum SNR such that the error probability of layer l, $p_{err,l}$, satisfies $p_{err,l} < \epsilon_{th}$, where ϵ_{th} is any arbitrary maximum error threshold defined or tolerable by the application or hardware decoder. Note that $\gamma_{th,l}$ is a function of $p_{err,l}$ and hence, is also a function of the power allocated for layer l in the SPC broadcast.

Symbol error expression governed by the average SNR can now be derived for each channel category. Although symbol error formulations have been previously derived in [56] for any general SIC-based multi-level SPC constellations, we only need to consider the special two-layer SSC-SPC case such that $L = 2$. Define the error probabilities for layer 1 and layer 2 from SIC-based SPC demodulation as the base layer symbol error (BSE) and compound symbol error (CSE), respectively. Their expressions have been extensively studied and derived in [57] and are briefly summarized below for use in conjunction with further analytical models to appear.

For each channel category, its BSE and CSE can be derived based on the categorial average SNR $\overline{\gamma}_l = \frac{E'}{N_0}$ subject to AWGN power $\frac{N_0}{2}$. Let $E_1 = \beta E'$ and $E_2 = (1-\beta)E'$, where β is any power allocation configuration for any two-layer SPC transmission employing m_1-QAM and m_2-QAM for layers 1 and 2, respectively. Each SPC symbol can thus be represented by a (x_i, x'_j) pair, respectively denoting the random variable representing the symbol's abscissa and ordinate position in a signal constellation illustrated in Fig. 4.3:

$$x_i \sim N\left(z_1(i)\sqrt{\tfrac{E_1}{\alpha_{m_1}}} + z_2(i)\sqrt{\tfrac{E_2}{\alpha_{m_2}}}, \tfrac{N_0}{2}\right), \tag{4.6}$$

$$x'_j \sim N\left(z'_1(j)\sqrt{\tfrac{E_1}{\alpha_{m_1}}} + z'_2(j)\sqrt{\tfrac{E_2}{\alpha_{m_2}}}, \tfrac{N_0}{2}\right), \tag{4.7}$$

for two scenarios

$$\left\{i, j \in \mathbb{N}^0 | i \leq I = \sqrt{m_2} - 1, j \leq J = \tfrac{1}{2}\sqrt{m_2} - 1\right\}, \tag{4.8}$$

$$\left\{i, j \in \mathbb{N}^0 | i, j \leq I = J = \sqrt{\tfrac{m_1 m_2}{4}} - 1\right\}, \tag{4.9}$$

where α_{m_1} and α_{m_2} are coefficients to normalize the symbol energy for layer 1 and layer 2 to E_1 and E_2, respectively. α_{m_1}, α_{m_2} and z are summarized in [57].

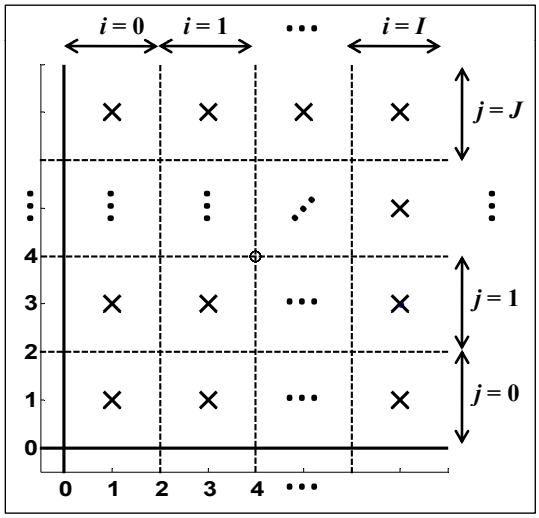

Figure 4.3: First quadrant of general m_1-QAM/m_2-QAM SPC symbol constellation with decision regions indexed by i and j.

Recall the SIC-based SPC demodulation process. In the first stage, an m_1-QAM detector attempts recovery of the layer 1 bitstream. Define $P_{i,1}$ and $P'_{j,1}$ as the correctness probability, which is the probability that the respective abscissa and ordinate components of the SPC symbol, located in region i and j, is found inside its correct layer 1 decision region, respectively. The average BSE of the SPC symbol is then expressed as:

$$p_{err,1} = 1 - \tfrac{4}{m_1 m_2} \sum_{i,j} P_{i,1} P'_{j,1}. \tag{4.10}$$

If layer 1 is correctly decoded, the m_2-QAM detector decodes the post-SIC signal for the layer 2 bitstream with a conditional error probability denoted by $p_{m_2\text{-QAM}}$. The CSE can then be expressed as follows, reflecting its dependency on the BSE:

$$p_{err,2} = 1 - (1 - p_{m_2\text{-QAM}})\,(1 - p_{err,1})\,. \tag{4.11}$$

It should be noted that each SPC symbol has a non-uniform error probability at each point in the signal constellation diagram. Specifically in Fig. 4.3, points in the set $\{(x_i, x'_j) : i <$

$I, j < J\}$ have different error probabilities than points located in regions indexed by $i = I$ or $j = J$. Hence, (4.10)-(4.11) are simply averages of the error probability of all points, corresponding to the assumption that each point is equally likely to occur.

The derivations in this subsection are applicable to all channels. To distinguish between the *s-d*, *s-r*, and *r-d* channels, the superscript notation is adopted such that $p^y_{err,1}$ and $p^y_{err,2}$ respectively denotes the BSE and CSE for channel y, where $y \in \{sd, sr, rd\}$. The same notation is applied for $\overline{\gamma}^y_l$ and p^y_l to denote the average SNR and realization probability of category l along channel y.

4.3.2 Proposed EED Model

The proposed EED model aims to quantify the distortion between the original source and its reconstruction at the destination, which is solely determined by the conditions of the three wireless channels. Accordingly, the destination node is subject to a number of channel realization types (RTs) governed by the information received and decoded from both source and relay channels.

The possible RTs are summarized in Table 4.1, in which three groups are classified according to the relay channel condition: Group $\mathcal{A}$ RTs fail in decoding layer 1 of the SPC symbol from the relay such that the entire information is lost; Group $\mathcal{B}$ RTs can only decode layer 1 from the relay but fails in decoding layer 2; and Group $\mathcal{C}$ RTs can decode both layers from the relay channel and obtain complete information from the received SPC symbol. Each group can be further classified according to the *s-d* channel condition in the same way, where a total of nine end-to-end RTs exist as shown in the table.

Let each of the RTs be indexed by k. The expected EED is the summation of the EED of each RT weighted by its corresponding probability:

$$\bar{D} = \sum_k \tilde{p}_k D_k, \tag{4.12}$$

where $\tilde{p}_k$ denotes the realization probability of RT k and satisfies $\sum \tilde{p}_k = 1$. Expressions

for the set of $\tilde{p}_k$ are expressed as follows in terms of expressions from (4.4):

$$\tilde{p}_{\mathcal{A}_i} = p_i^{sd}\left[p_0^{sr} + (1-p_0^{sr})p_0^{rd}\right], \tag{4.13}$$

$$\tilde{p}_{\mathcal{B}_i} = p_i^{sd}\left[p_1^{sr}(1-p_0^{rd}) + p_2^{sr}p_1^{rd}\right], \tag{4.14}$$

$$\tilde{p}_{\mathcal{C}_i} = p_i^{sd}p_2^{sr}p_2^{rd}, \tag{4.15}$$

where $i = 0, 1, 2$.

Derivation of the EED for each RT, D_k, first requires two EED formulations: one for the RT that is able to reconstruct the original source at the lower resolution, and the other for that at the higher resolution. Denote the original real-valued source as $\boldsymbol{z}$, a k-dimensional real-valued vector source over the Euclidean space Λ with a probability density function $f(\boldsymbol{z})$, zero mean, and variance per dimension $\sigma^2 = \frac{1}{k}\int_\Lambda \|\boldsymbol{z}\|^2 f(\boldsymbol{z})d\boldsymbol{z}$.

Referring back to Fig. 4.1, suppose $\boldsymbol{z}$ is to be encoded into a scalably encoded two-resolution source using a two-resolution vector quantizer for transmission over an arbitrary discrete memoryless broadcast channel with CRC, and characterized by a matrix of transition probabilities $\Pr\{(\hat{r},\hat{s})|(r,s)\}$, where (r,s) and $(\hat{r},\hat{s})$ respectively denote the channel input and output symbols. For the base layer, the source quantizer partitions Λ into N_1 disjoint regions denoted by $\{A_1, \cdots, A_{N_1}\}$, and represents them with respective codeword vectors $\{\boldsymbol{z}_1, \cdots, \boldsymbol{z}_{N_1}\}$. For the enhancement layer, the quantizer further partitions each of the N_1 regions into N_2 subregions denoted by $\{A_{i1}, \cdots, A_{iN_2}\}$, and represents them with respective codeword vectors $\{\boldsymbol{z}_{i1}, \cdots, \boldsymbol{z}_{iN_2}\}$. Let $i = 1, \cdots, N_1$ and $j = 1, \cdots, N_2$ index

Table 4.1: RTs based on base (B) or enhancement (E) layer received (✓) or lost (×) from source or relay channels.

Group:	$\mathcal{A}$			$\mathcal{B}$			$\mathcal{C}$		
RT $k=$	$\mathcal{A}_0$	$\mathcal{A}_1$	$\mathcal{A}_2$	$\mathcal{B}_0$	$\mathcal{B}_1$	$\mathcal{B}_2$	$\mathcal{C}_0$	$\mathcal{C}_1$	$\mathcal{C}_2$
B (source)	×	✓	✓	×	✓	✓	×	✓	✓
E (source)	×	×	✓	×	×	✓	×	×	✓
B (relay)	×	×	×	✓	✓	✓	✓	✓	✓
E (relay)	×	×	×	×	×	×	✓	✓	✓

the codeword vectors of the base and enhancement layers, respectively. The original source $\boldsymbol{z}$ is thus represented by (i, j) such that the receiver able to decode i reconstructs $\boldsymbol{z}$ at the lower resolution, while decoding both i and j enables the higher resolution reconstruction of $\boldsymbol{z}$.

Let $\pi_t(i, j) = (\pi_{tb}(i), \pi_{te}(j|i)) = (r, s)$ be a particular index assignment mapping (i, j) to (r, s) in a one-to-one manner such that $i \in \{1, \cdots, N_1\} = m_{\rm b}$ and $j \in \{1, \cdots, N_2\} = m_2$ are mapped to $r \in m_{\rm b}$ and $s \in m_2$, respectively. The broadcast channel takes $(r, s) \in m_{\rm b} \times m_2 = m_{\rm e}$ as input and outputs $(\hat{r}, \hat{s}) \in \{r, {\rm e}\} \times \{s, {\rm e}\}$, where e indicates detected error. Define $\tilde{p}_{err,1} \triangleq \Pr\{\hat{r} = {\rm e}\}$ and $\tilde{p}_{err,2} \triangleq \tilde{p}_{err,1} + \Pr\{\hat{r} = r, \hat{s} = {\rm e}\}$ such that $(1 - \tilde{p}_{err,2}) = \Pr\{\hat{r} = r, \hat{s} = s\}$, where $\tilde{p}_{err,w}$ denotes the error probability of decoding up to layer w. With the assumption that (r, s) is uniformly distributed over $m_{\rm e}$, where $|m_{\rm e}| = N_1 N_2$ given $\{\Pr((\hat{r}, \hat{s})|(r, s))\}$, we have

$$\tilde{p}_{err,1} = \frac{1}{N_1 N_2} \sum_{r=1}^{N_1} \sum_{s=1}^{N_2} \Pr\left\{\hat{r} = {\rm e}|(r, s)\right\},$$

$$\tilde{p}_{err,2} = \tilde{p}_{err,1} + \frac{1}{N_1 N_2} \sum_{r=1}^{N_1} \sum_{s=1}^{N_2} \Pr\left\{(r, \hat{s} = e)|(r, s)\right\}.$$

Based on the symbol selector output given $(\hat{r}, \hat{s})$, the receiver has three possible outputs: $\boldsymbol{z}_{ij}$ if $\hat{r} \neq {\rm e}$, $\hat{s} \neq {\rm e}$; $\boldsymbol{z}_i$ if $\hat{r} \neq {\rm e}$, $\hat{s} = {\rm e}_2$; and $E[\boldsymbol{z}]$ if $\hat{r} = {\rm e}$. Given π_t, the crossover error probabilities from codeword vector $\boldsymbol{z}_{ij}$ to each of the three outputs are related to the channel transition error probabilities as follows:

$$p_e^{\pi_t}(\boldsymbol{z}_{ij}|\boldsymbol{z}_{ij}) = \Pr\{(r, s)|(r, s)\};$$
$$p_e^{\pi_t}(\boldsymbol{z}_i|\boldsymbol{z}_{ij}) = \Pr\{(r, \hat{s} = {\rm e})|(r, s)\};$$
$$p_e^{\pi_t}(E[\boldsymbol{z}]|\boldsymbol{z}_{ij}) = \Pr\{\hat{r} = {\rm e}_1|(r, s)\}.$$

Note that output of the source mean $E[\boldsymbol{z}]$ when error is detected in the base layer information was shown to be optimal in [6] for random index assignments.

The EED is defined as the mean squared error distortion between $\boldsymbol{z}$ and $\hat{\boldsymbol{z}} \in \{\boldsymbol{z}_{ij}, \boldsymbol{z}_i, E[\boldsymbol{z}]\}$.

Hence, with the codeword crossover probabilities defined as above for some given index assignment π_t, the EED is expressed as follows:

$$\begin{aligned} D_h^{\pi_t} \triangleq & \frac{1}{k}\sum_{i,j}\int_{z\in A_{ij}} \|\boldsymbol{z}-\boldsymbol{z}_{ij}\|^2 p_e^{\pi_t}(\boldsymbol{z}_{ij}|\boldsymbol{z}_{ij}) f(\boldsymbol{z}) d\boldsymbol{z} \\ & + \frac{1}{k}\sum_{i,j}\int_{z\in A_{ij}} \|\boldsymbol{z}-\boldsymbol{z}_{i}\|^2 p_e^{\pi_t}(\boldsymbol{z}_{i}|\boldsymbol{z}_{ij}) f(\boldsymbol{z}) d\boldsymbol{z} \\ & + \frac{1}{k}\sum_{i,j}\int_{z\in A_{ij}} \|\boldsymbol{z}\|^2 p_e^{\pi_t}(E[\boldsymbol{z}]|\boldsymbol{z}_{ij}) f(\boldsymbol{z}) d\boldsymbol{z}. \end{aligned} \tag{4.16}$$

Now consider an uniform random selection of the index assignment mapping π_t over all possible $(N_1!)(N_2!)^{N_1}$ assignment mappings. Expectation taken over π_t for each of the codeword crossover error probabilities are summarized as follows:

$$\begin{aligned} E_{\pi_t} p_e^{\pi_t}(E[\boldsymbol{z}]|\boldsymbol{z}_{ij}) &= \frac{(N_1-1)!(N_2-1)!(N_2!)^{N_1-1}}{(N_1!)(N_2!)^{N_1}} \\ &\quad \times \sum_{r=1}^{N_1}\sum_{s=1}^{N_2} \Pr\{\hat{r}=\mathrm{e}|(r,s)\} \\ &= \tilde{p}_{err,1}; \end{aligned} \tag{4.17}$$

$$\begin{aligned} E_{\pi_t} p_e^{\pi_t}(\boldsymbol{z}_i|\boldsymbol{z}_{ij}) &= \frac{(N_1-1)!(N_2-1)!(N_2!)^{N_1-1}}{(N_1!)(N_2!)^{N_1}} \\ &\quad \times \sum_{r=1}^{N_1}\sum_{s=1}^{N_2} \Pr\{(r,\hat{s}=\mathrm{e}|(r,s)\} \\ &= \tilde{p}_{err,2} - \tilde{p}_{err,1}. \end{aligned} \tag{4.18}$$

Finally, substitute (4.17)-(4.18) into $D_h \triangleq E_{\pi_t} D_h^{\pi_t}$, which denotes the EED averaged

over all possible π_t as follows:

$$\begin{aligned} D_h &= (1-\tilde{p}_{err,2})\frac{1}{k}\sum_{i,j}\int_{z\in A_{ij}}\|\boldsymbol{z}-\boldsymbol{z}_{ij}\|^2 f(\boldsymbol{z})d\boldsymbol{z} \\ &\quad + (\tilde{p}_{err,2}-\tilde{p}_{err,1})\frac{1}{k}\sum_{i}\int_{z\in A_{i}}\|\boldsymbol{z}-\boldsymbol{z}_{i}\|^2 f(\boldsymbol{z})d\boldsymbol{z} \\ &\quad + (\tilde{p}_{err,1})\frac{1}{k}\sum_{i,j}\int_{z\in A_{ij}}\|\boldsymbol{z}\|^2 f(\boldsymbol{z})d\boldsymbol{z} \\ &= D_{Q_h}(1-\tilde{p}_{err,2}) + D_{Q_l}(\tilde{p}_{err,2}-\tilde{p}_{err,1}) + \sigma^2\tilde{p}_{err,1}. \end{aligned} \tag{4.19}$$

For the receiver seeking only lower resolution reconstruction, the substitution of $\tilde{p}_{err,2}=1$ in the above equation yields

$$D_l = D_{Q_l}(1-\tilde{p}_{err,1}) + \sigma^2\tilde{p}_{err,1}. \tag{4.20}$$

Under random index assignment, (4.19) and (4.20) are closed-form, non-asymptotic, evaluations of the EED for the receiver able to reconstruct the source at the lower and higher resolutions, respectively, with $\tilde{p}_{err,w}$ denoting the average error probability for the receiver to decode up to layer w, and D_{Q_l} and D_{Q_h} the quantization distortion from the reconstruction of $\boldsymbol{z}$ at the lower and higher resolutions, respectively. Note that (4.19)-(4.20) are applicable to the transmission of any real-valued continuous source with variance σ^2 after being scalably encoded into two resolutions characterized by D_{Q_l} and D_{Q_h}, and are obviously variations of the formulations from earlier chapters.

In this chapter, we consider the transmission of a real-valued, unity variance Gaussian source over the three-node decode-and-forward relay network. As our focus at this point turns to capture the effect of the relay channel on the system EED, we approximate the quantization distortion of the source by its rate-distortion function $D_Q = 2^{-2R}$, when R bits describe each symbol. Although use of the rate-distortion function to describe the quantization distortion is only achievable in the infinity limit of the source coding rate, we still maintain our non-asymptotic assumption on the channel side by capturing the nonzero error probabilities of the channel for channel codes with finite block lengths.

The channels of the considered three-node relay network are independent and characterized by BSE and CSE expressions as derived in Section 4.3.1. Thus, the EED for a particular RT k can be expressed by either (4.19) or (4.20) depending on its capability of decoding up to layer w at the destination node with error probability $\tilde{p}_{err,w}^{k}$. At the destination node, RT k able to decode up to layer w would obtain a rate of $\sum_{j=1}^{w} R_j$ [9], where R_j is the rate chosen to represent layer j of the scalably encoded source.

We begin with the most general RT $k = \mathcal{C}_2$, where all $L = 2$ layers of the SSC-SPC architecture are decodable from both source and relay channels for an EED expressed as:

$$\begin{aligned} D_{\mathcal{C}_2} = {} & 2^{-2(R_1+R_2)} \left(1 - \tilde{p}_{err,2}^{\,\mathcal{C}_2}\right) \\ & + 2^{-2R_1} \left(\tilde{p}_{err,2}^{\,\mathcal{C}_2} - \tilde{p}_{err,1}^{\,\mathcal{C}_2}\right) + \sigma^2 \tilde{p}_{err,1}^{\,\mathcal{C}_2}, \end{aligned} \tag{4.21}$$

where

$$\tilde{p}_{err,2}^{\,\mathcal{C}_2} = p_{err,2}^{sd} \left[1 - (1 - p_{err,2}^{sr})(1 - p_{err,2}^{rd})\right], \tag{4.22}$$

$$\tilde{p}_{err,1}^{\,\mathcal{C}_2} = p_{err,1}^{sd} \left[1 - (1 - p_{err,1}^{sr})(1 - p_{err,1}^{rd})\right], \tag{4.23}$$

and $R_1 = \log_2 m_1$ and $R_2 = \log_2 m_2$ are the respective number of bits allocated for the base and enhancement layers per source symbol under the two-layer SSC-SPC architecture.

EED expressions for the remaining eight RTs are in reduced forms of the most general RT given in (4.21). For RT $k = \mathcal{C}_1$, layer 2 is lost along the source channel for an EED identical to (4.21) with:

$$\tilde{p}_{err,2}^{\,\mathcal{C}_1} = 1 - (1 - p_{err,2}^{sr})(1 - p_{err,2}^{rd}); \tag{4.24}$$

$$\tilde{p}_{err,1}^{\,\mathcal{C}_1} = p_{err,1}^{sd} \left[1 - (1 - p_{err,1}^{sr})(1 - p_{err,1}^{rd})\right]. \tag{4.25}$$

Similarly for RT $k = \mathcal{C}_0$ when both layers are lost on the s-d channel,

$$\tilde{p}_{err,2}^{\,\mathcal{C}_0} = 1 - (1 - p_{err,2}^{sr})(1 - p_{err,2}^{rd}), \tag{4.26}$$

$$\tilde{p}_{err,1}^{\,\mathcal{C}_0} = 1 - (1 - p_{err,1}^{sr})(1 - p_{err,1}^{rd}). \tag{4.27}$$

For RTs in Group $\mathcal{B}$, only layer 2 is decodable from the relay channel. For RT $k = \mathcal{B}_2$ where both layers are still decoded from the source channel, the EED is given by:

$$\begin{aligned} D_{\mathcal{B}_2} &= 2^{-2(R_1+R_2)} \left(1 - p_{err,2}^{sd}\right) \\ &\quad + 2^{-2R_1} \left(p_{err,2}^{sd} - \tilde{p}_{err,1}^{\mathcal{B}_2}\right) + \sigma^2 \tilde{p}_{err,1}^{\mathcal{B}_2}, \end{aligned} \tag{4.28}$$

where

$$\tilde{p}_{err,1}^{\mathcal{B}_2} = p_{err,1}^{sd} \left[1 - (1 - p_{err,1}^{sr})(1 - p_{err,1}^{rd})\right]. \tag{4.29}$$

RT $k = \mathcal{B}_1$ loses only layer 2 while RT $k = \mathcal{B}_0$ loses both layers from the source channel. The EEDs for each are expressed as:

$$\begin{aligned} D_{\mathcal{B}_1} &= 2^{-2R_1} \left(1 - p_{err,1}^{sd} \left[1 - (1 - p_{err,1}^{sr})(1 - p_{err,1}^{rd})\right]\right) \\ &\quad + \sigma^2 p_{err,1}^{sd} \left[1 - (1 - p_{err,1}^{sr})(1 - p_{err,1}^{rd})\right]; \end{aligned} \tag{4.30}$$

$$\begin{aligned} D_{\mathcal{B}_0} &= 2^{-2R_1} (1 - p_{err,1}^{sr})(1 - p_{err,1}^{rd}) \\ &\quad + \sigma^2 \left[1 - (1 - p_{err,1}^{sr})(1 - p_{err,1}^{rd})\right]. \end{aligned} \tag{4.31}$$

When the RTs in Group $\mathcal{A}$ lose both layers from the relay channel, the EED expressions simplify further:

$$\begin{aligned} D_{\mathcal{A}_2} &= 2^{-2(R_1+R_2)} \left(1 - p_{err,2}^{sd}\right) \\ &\quad + 2^{-2R_1} \left(p_{err,2}^{sd} - p_{err,1}^{sd}\right) + \sigma^2 p_{err,1}^{sd}; \end{aligned} \tag{4.32}$$

$$D_{\mathcal{A}_1} = 2^{-2R_1} \left(1 - p_{err,1}^{sd}\right) + \sigma^2 p_{err,1}^{sd}; \tag{4.33}$$

$$D_{\mathcal{A}_0} = \sigma^2. \tag{4.34}$$

Although the derived EED model is for only the two-layer SSC-SPC pairing, the system can be straightforwardly extended to any number of layers at the expense of significantly higher complexity due to the increased number of channel types with the number of layers. For example, a system with three or four layers has 16 or 25 channel types, respectively.

4.3.3 Power Allocation Optimization

Section 4.3.2 detailed a comprehensive EED derivation of the SSC-SPC architecture depicted in Fig. 4.1 under the fundamental three-node relay network. From given channel statistics of the *s-d*, *s-r*, and *r-d* channels as well as the rates of the two layers at the source, we seek to optimally configure the SPC power allocation parameters at the source and relay nodes, respectively denoted by β_1 and β_2. Formally, the optimization problem is defined as follows:

$$\underset{\beta_1,\beta_2}{\text{minimize}} \quad \sum_k \tilde{p}_k D_k, \tag{4.35}$$

where D_k is the EED for RT k. Due to the unfortunate complexity of the EED model, we solve the power allocation optimization problem through a numerical search method in the next section.

4.4 Numerical Evaluation

In this section, the proposed EED model is applied from two perspectives to justify a variety of concepts employed in the entire system model. We first demonstrate its advantage in EED reductions by using the SSC-SPC architecture in the considered three-node relay network in comparison to a number of counterparts. We then perform power allocation optimization based on the developed EED model via numerical analysis, and demonstrate the performance impairment on the EED in the event that the same task is performed on a traditional abstract channel capacity formulation.

4.4.1 SSC-SPC versus Conventional Schemes

We first demonstrate achievable gains through the unique application of the SSC-SPC architecture in a relay network against a number of variations, including a mono-modulated

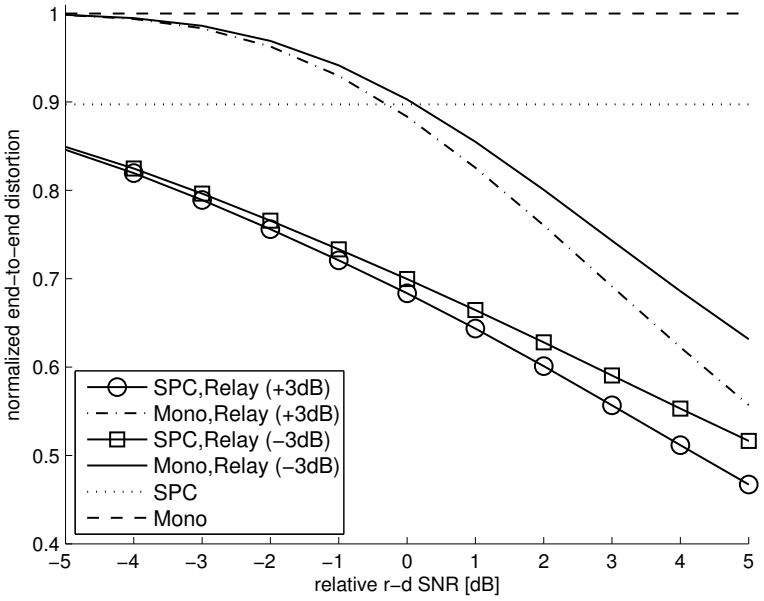

Figure 4.4: Normalized EED under *poor* source channel majority and relative *s*-*r* channel SNR $= -3, +3$ dB.

system with and without the relay node, and an SPC-modulated system without the relay. Performance gains are quantified in terms of EED reductions under various network conditions.

In the numerical evaluation, we consider the employment of two-layered SPC with BPSK ($m_1 = 2$) and QPSK ($m_2 = 4$) selected as layer 1 and layer 2 to modulate the base and enhancement layers of the scalably encoded source, respectively. Whenever applicable, the SPC power allocation parameters β_1 and β_2 are configured to minimize the EED based on the optimization problem stated in (4.35). All three *s*-*d*, *s*-*r*, and *r*-*d* channels are modeled under the Nakagami m-distribution with $m = 1$. Division of each channel into categories as outlined in Section 4.3.1 is based on $\epsilon_{th} = 10^{-3}$. When considering schemes with no relay, the source node transmits each symbol twice to achieve a fair comparison to the proposed system model.

We examine four scenarios with respect to varying *r*-*d* channels as shown in Fig. 4.4-4.5, each with good (or poor) *s*-*d* and *s*-*r* channels. Specifically within each figure, results

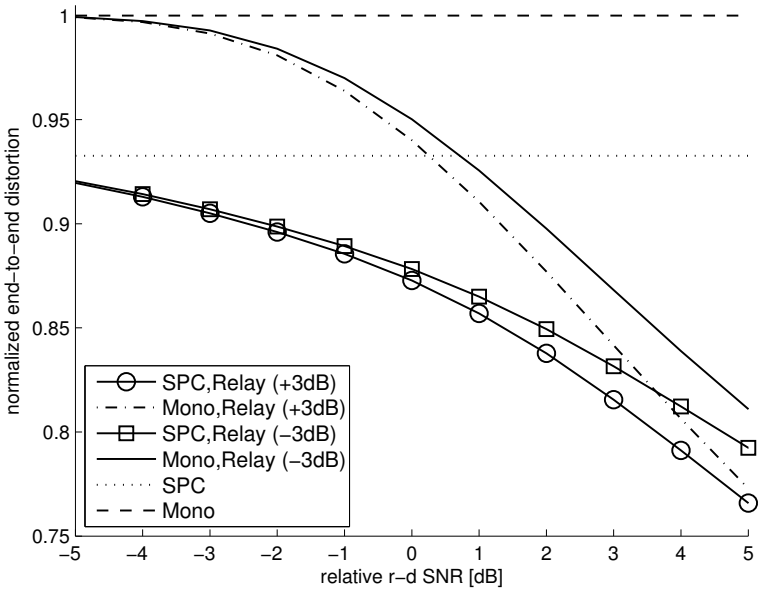

Figure 4.5: Normalized EED under *good* source channel majority and relative s-r channel SNR $= -3, +3$ dB.

involving the relay node considers an average SNR along the s-r channel that is -3 dB or $+3$ dB relative to the s-d channel, while average SNRs for the s-d channel itself are chosen to vary its proportion of faded channel categories captured through p_0^{sd}, p_1^{sd}, and p_2^{sd} along the source channel: either the poor channel majority corresponding to $p_0^{sd} > 2\left(p_1^{sd} + p_2^{sd}\right)$, or good channel majority corresponding to $p_2^{sd} > 2\left(p_0^{sd} + p_1^{sd}\right)$. The system EED is examined with respect to varying the average SNR of the r-d channel from -5 dB to $+5$ dB relative to that of the s-d channel.

Four schemes are examined in each scenario: (i) mono modulation without relay; (ii) SSC-SPC without relay; (iii) mono modulation with relay; and (iv) SSC-SPC with relay. All results are normalized according to the results of (i). From Fig. 4.4 and Fig. 4.5, it is clear that scenario (iv), where deployment of the SSC-SPC architecture is considered over the three-node relay network, the EED of the system can be considerably reduced from the other schemes.

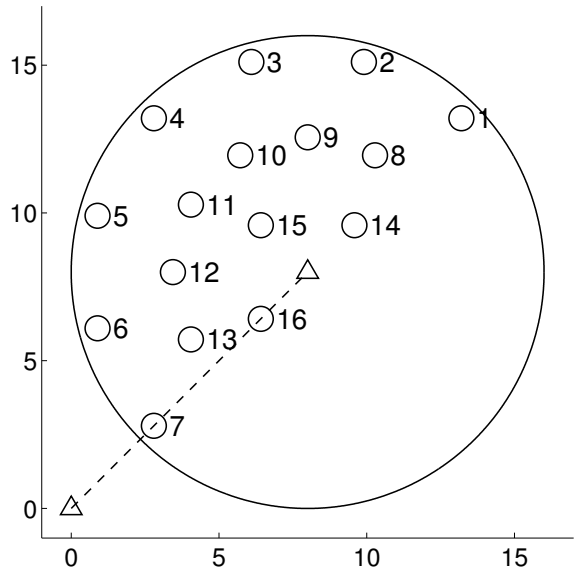

Figure 4.6: Topology of source and relay nodes (△), and considered destination nodes (◯).

4.4.2 Power Allocation: EED versus Capacity

This subsection provides comparison results between the proposed EED model and a traditional distortion model based on the abstract concept of channel capacity through the optimal configuration of SPC power allocation pair (β_1, β_2). We demonstrate the degraded EED performance that results due to the use of the abstract model in disregarding symbol losses caused by wireless channel conditions. The capacity-based distortion (CBD) model for the two-layered SSC-SPC architecture is summarized in [58].

We extend the study of the proposed model in the previous section to a practical network topology shown in Fig. 4.6, where the source and relay nodes are respectively located at $(0, 0)$ and $(8, 8)$, while considering 16 possible positions for the destination node within proximity of the semi-circle (due to symmetry). The 16 points in the figure correspond to 16 pairs of s-d and r-d channel SNRs, which are governed by a path loss constant of $\alpha = 3$ and a relay transmit power 3 dB below that of the source node. Let (β_1', β_2') and (β_1^*, β_2^*) denote the optimizers for the CBD and EED model, respectively.

Analysis of the CBD model is first conducted over all possible power allocation config-

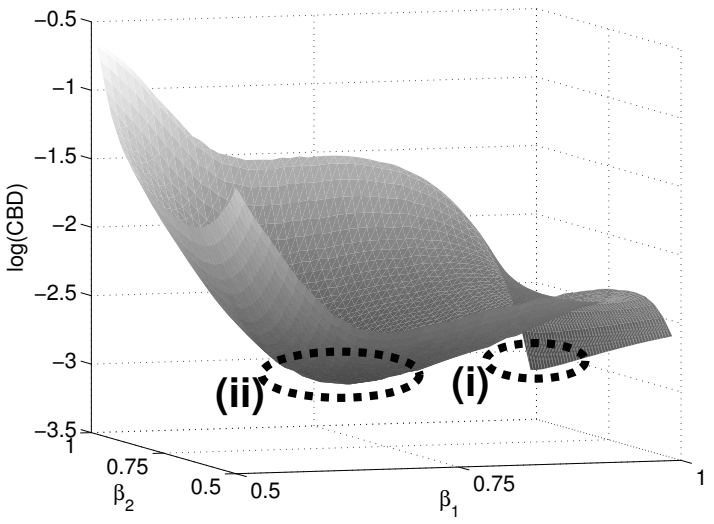

Figure 4.7: General behaviour of the capacity-based distortion measure.

urations, as shown in Fig. 4.7 for a particular destination node 12. It is representative of the behaviour of CBD over all possible power allocation configurations for any destination node in that it is non-convex and has a global optimizer located at one of two possible local minimizers. As annotated on Fig. 4.7, these two local minimizers for the CBD always occur under two competing power allocation configurations: (i) $\beta_1 \approx 1$, $\beta_2 \approx 1$; (ii) $\beta_1 \approx \frac{2}{3}$, $\beta_2 \approx \frac{2}{3}$. In (i), all power is allocated for layer 1, whereas in (ii), the power allocation favors a balance between layer 1 and layer 2 to minimize distortion while accounting for the dependency of layer 2 on layer 1.

The minimized CBD for these two configurations vary depending on network channel conditions, but since the CBD model disregards channel errors, the two local optimizer pairs always occur very close to the (β_1, β_2) values defined by the two configurations. The global optimizer pair (β_1', β_2') is thus one of the two above configurations that achieves a lower distortion depending on the network channel conditions. Configuration (i) yields lower CBD when the *s-d* channel is particularly poor (nodes 1-5, 8-11) to focus all available channel resources to secure layer 1, in contrast to the scenario where either the source or relay channel are at least in moderate conditions to favor configuration (ii).

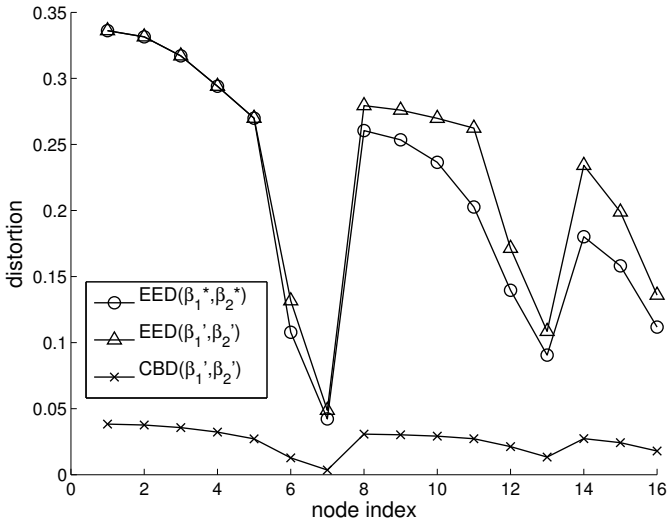

Node	Gap
1-5	0%
6	22.1%
7	15.6%
8	7.3%
9	8.9%
10	14.1%
11	29.5%
12	22.8%
13	19.9%
14	30.0%
15	25.8%
16	21.6%

Figure 4.8: Distortion and gap between CBD and EED models for each node.

Fig. 4.8 plots the minimum CBD and EED achieved through the optimal configuration of the power allocation parameter pair (β_1, β_2) for each of the 16 destination node positions. It is immediately clear and expected that the minimized distortion derived in CBD is significantly lower than that by the proposed EED model for all destinations; since the CBD is based on the channel capacity without taking symbol losses over the noisy wireless channels into consideration, it can only serve as a very rough lower bound on the distortion experienced by the end-receiver.

Fig. 4.8 also demonstrates the suboptimal EED performance that occurs if the optimizers for CBD, (β_1', β_2'), were awkwardly applied in the derived EED model, yielding gaps that could be as high as 30% for certain destination locations. Such behaviour is expected, since solving the power allocation problem according to the CBD model ignores the loss of source symbols over the wireless channels. Moreover, the CBD model is based on the channel capacities of each channel as opposed to any specific employed modulation schemes. Hence, configuration of power allocation based on CBD is demonstrated to be suboptimal in terms of the EED performance at the destination node, which has been appropriately quantified by the proposed EED model.

Table 4.2: Optimal (β_1, β_2) parameters for the CBD and EED models.

Nodes	**Network Channel Conditions (NC)**	**CBD**		**EED**	
		β_1'	β_2'	β_1^*	β_2^*
(a) 1-5	poor *s-d* and *r-d*	≈ 1	≈ 1	≈ 1	≈ 1
(b) 6-7	good *s-d*, poor *r-d*	$\approx \frac{2}{3}$	$\approx \frac{2}{3}$	0.75	0.77
(c) 8-11	poor *s-d*, moderate *r-d*	≈ 1	≈ 1	0.79-0.85	0.85
(d) 12-13	moderate *s-d* and *r-d*	$\approx \frac{2}{3}$	$\approx \frac{2}{3}$	0.74	0.85
(e) 14-16	good *r-d*	$\approx \frac{2}{3}$	$\approx \frac{2}{3}$	0.74-0.82	0.96

Behaviour of the gap from optimality when employing (β_1', β_2') as opposed to (β_1^*, β_2^*) can be split into five categories according to the network conditions (NCs). Table 4.2 depicts the five NCs upon which each of the 16 nodes belongs: (a) nodes 1-5; (b) nodes 6-7; (c) nodes 8-11; (d) nodes 12-13; and (e) nodes 14-16. The nodes that belong in NC(a) exhibit zero gap between the CBD and EED model. In such scenario, the conditions of both the source and relay channel are very poor such that the optimal solution for both models targets to allocate nearly all power for layer 1 for $\beta_1 \approx 1$ and $\beta_2 \approx 1$. Therefore, the resultant EED performance is the same under identical optimal power allocation configurations, hence yielding zero gap between the results of the CBD and EED models.

In NC(b), NC(d), and NC(e), the CBD model results in configuration (ii) (i.e., $\beta_1 \approx \frac{2}{3}$, $\beta_2 \approx \frac{2}{3}$) as the global optimizer attempts to a moderate balance between layer 1 and layer 2 power allocation, which also occurs in the EED model but at different (β_1^*, β_2^*). Disregarding symbol loss caused by the noisy channel in CBD yields a suboptimal power allocation configuration, resulting in potentially non-trivial gaps between the CBD and EED models. Nodes in NC(c) have the same *r-d* channel condition as NC(d), but with poorer *s-d* channels which forces the CBD to a slightly lower distortion with configuration (i) (i.e., $\beta_1 \approx 1$, $\beta_2 \approx 1$) instead of (ii). On the other hand, the accounting for symbol losses in the EED model results in optimal (β_1^*, β_2^*) values within the range of NC(b), NC(d), and NC(e).

Lastly, β_2^* for the EED model is seen in Table 4.2 to behave in an interesting manner that warrants some discussion. When the r-d channel is poor, it is expected that β_2^* should occur near unity to better secure layer 1 information. For nodes with a moderate r-d channel, however, some of the channel resources are transferred from layer 1 to layer 2 for β_2^* to fall within 0.77-0.85. It may thus be surprising that as the r-d channel further improves, β_2^* begins to asymptotically approach unity once again. This phenomenon occurs because improving the r-d channel reduces both its BSE and CSE; however, the absolute reductions to the CSE are much larger than BSE since the BSE is already asymptotically small in high r-d channel SNRs. Since increasing β_2 trades increased CSE for reduced BSE, β_2^* increases to allow for a more balanced reduction of both BSE and CSE in reducing EED. Such behavior is observed for nodes in NC(e) with $\beta_2^* = 0.96$.

4.5 Summary

This chapter investigates a layered joint source-channel coding architecture realized through the coupling of scalable source coding (SSC) with superposition coding (SPC) in a decode-and-forward three-node relay network. Through non-asymptotic theoretical analysis, a practical and computable measure of EED is derived to enable performance evaluation of the considered JSCC system under any channel condition with arbitrarily large channel error probabilities. Based on the derived EED models, numerical experiments over a wide range of channel conditions demonstrate significant performance gains by using the considered SSC-SPC architecture over a number of legacy implementations. Furthermore, solutions to the power allocation optimization problem show significant gaps of achievable EED in the case that the system operates based on suboptimal power allocation configurations derived from asymptotic formulations that disregard channel errors. Insights on the sensitivity of such EED gaps to suboptimal configurations are provided via extensive discussions in relation to the channel conditions of the fundamental three-node relay channel.

Chapter 5

Conclusion and Future Work

This thesis considers the application of joint source-channel coding principles to multimedia communications over point-to-point, broadcast, and relay channels. From the perspective of end-to-end distortion, the thesis targets non-asymptotic theoretical analysis to pursue insights into practical designs. In this final chapter, the motivation, background, and contributions of this thesis are summarized, along with ongoing open problems that are left for future investigation.

5.1 Conclusion

The fundamental motivation behind joint source-channel coding is inspired by the unknown optimality of separate source-channel coding for practical systems that must always operate in the finite block length regime, thus causing the channel error probability for a system employing *any* channel code to be strictly greater than zero. However, such simple fact does not directly imply the breakdown of Shannon's separation result of optimality under separate source and channel coding design. To demonstrate the separation theorem's invalidity, we must identify some scenarios in which gains of joint versus separate source-channel coding can be quantified, and do so under an optimal separate design setting.

Motivated by the above, Chapter 2 revisits the validity of the separation theorem in the finite block length regime for point-to-point channels, aiming to disprove the theorem by demonstrating the performance gains of designing source quantizers that are tailored to the channel statistics of an optimal channel code. The statistics of the optimal channel code are governed by recent advancements in finite block length analysis, which provides an accurate characterization of the tradeoff between the error probability of the channel under optimal channel coding, and the source coding rate, or equivalently in this thesis, the quantization rate. Under the optimal tradeoff between the source quantization rate and channel block error probability, the channel-optimized source quantizer is demonstrated to outperform the optimal Lloyd-Max separate quantizer from the perspective of end-to-end distortion, which is computable in closed-form when assuming a random index mapping between source and channel coding symbols. With this, we can firmly conclude that the separation of source and channel coding no longer holds in the finite block length regime. Furthermore, we demonstrate that the application of JSCC techniques may yield significant reductions to the end-to-end distortion of the system under certain channel conditions or settings, hence justifying their required increase in design and operation complexity for their implementation in practical systems.

With the conclusion of the invalidity of separate source and channel coding from Chapter 2 even under optimal channel coding, we are further motivated to improve JSCC systems for broadcast applications that must tolerate potentially large and fixed channel error probabilities from operating with finite block lengths. Beyond the advantages of using channel-optimized source quantizers, we identify room for further reductions to the end-to-end distortion through the augmentation of error detection codes into source coding to tradeoff quantization rate and error detection capability under fixed channel coding statistics. In Chapter 3, we consider the augmentation of cyclic redundancy checks (CRC) as the error detection code in conjunction with the multiresolution quantizer to serve as the scalable source coding (SSC) portion of the system. The SSC is paired with layered modulation to serve as a superposition channel code (SPC). Under the assumption of random index assignments, a closed-form formula for the weighted end-to-end distortion is derived for a JSCC system consisting of MRVQ, RIA, CRC, and SPC. The EED formula

allows for further derivation of necessary optimality conditions, which serve as guidelines for algorithm development in designing the noisy MRVQ in conjunction with CRC.

The numerical results in Chapter 3 show significant EED reductions due to trading off some quantization rate to enable inclusion of CRC data without loss of bandwidth. The reductions to EED when employing CRC are observed for both the point-to-point AWGN channel as well as the Gaussian broadcast channel over a wide range of channel conditions. Moreover, the results reveal some interesting insights of the system when employing optimal CRCs, such as the counterintuitive behaviour of increasing EED reductions with improving channel conditions for both considered channels. In the point-to-point case, this is due to sacrificing more quantization rate to enable an effective CRC implementation when the channel is worse; as a result, the reductions to EED are largely offset by the increase in quantization distortion. As the channel improves, less quantization rate needs to be sacrificed for CRC, resulting in significantly more reductions to the EED. This behaviour also applies for the worse channel receiver in the broadcast case, as it behaves like the point-to-point case with interest in only the lower resolution reconstruction of the original source. However, the same trend is also observed for the other receiver, due to the increasingly likelihood for both CRCs to be utilized under better channel conditions, as opposed to discarding the higher resolution CRC data once an error is detected for the lower resolution. Nonetheless, from all of the numerical results, it can be concluded that for applications that are constantly subject to nonzero error probabilities under any channel code, inclusion of error detection at the application layer is considered to be rather effective in further improving the end-to-end performance of JSCC systems.

Due to the positive reductions to EED achievable by the pairing of scalable source codes with superposition channel codes in the broadcast scenario, Chapter 4 further extends their consideration into a three-node relay network. Maintaining analyses on a non-asymptotic basis, a practical and computable measure of the end-to-end distortion is derived to evaluate the performance for such setting under any relay channel conditions with potentially large channel error probabilities. The advantages of applying JSCC principles in the relay network is demonstrated through numerical experiments, revealing significant performance advantages of the relay-assisted transmission in exploiting the possible increase in trans-

mission diversity, in addition to the SSC-SPC pairing itself in tackling channel fluctuations caused by fading.

To demonstrate the importance of analyzing JSCC systems under non-asymptotic techniques and settings, Chapter 4 also considers the problem of power allocation configuration that is necessary for the optimal performance of superposition coding. We provide some insight into the relationship between relay channel conditions and power allocation configurations, and quantify the performance gaps between solutions based on capacity-based metrics that disregard channel errors, and those based on the end-to-end distortion of the system. Numerical results show that solutions based on the capacity-based metrics result in a potentially large sub-optimality in the end-to-end distortion performance of the considered JSCC system. Although our analysis is only one JSCC setup of many, we conclude that consideration of JSCC systems from a non-asymptotic setting is not only more meaningful, but also reveals more relevant insight into practical system design. In this thesis, we accomplish analysis under non-asymptotic scenarios by maintaining the end-to-end distortion as the performance measure for system evaluation throughout the entirety of the thesis.

5.2 Future Work

The chapters in this thesis tackle a variety of related problems in joint source-channel coding. For each topic of interest, there are still open problems that have been left for future investigation. In this section, we briefly discuss them, and include some intermediate results of currently ongoing investigations.

5.2.1 Separation of Source and Channel Coding

Chapter 2 investigates the validity of Shannon's separation theorem on the optimality of separate source and channel coding design in the finite block length regime. From the perspective of end-to-end distortion, the results show that there indeed exist scenarios where

JSCC achieves reductions to the EED of a separate source-channel coding system with an optimal channel code. Although such results already imply that source and channel coding separation is no longer valid in the finite block length regime, there is room to further develop this problem in a mathematically rigorous manner. Doing so would help characterize the relationship between the quantity of the EED reduction to the system setting or channel conditions, potentially revealing deeper insight as to when the performance advantages of joint source-channel coding justifies the increased design or operation complexity in practical multimedia communication systems.

To fully solve this problem, one strategy is to derive the converse bound of the separate source-channel coding system, and show that the EED of such system is strictly greater than a particular achievability of the JSCC case. Since the derivation of the required converse and achievability may be difficult for the general case, this subsection summarizes some initial results for the case of high-rate quantization to allow some analysis using point density analysis techniques. We provide a derivation of the converse EED bound under high-rate quantization for the separate design system, where the quantizer only targets the minimization of the quantization distortion as opposed to the end-to-end distortion. The achievability of the JSCC system employing channel-optimized vector quantizers remains an open problem.

Let $\boldsymbol{z}$ be a k-dimensional Gaussian source with a probability density function $f(\boldsymbol{z})$. Suppose $\boldsymbol{z}$ is to be quantized by a N-level vector quantizer with $N \gg k$ for high-rate quantization. Applying point density analysis as in [59] and [60], the quantization distortion D_Q can be lower bounded as follows:

$$\begin{aligned} D_Q &\geq \frac{1}{k}\left(\frac{k}{k+2}\right)(NB_k)^{-\frac{2}{k}}\left[\int f(\boldsymbol{z})^{\frac{k}{k+2}}d\boldsymbol{z}\right]^{\frac{k+2}{k}} \\ &= \frac{1}{k}\left(\frac{k}{k+2}\right)(NB_k)^{-\frac{2}{k}}\left[\left(2\pi\sigma^2\right)^{\frac{k}{k+2}}\left(\frac{k+2}{k}\right)^{\frac{k}{2}}\right]^{\frac{k+2}{k}} \\ &= \frac{2\pi\sigma^2}{k}\left(\frac{k+2}{k}\right)^{\frac{k}{2}}(B_kN)^{-\frac{2}{k}}, \end{aligned} \tag{5.1}$$

where B_k is the volume of the k-sphere, expressed as

$$B_k = \frac{\pi^{\frac{k}{2}}}{\Gamma\left(\frac{k}{2}+1\right)},$$

and $\Gamma(\cdot)$ is the gamma function.

Combining the above yields

$$D_Q \geq \frac{2\sigma^2}{k}\left(\frac{k+2}{k}\right)^{\frac{k}{2}}\left[\frac{\Gamma(\frac{k}{2}+1)}{N}\right]^{\frac{2}{k}}. \tag{5.2}$$

Similarly suppose $N \gg k$, use point density analysis to approximate S_Q as follows:

$$S_Q \approx \frac{1}{k}\int \frac{|\boldsymbol{z}|^2 N\lambda(\boldsymbol{z})d\boldsymbol{z}}{N} = \frac{1}{k}\int |\boldsymbol{z}|^2\lambda(\boldsymbol{z})d\boldsymbol{z}, \tag{5.3}$$

where to minimize the quantization distortion, $\lambda(\boldsymbol{z})$ is expressed as

$$\lambda(\boldsymbol{z}) = \frac{f(\boldsymbol{z})^{\frac{k}{k+2}}}{\int_\Lambda f(\boldsymbol{z})^{\frac{k}{k+2}}d\boldsymbol{z}}. \tag{5.4}$$

For a k-dimensional Gaussian source, $\lambda(\boldsymbol{z})$ can be computed as

$$\lambda(\boldsymbol{z}) = \frac{f(\boldsymbol{z})^{\frac{k}{k+2}}}{(2\pi\sigma^2)^{\frac{k}{k+2}}\left(\frac{k+2}{k}\right)^{\frac{k}{2}}} \tag{5.5}$$

to yield

$$S_Q \approx \left(\frac{k+2}{k}\right)\sigma^2. \tag{5.6}$$

From (2.2), the end-to-end distortion (EED) is expressed as:

$$\bar{D} = \left(1 - \frac{\epsilon N^k}{N^k - 1}\right) D_Q + \frac{\epsilon N^k}{N^k - 1}(\sigma^2 + S_Q), \tag{5.7}$$

which for $N \gg k$, is lower bounded as

$$\begin{aligned}\bar{D} &\geq \left(1 - \frac{\epsilon N^k}{N^k - 1}\right) \frac{2\sigma^2}{k} \left(\frac{k+2}{k}\right)^{\frac{k}{2}} \left[\frac{\Gamma(\frac{k}{2}+1)}{N}\right]^{\frac{2}{k}} + \frac{\epsilon N^k}{N^k - 1}\left[\sigma^2 + \left(\frac{k+2}{k}\right)\sigma^2\right] \\ &\approx (1-\epsilon)\frac{2\sigma^2}{k}\left(\frac{k+2}{k}\right)^{\frac{k}{2}} \left[\frac{\Gamma(\frac{k}{2}+1)}{N}\right]^{\frac{2}{k}} + \epsilon\left[\sigma^2 + \left(\frac{k+2}{k}\right)\sigma^2\right]. \end{aligned} \tag{5.8}$$

For the highest quantization rate, i.e., $k = 1$, the above reduces to

$$\begin{aligned}\bar{D} &\geq (1-\epsilon)\sigma^2 \frac{2\sqrt{3}}{4}\pi N^{-2} + 4\sigma^2\epsilon \\ &\approx \sigma^2\left[\frac{\sqrt{3}\pi(1-\epsilon)}{2N^2} + 4\epsilon\right]. \end{aligned} \tag{5.9}$$

5.2.2 Noisy Quantization with Error Correction Codes

In Chapter 3, the usage of error detection codes is considered for the purpose of reducing the end-to-end distortion of the system by reducing the effects of the scatter factor for incorrectly decoded source symbols. In this subsection, we suggest further possible reductions to the system EED using error correction codes.

Consider the EED for the point-to-point channel under random index assignments in (3.9), and restated as follows for clarity:

$$D_b^{\Pi} = \left(1 - p_{bd} - \frac{N_1 p_{bu}}{N_1 - 1}\right) D_{Q_b} + \left(\frac{N_1 p_{bu}}{N_1 - 1}\right)\left(\sigma^2 + S_{Q_b}\right) + p_{bd}\sigma^2.$$

Observe from (3.9) that addition of error detection codes significantly reduces the effects of the scatter factor to only undetected symbol errors, occurring with probability $p_{bu} \ll$

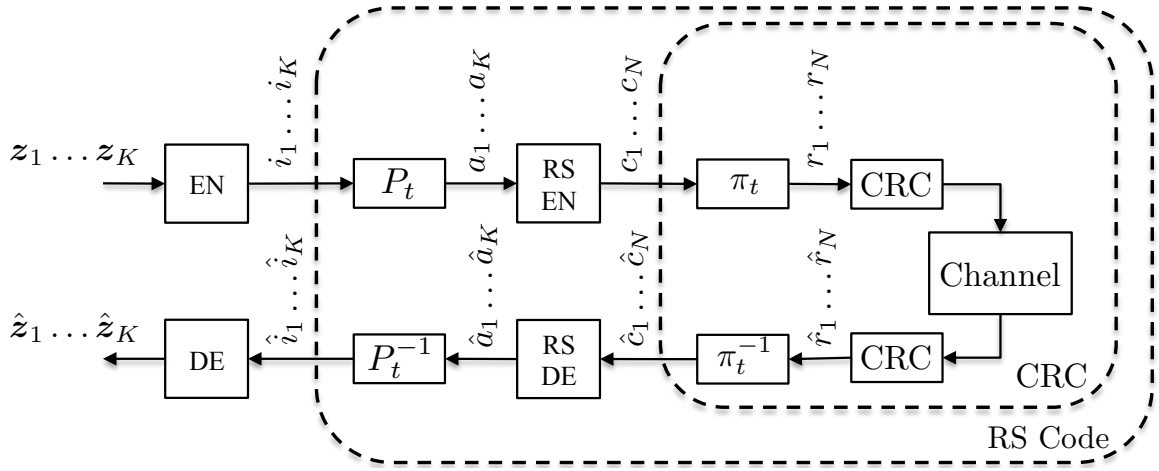

Figure 5.1: A tandem source-channel point-to-point system with error correcting codes over a channel with both erasures and errors.

$p_{bd} + p_{bu}$. As a result, the EED is reduced since all detected errors have their distortion contribution to EED reduced from $(\sigma^2 + S_{Q_b})$ to σ^2. At this point, due to the addition of error detection codes, the contribution of the $p_{bd}\sigma^2$ term may become significant under certain channel conditions, hence motivating us to employ error correction codes in hopes of correcting some of the detected errors, also known as erasures, to further reduce the EED of the system.

With reference to Fig. 5.1, consider employing Reed-Solomon (RS) codes for only erasure correction on top of the original JSCC system with error detection. Suppose K samples of the vector source $\boldsymbol{z}$, $\{\boldsymbol{z}_1, \ldots, \boldsymbol{z}_K\}$ are each mapped to a particular quantizer index to yield K quantizer indices denoted by $\{i_1, \ldots, i_K\}$. Let $P_t(\{i_1, \ldots, i_K\}) = \{a_1, \ldots, a_K\}$ be a random permutation linking the K outputs of the quantizer output to the RS encoder input. The RS encoder outputs $N \geq K$ symbols, $\{c_1, \ldots, c_N\}$, where $c_x = a_x$ for $x = 1, \ldots, K$. Each of the N RS encoder outputs are linked to the CRC-coded channel with random index assignment, as in Chapter 3.

Approximate the CRC-coded channel in Fig. 5.1 as a non-binary erasure channel to simplify Fig. 5.1 to Fig. 5.2. Due to employment of random index assignments in Fig. 5.1, the non-binary erasure channel can be characterized by an average erasure probability p_1.

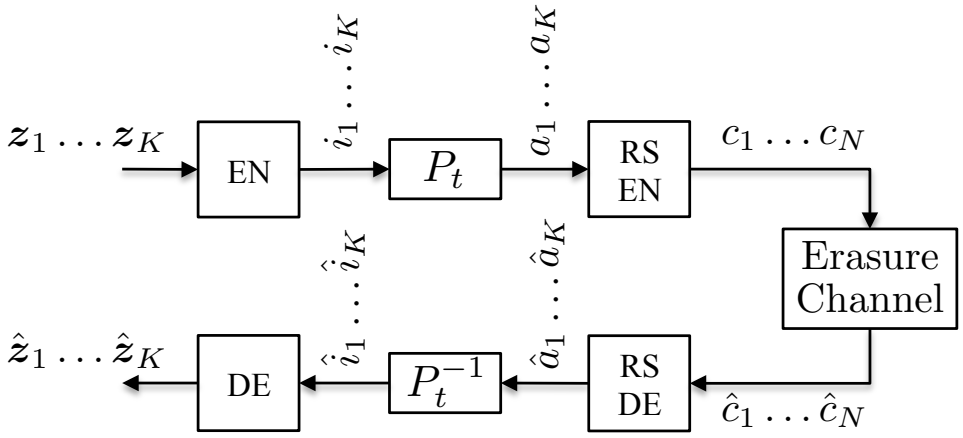

Figure 5.2: A tandem source-channel point-to-point system with error correcting codes over an erasure channel.

Let $\mathcal{A}_n = \{\hat{\boldsymbol{a}} : d(\hat{\boldsymbol{a}}, \boldsymbol{a}) = n\}$, where $\boldsymbol{a} = a_1 \dots a_K$, $\hat{\boldsymbol{a}} = \hat{a}_1 \dots \hat{a}_K$, and $d(\cdot, \cdot)$ denotes the Hamming distance between the two arguments. Consider a particular $\hat{\boldsymbol{a}}_n \in \mathcal{A}_n$ where $\hat{a}_1 = \cdots = \hat{a}_n = \mathrm{e}, \hat{a}_{n+1} = a_{n+1}, \dots, \hat{a}_K = a_K$; specifically, the $\hat{\boldsymbol{a}}_n$ corresponds to $\boldsymbol{a}$ with erasure occurring for the first n elements. For this error pattern, suppose the permutation P_t linking $\boldsymbol{i}$ and $\boldsymbol{a}$ is randomly and uniformly selected. Taking expectation over all possible permutations, the probability of $\boldsymbol{z}_x$ being erased for $\hat{\boldsymbol{a}} = \hat{\boldsymbol{a}}_n$ is given by

$$\begin{aligned} E_{P_t}\left[p_b^{P_t}\left(\hat{i}_x = \mathrm{e}, \hat{\boldsymbol{a}}_n\right)\right] &= \frac{1}{K!}\sum_{t=1}^{K!} p_b^{P_t}\left(\hat{i}_x = \mathrm{e}, \hat{\boldsymbol{a}}_n\right) = \frac{1}{K!}\sum_{p=1}^{n}\sum_{t:i_x=a_p} \Pr(\hat{\boldsymbol{a}}_n) \\ &= \frac{n}{K}\Pr(\hat{\boldsymbol{a}}_n). \end{aligned} \tag{5.10}$$

Summing over all possible $\hat{\boldsymbol{a}}_n \in \mathcal{A}_n$ for $n = 1, \dots, K$ results in the average probability of erasure for $\boldsymbol{z}_x$:

$$\begin{aligned} E_{P_t} p_b^{P_t}\left(\hat{i}_x = \mathrm{e}\right) &= \sum_{n=1}^{K}\sum_{\hat{\boldsymbol{a}}_n \in \mathcal{A}_n} E_{P_t} p_b^{P_t}\left(\hat{i}_x = \mathrm{e}, \hat{\boldsymbol{a}}_n\right) = \sum_{n=1}^{K}\sum_{\hat{\boldsymbol{a}}_n \in \mathcal{A}_n} \frac{n}{K}\Pr(\hat{\boldsymbol{a}}_n) \\ &= \sum_{n=1}^{K} \frac{n}{K}\Pr\left\{d(\hat{\boldsymbol{a}}, \boldsymbol{a}) = n\right\} \triangleq p_{d_1}. \end{aligned} \tag{5.11}$$

Let n_e denote the number of erasures caused by the erasure channel such that $n_e = d(\hat{\boldsymbol{c}}, \boldsymbol{c})$, where $\boldsymbol{c} = c_1 \dots c_N$ and $\hat{\boldsymbol{c}} = \hat{c}_1 \dots \hat{c}_N$. Suppose the RS code can correct all erasures if $n_e \leq N - K$; otherwise, trash $\hat{c}_{K+1} \dots \hat{c}_N$ and let $\hat{a}_p = \hat{c}_p$ for $p = 1, \dots, K$. Hence, any erasure occurring in $\hat{\boldsymbol{a}}$ implies RS correction failure. RS decoding in this manner allows p_{d_1} to be further simplified as follows:

$$\begin{aligned}
p_{d_1} &= \sum_{n=1}^{K} \frac{n}{K} \Pr\left\{d(a_1 \dots a_K, \hat{a}_1 \dots \hat{a}_K) = n\right\} \\
&= \sum_{n=1}^{K} \frac{n}{K} \Pr\left\{d(c_1 \dots c_K, \hat{c}_1 \dots \hat{c}_K) = n, d(c_1 \dots c_N, \hat{c}_1 \dots \hat{c}_N) > N - K\right\} \\
&= \sum_{n=1}^{K} \frac{n}{K} \Pr\left\{d(c_1 \dots c_K, \hat{c}_1 \dots \hat{c}_K) = n\right\} \Pr\left\{d(c_{K+1} \dots c_N, \hat{c}_{K+1} \dots \hat{c}_N) > N - K - n\right\} \\
&= \sum_{n=1}^{K} \frac{n}{K} \left[\binom{K}{n} p_1^n (1 - p_1)^{K-n}\right] \left[\sum_{t=\max(0, N-K-n+1)}^{N-K} \binom{N-K}{t} p_1^t (1 - p_1)^{N-K-t}\right] \quad (5.12)
\end{aligned}$$

The EED for any single source symbol $\boldsymbol{z}_x$ in the system in Fig. 5.2 is expressed as follows under random permutation assignment.

$$\begin{aligned}
E_{P_t} D_b^{P_t} &= \frac{1}{k} \sum_{i_x=1}^{N_1} \int_{\boldsymbol{z}_x \in A_{i_x}} \|\boldsymbol{z}_x - \boldsymbol{z}_{i_x}\|^2 E_{P_t} p_b^{P_t} \left(\hat{i}_x = i_x\right) f(\boldsymbol{z}_x) \mathrm{d}\boldsymbol{z}_x \\
&\quad + \frac{1}{k} \sum_{i_x=1}^{N_1} \int_{\boldsymbol{z}_x \in A_{i_x}} \|\boldsymbol{z}_x\|^2 E_{P_t} p_b^{P_t} \left(\hat{i}_x = \mathrm{e}\right) f(\boldsymbol{z}_x) \mathrm{d}\boldsymbol{z}_x \\
&= (1 - p_{d_1}) D_Q + p_{d_1} \sigma^2 \quad (5.13)
\end{aligned}$$

From (5.13), we see that the optimal separate quantizer actually minimizes the EED of the system with RS code under the assumption that the employed CRC detects all errors. Since there is no closed-form expression for the EED to include the effects of imperfect CRC error detection, performance evaluations require the use of simulations, which are generated from Gaussian random variables with sample sizes on the order of $\mathcal{O}(10^8)$.

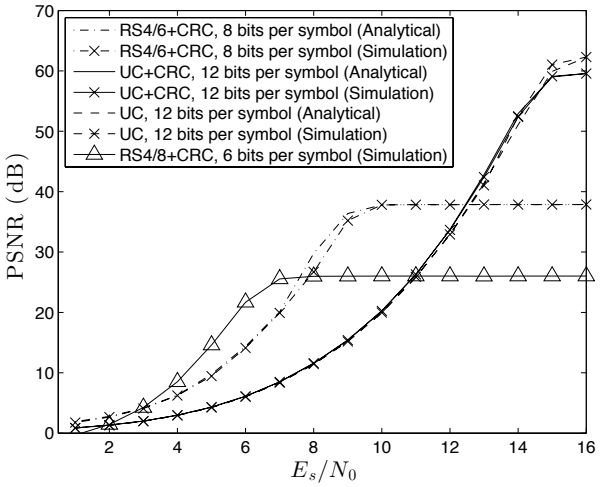

Figure 5.3: Results comparing uncoded (UC) with and without CRC for error detection and Reed-Solomon codes for error correction over various QPSK channel SNR E_s/N_0.

Fig. 5.3 summarizes the PSNR performance of a number of schemes that can be largely categorized as: 1) uncoded, where all bits are reserved for source quantization; 2) uncoded with CRC only, where the optimal tradeoff between quantization and CRC bits are considered; and 3) RS code with CRC, where the optimal tradeoff between quantization, CRC, and RS code is considered. For a fair comparison, $K = 4$ is fixed over 24 uses of the QPSK modulation scheme for a total block length of 48 bits. For 1) and 2), existing closed-form expressions from earlier chapters are used to analytically evaluate the EED. Simulation results for these categories are also included for verification purposes. The analytical results for 3) are based on (5.13), which is only an approximation as CRC cannot detect all error patterns, and hence such category relies on simulations for accurate results.

Fig. 5.3 shows that the joint use of RS code and CRCs can significantly increase the system PSNR performance, as opposed to employing only CRCs. The gains are also visibility dependent on the channel conditions and as expected, the optimal RS code rate decreases as the channel condition worsens. These preliminary results show that it is worthwhile to investigate the addition of error correction codes on top of error detection codes, especially for scenarios with large channel error probabilities, resulting in the source variance term dominating the end-to-end distortion of the system with only CRC.

Bibliography

[1] A. Goldsmith and M. Effros, "Joint Design of Fixed-Rate Source Codes and Multiresolution Channel Codes," *IEEE Trans. Commun.*, vol. 46, no. 10, pp. 1301-1312, Oct. 1998.

[2] A. Kurtenbach and P. Wintz, "Quantizing for noisy channels," *IEEE Trans. Commun. Technol.*, vol. COM-17, pp. 291-302, Apr. 1969.

[3] N. Farvardin and V. Vaishampayan, "Optimal Quantizer Design for Noisy Channels: an Approach to Combined Source-Channel Coding," *IEEE Trans. Inf. Theory*, vol. IT-33, pp. 827-838, Nov. 1987.

[4] N. Farvardin and V. Vaishampayan, "On the performance and complexity of channel-optimized vector quantizers," *IEEE Trans. Inf. Theory*, vol. 37, no. 1, pp. 155-160, Jan. 1991.

[5] H. Kumazawa, M. Kasahara, and T. Namekawa, "A construction of vector quantizers for noisy channels," Electron. Eng. Japan, vol. 67-B, pp. 39-47, 1984.

[6] X. Yu, H. Wang, and E.-H. Yang, "Design and analysis of optimal noisy channel quantization with random index assignment," *IEEE Trans. Inf. Theory*, vol. 56, no. 11, pp. 5796-5804, Nov. 2010.

[7] F. Teng, E.-H. Yang, and X. Yu, "Optimal Multiresolution Quantization for Broadcast Channels with Random Index Assignment," *Proc. IEEE Intern. Symp. Inf. Theory*, Austin, TX, Jun. 2010, pp. 181-185.

[8] J. She, F. Hou, P.-H. Ho, and L.-L. Xie, "IPTV over WiMAX: Key Success Factors, Challenges and Solutions," *IEEE Commun. Mag.*, vol. 45, no. 8, pp. 87-93, Aug. 2007.

[9] C. Ng, D. Gündüz, A.J. Goldsmith, and E. Erkip, "Distortion Minimization in Gaussian Layered Broadcast Coding with Successive Refinement," *IEEE Trans. Inf. Theory*, vol. 55, no. 11, pp. 5074-5086, Nov. 2009.

[10] J. She, X. Yu, P.-H. Ho and E.-H. Yang, "A Cross-Layer Design Framework for Robust IPTV Services over IEEE 802.16 Networks," *IEEE J. Sel. Areas on Commun.*, vol. 27, no. 2, pp. 235-245, Feb. 2009.

[11] C. Tian, A. Steiner, S. Shamai, S. N. Diggavi, "Successive Refinement Via Broadcast: Optimizing Expected Distortion of a Gaussian Source Over a Gaussian Fading Channel," *IEEE Trans. Inf. Theory*, vol. 54, no. 7, pp. 2903-2918, Jul. 2008.

[12] D. Gündüz, E. Erkip, A. Goldsmith, and H. Poor, "Reliable Joint Source-Channel Cooperative Transmission Over Relay Networks," *IEEE Trans. Inf. Theory*, vol. 59, no. 4, pp. 2442-2458, Apr. 2013.

[13] M. Yuksel and E. Erkip, "Broadcast Strategies for the Fading Relay Channel," *Proc. IEEE Military Commun. Conf.*, Nov. 2004. vol. 2, pp. 1060-1065.

[14] H. Y. Shutoy, D. Gündüz, E. Erkip, and Y. Wang, "Cooperative Source and Channel Coding for Wireless Multimedia Communications," *IEEE J. Sel. Topics Signal Process.*, vol. 1, no. 2, pp. 295-307, Aug. 2007.

[15] U. Sethakaset, T. Quek, and S. Sun, "Joint Source-Channel Optimization over Wireless Relay Networks," *IEEE Trans. Commun.*, vol. 59, no. 4, pp. 1114-1122, Apr. 2011.

[16] D. Gündüz and E. Erkip, "Source and Channel Coding for Cooperative Relaying," *IEEE Trans. Inf. Theory*, vol. 53, no. 10, pp. 3454-3475, Oct. 2007.

[17] A. Steiner and S. Shamai, "Single-user broadcasting protocols over a two-hop relay fading channel," *IEEE Trans. Inf. Theory*, vol. 52, no. 11, pp. 4821-4838, Nov. 2006.

[18] J. Wui and D. Kim, "Optimal Power Allocation Between Unicast and Multicast Messages in Wireless Relay-Multicasting Networks Using Superposition Coding," *IEEE Commun. Letters*, vol. 15, no. 11, pp. 1159-1161, Nov. 2011.

[19] D. Gündüz and E. Erkip, "Reliable Cooperative Source Transmission with Side Information," *Proc. IEEE Inform. Theory Workshop*, Bergen, Norway, Jul. 2007, pp. 1-5.

[20] A. Avestimehr and D. Tse, "Outage Capacity of the Fading Relay Channel in the Low SNR Regime," *IEEE Trans. Inf. Theory*, vol. 53, no. 4, pp. 1401-1415, Apr. 2007.

[21] T. Holliday and A. Goldsmith, "Optimizing End-to-End Distortion in MIMO Systems," *Proc. IEEE Intern. Symp. Inf. Theory*, Adelaide, SA, Sep. 2005, pp. 1671-1675.

[22] J. Chen and D.T.M. Slock, "Bounds on Optimal End-to-End Distortion of MIMO Links," *Proc. IEEE Intern. Conf. on Commun.*, Beijing, China, May 2008, pp. 1377-1381.

[23] I. Kozintsev and K. Ramchandran, "Robust Image Transmission Over Energy-Constrained Time-Varying Channels Using Multiresolution Joint Source-Channel Coding," *IEEE Trans. Signal Process.*, vol. 46, no. 4, pp. 1012-1026, Apr. 1998.

[24] S. Lloyd, "Least squares quantization in PCM," *IEEE Trans. Inf. Theory*, vol. IT-28, no. 2, pp. 129-137, Mar. 1982.

[25] J. Max, "Quantizing for minimum distortion," *IRE Trans. Inf. Theory*, vol. IT-6, pp. 7-12, Mar. 1960.

[26] K. Zeger and V. Manzella, "Asymptotic bounds on optimal noisy channel quantization via random coding," *IEEE Trans. Inf. Theory*, vol. 40, no. 6, pp. 1926-1938, Nov. 1994.

[27] "Evolved universal terrestrial radio access (e-utra); multiplexing and channel coding," 3GPP Technical Specification 36.212, www.3gpp.org.

[28] J. Ho, J. Meng, and E.-H. Yang, "On Separation of Source and Channel Coding in the Finite Block Length Regime," *Proc. Canadian Workshop Inform. Theory*, Toronto, ON, Jun. 2013, pp. 97-100.

[29] J. Ho and E.-H. Yang, "Designing Optimal Multiresolution Quantizers with Error Detecting Codes," *IEEE Trans. Wireless Commun.*, vol. 12, no. 7, pp. 3588-3599, Jul. 2013.

[30] J. Ho and E.-H. Yang, "Optimal Multiresolution Quantization with Error Detecting Codes for Broadcast Channels," *Proc. IEEE Intern. Symp. Inform. Theory*, Istanbul, Turkey, Jul. 2013, pp. 554-558.

[31] J. Ho and P.-H. Ho, "On Transmission of Multiresolution Gaussian Sources over Noisy Relay Networks," *IEEE Trans. Wireless Commun.*, vol. 12, no. 7, pp. 3170-3179, Jul. 2013.

[32] J. Ho and P.-H. Ho, "Reducing End-to-End Distortion in Noisy Wireless Relay Networks," *Proc. IEEE Global Commun. Conf.*, Anaheim, CA, Dec. 2012, pp. 5669-5674.

[33] J. Ho, J. She, and P.-H. Ho, "Successive Refinement Relaying Strategies in Coded Wireless Multicast Networks," *Proc. IEEE Intern. Conf. Commun.*, Kyoto, Japan, Jun. 2011, pp. 1-6.

[34] J. Ho and P.-H. Ho, "On Optimal Power Allocation of Layered Coding in Noisy Wireless Relay Networks," *Proc. Intern. Symp. Wireless Personal Multimedia Commun.*, Taipei, Taiwan, Sept. 2012, pp. 321-325.

[35] J. Ho and E.-H. Yang, "Cross-Layer Coding Optimization for Mobile IPTV Delivery," *IEEE COMSOC MMTC E-Letter*, Jan. 2011.

[36] V. Kostina and S. Verdú, "Fixed-Length Lossy Compression in the Finite Blocklength Regime," *IEEE Trans. Inf. Theory*, vol. 58, no. 6, pp. 3309-3338, Jun. 2012.

[37] E.-H. Yang and J. Meng, "Jar Decoding: Non-asymptotic Converse Coding Theorems, Taylor-Type Expansion, and Optimality," submitted to *IEEE Trans. Inf. Theory*, Apr. 2012, and online available: http://arxiv.org/abs/1204.3658.

[38] E.-H. Yang and J. Meng, "Channel Capacity in the Non-asymptotic Regime: Taylor-type Expansion and Computable Benchmarks," *Proc. Allerton Conf.*, Monticello, IL, Oct. 2012., pp. 278-285.

[39] Y. Polyanskiy, H. V. Poor, and S. Verdú, "Channel Coding Rate in the Finite Blocklength Regime," *IEEE Trans. Inf. Theory*, vol. 56, no. 5, pp. 2307-2359, May 2010.

[40] J. Meng and E.-H. Yang, "Constellation and Rate Selection in Adaptive Modulation and Coding based on Finite Blocklength Analysis," *Proc. IEEE Wireless Commun. Net. Conf.*, Shanghai, China, Apr. 2013.

[41] P. Vitthaladevuni and M. Alouini, "A Recursive Algorithm for the Exact BER Computation of Generalized Hierarchical QAM Constellations," *IEEE Trans. Inf. Theory*, vol. 49, no. 1, pp. 297-307, Jan. 2003.

[42] S. Dumitrescu, "Fast Encoder Optimization in Multi-resolution Scalar Quantizer Design," *IEEE Trans. Inf. Theory*, vol. 57, no. 3, pp. 1520-1529, Mar. 2011.

[43] H. Brunk and N. Farvardin, "Fixed-rate successively refinable scalar quantizers," *Proc. DCC96*, Snowbird, Utah, March 1996, pp. 250-259.

[44] M. Effros and D. Dugatkin, "Multiresolution Vector Quantization," *IEEE Trans. Inf. Theory*, vol. 50, no. 12, pp. 3130-3145, Dec. 2004.

[45] B. Hochwald and K. Zeger, "Tradeoff Between Source and Channel Coding," *IEEE Trans. Inf. Theory*, vol. 43, no. 5, pp. 1412-1424, Sept. 1997.

[46] M. Scagliola, F. Perez-Gonzalez, and P. Guccione, "A Dirty Paper Scheme for Hierarchical OFDM," *Proc. IEEE Intern. Conf. on Commun.*, Kyoto, Japan, Jun. 2011., pp. 1-5.

[47] L. Cai, S. Xiang, Y. Luo, and J. Pan, "Scalable Modulation for Video Transmission in Wireless Networks," *IEEE Trans. Vehicular Tech.*, vol. 60, no. 9, pp. 4314-4323, Nov. 2011.

[48] *DVB-T standard: ETS 300 744, Digital Broadcast Systems for Television, Sound and Data Services: Framing Structure, Channel Coding and Modulation for Digital Terrestrial Television*, ETSI Draft, vol. 1.2.1, no. EN300 744, 1999-1.

[49] *Physical Layer for Ultra Mobile Broadband (UMB) Air Interface Specification*, TSG-C, 3GPP2 C.S0084-001-0 v3.0, 2008.

[50] P. Koopman and T. Chakravarty, "Cyclic Redundancy Code (CRC) polynomial selection for embedded networks," *Proc. Intern. Conf. Dependable Syst. and Networks*, Florence, Italy, Jun. 2004, pp. 145-154.

[51] F. Etemadi and H. Jafarkhani, "Rate and Power Allocation for Layered Transmission With Superposition Coding," *IEEE Signal Process. Letters*, vol. 14, no. 11, pp. 773-776, Nov. 2007.

[52] B.A. Heng, J.G. Apostolopoulos, and J.S. Lim, "End-to-end rate-distortion optimized mode selection for multiple description video coding," *Proc. IEEE Intern. Conf. Acoustics, Speech, and Signal Process.*, Philadelphia, PA, Mar. 2005, vol. 5, pp. 905-908.

[53] H. Yang and K. Rose, "Advances in Recursive Per-Pixel End-to-End Distortion Estimation for Robust Video Coding in H.264/AVC," *IEEE Trans. Circuits and Systems for Video Technology*, vol. 17, no. 7, pp. 845-856, Jul. 2007.

[54] J. Han, V. Melkote, and K. Rose, "A spectral approach to recursive end-to-end distortion estimation for sub-pixel motion-compensated video coding," *Proc. IEEE Intern. Conf. Acoustics, Speech, and Signal Process.*, Prague, Czech Republic, May 2011, pp. 825-828.

[55] M. Nakagami, "The m-distribution- A general formula of intensity distribution of rapid fading," *Statistical Methods in Radio Wave Propagation*, pp. 3-36, Pergamon Press, Oxford, England, 1960.

[56] P. K. Vitthaladevuni and M.-S. Alouini, "BER computation of 4/M- QAM hierarchical constellations," *IEEE Trans. Broadcast*, vol. 47, pp. 228-239, Sept. 2001.

[57] J. Ho, "Logical Superposition Coded Modulation for Wireless Video Multicasting," M.A.Sc. thesis, Dept. Elect. and Comput. Eng., Univ. of Waterloo, Waterloo, Canada, 2009.

[58] J. Ho. (2012) *On the Capacity of Relay Networks under Layered Joint Source-Channel Coding* [Online]. Available: `http://www.eng.uwaterloo.ca/~jc4ho/techrep.pdf`

[59] A. Gersho, "Asymptotically optimal block quantization," *IEEE Trans. Inf. Theory*, vol. 25., no. 4, pp. 373-380, Jul. 1979.

[60] P. Zador, "Asymptotic quantization error of continuous signals and the quantization dimension," *IEEE Trans. Inf. Theory*, vol. 28, no. 2, pp. 139-149, Mar. 1982.